STUDY OF POLARIMETRIC ANALYSIS OF PALSAR IMAGES FOR TERRAIN CLASSIFICATION

A DISSERTATION

Submitted in partial fulfillment of the requirements for the award of the degree of

MASTER OF TECHNOLOGY

in

ELECTRONICS AND COMMUNICATION ENGINEERING

(With Specialization in RF and Microwave Engineering)

By

POOJA MISHRA

DEPARTMENT OF ELECTRONICS AND COMPUTER ENGINEERING
INDIAN INSTITUTE OF TECHNOLOGY ROORKEE
ROORKEE -247 667 (INDIA)

JUNE, 2010

CANDIDATE'S DECLARATION

I hereby declare that the work, which is being presented in the dissertation entitled **"Study of Polarimetric Analysis of SAR Images for Terrain Classification"** in the partial fulfillment of the requirements for the award of degree of **Master of Technology** in **RF & Microwave Engineering** submitted in the Department of Electronics and Computer Engineering, Indian Institute of Technology Roorkee, Roorkee (INDIA), is an authentic record of my own work carried out under the guidance of Dr. Dharmendra Singh, Associate Professor, Department of Electronics and Computer Engineering, Indian Institute of Technology, Roorkee.

I have not submitted the matter embodied in this dissertation for the award of any other degree or diploma.

Dated: 11/06/10

Place: Roorkee

Pooja Mishra

CERTIFICATE

This is to certify that the above mentioned made by the candidate is correct to the best of my knowledge and beliefs.

Dated: 11/6/2010

Place: Roorkee

Dr. Dharmendra Singh
Associate Professor,
E&C Department
IIT Roorkee

ACKNOWLWDGEMENT

On the successful completion of this dissertation work I would like to take the opportunity to personally thank people behind the scene who help me in making it a possible task.

First of all I would like to express my deep and sincere gratitude to my supervisor, **Dr. Dharmendra Singh**, Associate Professor, Department of Electronic and Computer Engineering, Indian Institute of Technology Roorkee for his invaluable support throughout the dissertation work. His understanding, encouragement and personal guidance provided a good basis for the present dissertation work.

I wish to express my warm and sincere thanks to **Dr. S. N. Sinha**, Professor, **Dr. N. K. Agarwal**, Emeritus Fellow, **Dr. B. Sinha**, Emeritus Fellow, **Dr. M. V Kartikeyan,** Professor, **Dr. N. P. Pathak**, Assistant Professor and **Dr. A. Patnaik,** Assistant Professor, for their kind help, moral support and for all I have learned from them directly or indirectly in class room contact hours or at other times.

During this work I have collaborated with many colleagues, for whom I have great regard, and I wish to extend my warmest thanks to all who have helped me with my work in Remote Sensing Laboratory of Department of Electronic and Computer Engineering, Indian Institute of Technology Roorkee.

My special sincere heartfelt gratitude to my family, whose sincere prayer, best wishes and unflinching encouragement has been a constant source of strength to me during the entire work. Without their loving support and understanding it would have been impossible for me to finish this work.

(Pooja Mishra)

ABSTRACT

This work is intended to polarimetric analysis of PALSAR image in order to extract polarimetric SAR observables by means of SAR image processing techniques and classification algorithms. The polarimetric SAR observables possess useful intrinsic information, what makes SAR data (here PALSAR) useful for classification.

In the first part of the thesis, the basic concepts of radar polarimetry and state of the art of its application to remote sensing have been discussed with the aim to define established knowledge and possible future development of research.

The second section of the thesis consists of experimental part, which pursues two tasks. In order to accomplish first task, target decomposition theorems have been applied for extracting all relevant polarimetric parameters. The target decomposition theorems laid down the basis of classification, which is the second task of our experimental work. The purpose of this task is to evaluate possible differences between various SAR observables by performing classification. In this context various classification algorithms have been proposed namely, Parallelepiped, Minimum distance, Maximum likelihood and Decision tree classification. The effect of filtering and ensemble averaging on classification has also been evaluated. The SAR observables have been compared by accuracy estimate related to each classification algorithm. The accuracy estimate plays an important role in giving insight to usefulness of SAR observables by providing error in classification. The research work reaches its goal by comparing classification techniques by accuracy estimate as a key feature. The decision tree classifier is found to be best in terms of overall accuracy.

CONTENTS

CANDIDATE'S DECLARATION i

CERTIFICATE i

ACKNOWLWDGEMENT ii

ABSTRACT iii

Chapter 1. Introduction 1

1.1 Brief review 2

1.2 State of the art 3

1.3 Problem formulation 5

1.4 Motivation and scope 6

1.5 Aim and objective of the thesis 7

1.6 Organization of the thesis 8

Chapter 2. Radar Polarimetry background 9

2.1 Polarimetry basics 9

2.1.1 Polarization 10

2.1.2 Characterization of polarization state 11

2.1.3 Characterization of partially polarized wave 11

2.1.4 Mathematical representation of target scattering 12

2.2 Target decomposition theorem 15

2.2.1 Coherent target decomposition (CTD) 15

2.2.2 Incoherent target decomposition (ICTD) 17

2.3 Classification schemes 24

2.3.1 Supervised classification 25

2.3.2 Unsupervised classification 28

2.3.3 Non – parametric classifiers 30

2.4 Accuracy assessment 32
2.4.1 Kappa coefficient 32
2.4.2 Overall accuracy 33
2.4.3 Producer's accuracy 33
2.4.4 User's accuracy 33
Chapter 3. Methodology 34
3.1 Materials used 34
3.1.1 Study area 34
3.1.2 Data sets used 35
3.1.3 Software used 37
3.2 Pre-classification technique: a general overview 37
3.2.1 Data import 37
3.2.2 Polarimetric calibration 37
3.2.3 Speckle filtering 38
3.2.4 DEM extraction 39
3.2.5 Geocoding and radiometric calibration 39
3.3 Used target decomposition methods 40
3.3.1 Pauli decomposition 40
3.3.2 Eigen value decomposition 41
3.3.3 Three D decomposition 42
3.4 Classification techniques adopted 45
3.4.1 Decision tree classification 45
3.4.2 Classification based on 3 D decomposition 47
3.4.3 Classification based on Pauli decomposition 48
3.4.4 Classification based on Eigen value decomposition 49
3.4.5 Classification by combining intensities of various polarizations 49
Chapter 4. Results and discussion 50

4.1 Decomposition results 50

4.1.1 Results of three D decomposition 50

4.1.2 Results of Pauli decomposition 52

4.1.3 Results of eigen value decomposition 53

4.2 Effect of ensemble averaging on classification 54

4.3 Classification results 57

4.3.1 Results of decision tree classifier 57

4.3.2 Results of classification based on three D decomposition 58

4.3.3 Results of classification based on Pauli decomposition 60

4.3.4 Results of classification based on eigen value decomposition 63

Chapter 5. Comparison of results 80

Chapter 6. Conclusions 82

6.1 Concluding remarks 82

6.2 Future scope 83

References 84

Appendix 92

A. Classification results 92

B. MATLAB CODES 99

LIST OF FIGURES

Figure no.	Caption	Page no.
2.1	Polarization ellipse	9
2.2	Sketch of scattering mechanisms; (a) odd-bounce scattering,(b) even bounce scattering	16
2.3	Types of theoretical scatterers defined by Pauli;(a)sphere,(b)flat square plate,(c)dihedral corner reflector, trihedral with (d) quarter circular sides,(e) triangular sides ,(f) square sides.	17
2.4	Schematic representation of the range of α	20
2.5	Sketch of three scattering mechanisms used in the model	20
2.6	Sketch of four scattering mechanisms used in the model	23
2.7	Illustration of parallelepiped classification with parallelepipeds bound by maximum and minimum value of data elements	26
2.8	Parallelepiped classification for correlated data showing region of inseparability	27
2.9	An example of minimum distance classification	27
2.10	K – mean algorithm	29
2.11	Decision tree classification technique	31
3.1	Location of study area in map	34
3.2	Flow chart for pre-processing procedure	39
3.3	Flow chart of Pauli decomposition	40
3.4	Flow chart of eigen value decomposition	41
3.5	Flow chart of data pre-processing before 3-D decomposition (without polarimetric filtering)	43
3.6	Flow chart of data pre-processing before 3-D decomposition (with polarimetric filtering)	44
3.7	Algorithm for decision tree classification	47

4.1	Results of three D decomposition of image processed without polarimetric filtering: (a) decomposed image,(b) P_d,(c) P_v, (d) P_S	50
4.2	Results of three D decomposition of image processed with polarimetric filtering:(a)Decomposed image, (b) P_d, (c) P_S, (d) P_v	51
4.3	Results of Pauli decomposition: (a) Colour coded decomposed image, (b) Resized image of region Roorkee	52
4.4	Results of eigen value decomposition: (a) Entropy image, (b) Alpha image, (c) Anisotropy image, (d), (e) & (f) resized image of (region Roorkee) eigen value parameters entropy ,alpha and anisotropy respectively.	53
4.5	Accuracy estimate of classification tests based on three D decomposition by varying window sizes related to: (a) Parallelepiped, (b) Minimum distance, (c) Maximum likelihood classification	54
4.6	Kappa coefficient estimation of classification tests based on three D decomposition related to, (a) Parallelepiped, (b) Minimum distance, (c) Maximum Likelihood	56
4.7	Classification map based on decision tree classifier, (b) Resized image showing region Roorkee	57
4.8	Classification map based on 3 D decomposition (15x15 pixel averaging window:(a)Parallelepiped ,(b)Minimum distance, (c) Maximum likelihood	59
4.9	Accuracy estimate and (b) Kappa coefficient estimate of classifications based on three D decomposition (15x15 - pixel averaging window)	60
4.10	Classification map based on Pauli decomposition: (a) Parallelepiped, (b) Minimum distance, (c) Maximum likelihood, (d), (e) and (f) resized image of region Roorkee for (a) ,(b) and (c) respectively	61
4.11	Accuracy estimate ,(b) Kappa coefficient estimate of classifications based on Pauli decomposition	62
4.12	Classification map based on eigen value decomposition (by using parameters H/α):(a)Parallelepiped, (b) Minimum distance, (c) Maximum likelihood ,(d), (e) and (f) resized image of region Roorkee for (a) ,(b) and (c) respectively	63

4.13	Accuracy estimate and Kappa coefficient estimate of classifications based on eigen value decomposition by using parameters H/α.	64
4.14	Classification map based on eigen value decomposition (using parameters : H/A/α): (a) Parallelepiped, (b) Minimum distance, and (c) Maximum likelihood ; (d), (e) and (f) resized image of region Roorkee for (a) ,(b) and (c) respectively	65
4.15	Accuracy estimate and (b) Kappa coefficient estimate of classifications based on eigen value decomposition by using parameters H/A/α	66
4.16	Classification map based on fusion of intensity image of various polarizations by parallelepiped classification: (a) HH-HV, (b) HH-VV,(c) HV-VV, (d) HH-HV-VV, (e) LL-LR, (f) LL-RR, (g) LR-RR, (h) LL-LR-RR, (i) HH-HV-VV-LL, (j) HH-HV- VV-LL-LR, (k) HH-HV-VV-LL-LR-RR	68
4.17	Classification map of resized image based on fusion of intensity image of various polarizations by Parallelepiped classification: (a) HH-HV, (b) HH-VV,(c) HV-VV,(d) HH-HV-VV, (e) LL-LR, (f) LL-RR, (g) LR-RR, (h) LL-LR-RR, (i) HH-HV-VV -LL, (j) HH-HV-VV-LL-LR, (k) HH-HV-VV-LL-LR-RR	69
4.18	Accuracy estimate, (b) Kappa coefficient related to parallelepiped classification based on fusion of intensity images of various polarizations	70
4.19	Classification map based on fusion of intensity image of various polarizations by minimum distance classification: (a) HH-HV, (b) HH-VV,(c) HV-VV, (d) HH-HV-VV, (e) LL-LR, (f) LL-RR, (g) LR-RR, (h) LL-LR-RR, (i) HH-HV-VV-LL, (j) HH- HV-VV-LL-LR, (k) HH-HV-VV-LL-LR-RR	73
4.20	Classification map of resized image (Roorkee) based on fusion of intensity image of various polarizations by Minimum distance classification: (a) HH-HV, (b) HH-VV,(c) HV-VV, (d) HH-HV-VV, (e) LL-LR, (f) LL-RR, (g) LR-RR, (h) LL-LR-RR, (i) HH- HV-VV-LL, (j) HH-HV-VV-LL-LR, (k) HH-HV-VV-LL-LR-RR	74
4.21	Accuracy estimation, and (b) Kappa coefficient estimation related to minimum distance classification based on fusion of intensity images	75

4.22	Classification map based on fusion of intensity image of various polarizations by maximum likelihood classification: (a) HH-HV, (b) HH-VV,(c) HV-VV, (d) HH-HV-VV, (e) LL-LR, (f) LL-RR, (g) LR-RR, (h) LL-LR-RR, (i) HH-HV-VV-LL, (j) HH- HV-VV-LL-LR, (k) HH-HV-VV-LL-LR-RR	76
4.23	Classification map of resized image (Roorkee) based on fusion of intensity image of various polarizations by maximum likelihood classification: (a) HH-HV, (b) HH-VV,(c) HV-VV, (d) HH-HV-VV, (e) LL-LR, (f) LL-RR, (g) LR-RR, (h) LL-LR-RR, (i) HH- HV-VV-LL, (j) HH-HV-VV-LL-LR, (k) HH-HV-VV-LL-LR-RR	78
4.24	Accuracy estimation, and (b) Kappa coefficient estimation related to maximum likelihood classification based on fusion of intensity images	79

LIST OF TABLES

Table no.	Caption	Page no.
2.1	Polarisation descriptors for characteristic polarisation states	10
3.1	Polarization description of polarimetric data	35
3.2	File description of ALOS PALSAR L-1.1 data sets	36
3.3	Product description	30
3.4	Ground truth survey points for full scene of data sets	46
3.5	Ground truth survey points for region Roorkee only	48
4.1	Confusion matrix (pixel assignment) for accuracy assessment related to decision tree classifier	58
4.2	Confusion matrix of classification tests based on three D decomposition	59
4.3	Confusion matrix showing producer's accuracy for classifications based on Pauli decomposition	62
4.4	Confusion matrix showing producer's accuracy for classification tests based on H/α parameters	64
4.5	Confusion matrix showing producer's accuracy for classification tests based on H/A/α parameters	67
4.6	Confusion matrix showing producer's accuracy for parallelepiped classification based on fusion of intensity images	71
4.7	Confusion matrix showing producer's accuracy for minimum distance classification based on fusion of intensity images	72
4.8	Confusion matrix showing producer's accuracy for maximum likelihood classification based on fusion of intensity images	77
5.1	Classification performance estimate in terms of overall accuracy	80

CHAPTER 1. INTRODUCTION

1.1 Brief review

Quantitative assessment of land cover is required for every country in order to make proper planning against earth surface alteration, since land cover change is related to global change due to its interaction with climate, eco system process, bio-geochemical cycles, biodiversity and human activity. This information also assists in monitoring the dynamics of land use resulting out of changing demands of increasing population. Remote sensing plays an important role in classification.

Remote sensing is broadly defined as collecting and interpreting information about a target without being in physical contact with the object [1]. Based on the wavelength in which the system works, remote sensing is categorized into two different groups, i.e., optical and microwave. Optical remote sensing uses visible and infrared waves while microwave remote sensing uses radio waves.

As a microwave remote sensing RADAR (Radio Detection And Ranging) sends out electromagnetic pulses to detect targets which are ordinarily invisible to human eye due to darkness, fog, or far distance. The conventional radar systems were direct aperture radars. The information about the target was taken in the form of magnitude only and any information on phase was ignored because they used single fixed polarisation antenna for both transmission and reception. In those systems, for each resolution cell single backscattering coefficient was measured using a specific combination of transmit and receive polarization states in order to measure radar echo. Therefore target detection and identification was not possible because of the poor separability of different characteristic scatters at the ground [2]. The development of SAR sensors was a breakthrough in this field. SAR sensor being a polarization sensitive device considers full vector nature of electromagnetic wave.

A Synthetic Aperture Radar (SAR) system illuminates a scene with microwaves and records both the amplitude and the phase of the back-scattered radiation, making it a coherent imaging process. The received signal is sampled and converted into a digital image. The advent of SAR sensors lead to the concept of radar polarimetry. *Radar Polarimetry is the merging of the technological concept of radar (radio detection and ranging) and of the fundamental*

property of transverse nature of electromagnetic waves. It is the science of acquiring, processing and analyzing the polarization state of an EM field [3].

Fully polarimetric SAR acquires four channels to obtain the complete scattering matrix, wherein the signal is transmitted in two orthogonal polarizations and received at two orthogonal polarizations. With Polarimetric radars it has become possible to extract more information available than conventional radars due to the preservation of phase term. The incorporation of coherent polarimetric phase and amplitude into radar signal and image processing promises to bring about further improvements in monitoring capabilities in SAR image analysis. The phase information, along with the conventional magnitude data, can be used to study the scattering mechanisms and resolve the ambiguities about the source of scattering [3]. This unique characteristic of polarimetric imaging radar makes it a powerful tool for land cover classification. The possible reasons which make polarimetric SAR a useful tool to characterize various targets of ecosystem for classification are mentioned below:

- SAR being an active sensor is a day light acquisition system (unlike optical sensors).
- Most of the radar sensors exhibit all weather capability. It can be seen that atmospheric characteristics such as cloud, light rain, haze, and smoke has little effect on the capability of RADAR data acquisition system as attenuation of atmosphere is negligible for wavelengths $\lambda > 3$ cm [4].
- SAR is not only sensitive to the dielectric, physical and geometric properties of various land cover types, but is also sensitive to the relative proportion and distribution of various scatterers within an area-extended target.
- SAR not only provides ground surface information but can also be used for obtaining information beneath the ground (for certain moisture value and ground density) due to its capability to penetrate into soil and vegetation canopy.

Classification is an important step towards the retrieval of bio-geophysical parameters and a classification scheme directly based on polarimetric SAR data is useful to understand the characteristics of the Earth surface, particularly for the physical assessment of scatterers. Thus Polarimetric SAR images are widely used for terrain classification as they can extract geometrical properties (size, shape, orientation distribution and spatial arrangement of

objects) and physical information about the target like symmetry, non symmetry or irregularity of the target [5].

The present work is dedicated to the task of terrain classification of polarimetric **PALSAR (Phased Array L- band Synthetic Aperture Radar)** data by using various classification techniques. Classification of SAR images is required for various environmental and socioeconomic applications like agriculture monitoring, flood mapping, oil spill detection etc. Classification of image is done to identify different spectral classes present in it and their relation to some specific ground cover type. Classifying remotely sensed data into a thematic map is very challenging because it depends upon many factors, such as the complexity of the landscape in a study area, selected remotely sensed data. Also image processing and classification approaches, may affect the success of a classification.

1.2 State of the art

Polarimetry deals with the full vector nature of polarized (vector) electromagnetic waves throughout the frequency spectrum from Ultra-Low-Frequencies (ULF) to above the Far-Ultra-Violet (FUV). Where there are abrupt or gradual changes in the index of refraction (or permittivity, magnetic permeability, and conductivity), the polarization state of a narrow-band (single-frequency) wave is transformed, and the electromagnetic *"vector wave"* is re-polarized. When the wave passes through a medium of changing index of refraction, or when it strikes an object such as a radar target and/or a scattering surface and it is reflected; then, characteristic information about the reflectivity, shape and orientation of the reflecting body can be obtained by implementing *'polarization control"* [6,7]. The time-varying nature of the electric field vector generally forms an ellipse in a plane transverse to propagation. It plays an essential role in the interaction of electromagnetic "vector waves" with material bodies and the propagation medium. This polarization transformation behaviour, expressed in terms of the "polarization ellipse", is named "ellipsometry" in optical sensing and imaging, it is denoted "polarimetry" in radar and lidar–ladar sensing and imaging. The word "Polarimetry" has ancient Greek meaning of "measuring orientation and object shape" [8].

Ellipsometry started a new era in the 1940s with the significant advent of optical polarization phase control devices and the associated development of mathematical ellipsometry. Initial work on radar polarimetry is attributed to Sinclair [9], after whom the scattering matrix was named. The entries of this matrix represent backscattering for the four combinations of transmitted-received polarizations in an orthogonal basis and this matrix

depends upon the coordinate system, wavelength, target's shape, target's conductivity and target's aspect direction. The contribution of Deschamps [10] is also worth mentioning, who demonstrated geometrically the polarization property of electromagnetic wave.

Later an important pioneering work was done by Kennaugh [11], who demonstrated that there exist radar polarization states for which the radar receives minimum/maximum power. After four year of his research Graves introduced the concept of power scattering matrix for determining density of scattering field [12]. He also introduced the concept of directional Jones vector, which is widely used in polarimetry. The min/max polarization state theory of Kennaugh was extended primarily by Huynen, who introduced the "polarization fork" concept. It was the first generalization of the decomposition techniques which renewed the interest of the remote sensing community in radar polarimetry.

On the basis of work done by Sinclair and Kennaugh, Copeland [13] proposed a method of classification of radar targets by using polarization properties. After the important contribution of Huynen in radar polarimetry, Ioannidis [14] proposed a method to improve radar detection capability by discriminating radar target and clutter using polarization. An excellent contribution was made in the 1980s by Boerner and his co-workers in which, they showed the importance of polarization properties of scattering radiation with respect to inverse scattering and target identification [15, 16].

Since the 1980's, radar polarimetry, i.e., the utilization of complete electromagnetic vector wave information, has been gaining more and more recognition from many researchers. Since then radar polarimetry is used in conjunction with remote sensing and other fields and splendid results were achieved. Cloud and Pottier [17,18] gave important contribution in the field of target decomposition by introducing the concept of Anisotropy , alpha (α) and beta (β).Cloude and Pottier's parameters have become the standard tools for target characterization and have been used as the basis for the development of new classification methods introduced for the analysis of polarimetric data. Many approaches for unsupervised classification have been proposed notably by Pottier [19], Lee et al. [20, 21, 22], Ferro-Famil et al. [23, 24], Ouarzeddine et al. [25], Fang et al. [26], Park et al. [27], Praks et al. [28]. The comparison of classification performance by dual and fully polarized antenna was done by Lee et al. [29], in which they drew conclusion that fully polarimetric data performs better than dual polarized data.

Freeman [30] introduced the concept of three component scattering model, which have constantly been used as basis for classification. Based on the decomposition model proposed by

technique to classify PALSAR data through SAR observables obtained by target decomposition techniques. We also proposed decision tree classification based on the knowledge acquired by back-scattering coefficient. Decision rules are intended to be made on the basis of backscattering coefficient as information bearing feature. In order to compare the results of each classification technique extensively is required to be done.

Radar waves can interfere constructively or destructively to produce light and dark pixels known as speckle noise. Speckle noise is commonly observed in almost all SAR images. Speckle reduction affects the performance of classification. In this context effect of filtering on classification is proposed to be evaluated. Ensemble averaging also has a significant effect on classification performance. In this context, three D decomposition method is proposed to be used to see the effect of filtering and ensemble averaging.

1.4 Motivation and scope

Nearly every aspect of our lives is tied into the ground cover that surrounds us. Farms feed us, forests provide us with oxygen and building materials, rivers and lakes yield fresh water to drink, and cities shelter us. Each of these land covers has its own importance in the life of all living creature .When land covers change; our health, economy, and environment can all be affected. The detailed description of land cover change on earth can be obtained through appropriate terrain classification. Remote sensing plays an important role in terrain classification. Various classification algorithms have already been proposed, but further improvement is required. The limitation of these classification algorithms is that they necessitate prior information about study area. The aforementioned reasons were the driving force behind captivating the assignment of land cover classification. The motivation behind taking up the task of terrain classification through PALSAR data is to explore the maximum utilization of this polarimetric data in order to reduce the need of prior information.

The scope of this thesis is land cover classification using SAR image by rigorous polarimetric analysis. The scope lies in answering the questions:

i. **How accurately can land cover classification be performed using SAR imagery?**
ii. **Which classification algorithm can extract more physical information from SAR images?**
iii. **What are the challenges and limitations?**

The answer to these questions is worthwhile considering recent advancement in radar polarimetry and SAR technology, data analysis and processing techniques.

1.5 Aim and objective of the thesis

1.5.1 Aim

The aim of this dissertation work is to generate a land cover classification map by using various classification techniques and compare their results by using polarimetric PALSAR data. The present work is focused on the maximum utilization of polarimetric data in order to reduce the need of prior knowledge about the study area to be taken for classification. In this study we are planning to express polarimetric data in different ways in order to see substantial differences among a number of polarimetric observables in terms of the information they contain. The goal of this study is to suggest appropriate classification technique for land cover classification. The classification map so generated can be used in future to detect land cover change in particular build up land.

1.5.2 Objective

The objective of this thesis is to study polarimetric analysis of PALSAR images for land cover classification. The objectives of thesis are as follows:

- Study various polarimetric methods for terrain classification.
- Study the role of window size on classification.
- Study the effect of filtering on SAR images for flat terrain like-Roorkee.
- Apply various supervised classification techniques (Parallelepiped, Minimum distance, and Maximum likelihood) on PALSAR data in order to identify and map various land cover types.
- Quantify the relationship between backscatter and various land cover types and obtain land cover map using backscatter as information bearing feature.
- Perform accuracy assessments on the different classifications to determine the best approach and to quantify the expected level of accuracy.
- Critical comparison of all applied classification techniques.

Thus the overall objective is to distinguish the effect of each classifier on classification of a mixture of land cover types and put forward the appropriate method that classifies all the land cover types having satisfactory classification accuracy.

1.6 Organization of the thesis

The thesis consists of six chapters. In *chapter 2* basics of radar polarimetry i.e. basic wave and scattering concepts are discussed. This chapter includes mathematical formulation of basic scattering matrices, theoretical concept target decomposition theorems and classification techniques.

In *chapter 3,* the description of test site, along with the description of used SAR data and software is presented. This chapter also includes the methodology used for SAR data pre-processing, target decomposition theorems and land cover classification.

In *chapter 4* the results of all the methods discussed in chapter 2 are shown. The results of all the classification techniques are shown by confusion matrix. Effect of averaging window on decomposition is also presented in this chapter using 3 D decomposition.

In chapter 5 advantages and disadvantages of each classification techniques and their limitation is discussed.

Chapter 6 summarizes the obtained results by concluding remarks.

CHAPTER 2. RADAR POLARIMETRY BACKGROUND

In this chapter basic polarimetry concepts are discussed in brief. There are two main conceptual formalisms in polarimetry. The first one is a real space formalisms based on the Stokes Vector for the description of the polarimetric properties of waves and on the Mueller matrix, (in backscattering also known as Kennaugh matrix) for the polarimetric description of the scatterer. The second one is a complex space formalism based on the Jones vector for the analysis of wave polarization and on the covariance or coherency matrix for the description of the scattering process. Both formalisms are equivalent and can be changed unambiguously into another one. Since the processing of SAR data is done in complex domain therefore in this study complex domain formalism is chosen. Starting with polarization, which is the basis of radar polarimetry, mathematical formulation of all the matrices describing various scattering phenomenon are discussed in brief. Target decomposition theorems and various classification approaches used in dissertation are discussed in detail.

2.1 Polarimetry basics

2.1.1 Polarization

Concerning an EM monochromatic plane wave, the polarization describes the orientation of the electric field vector, in the plane perpendicular to the direction of propagation, as a function of time. At a fixed time the electric field is composed of two orthogonal sinusoidal waves with, in general, different amplitudes and phases at the origin. A plane electromagnetic wave is fully characterized by the parameters (magnitude, phase, and direction) of its electric vector *E(r, t)* given by

$$E(r,t) = E_x\hat{x} + E_y\hat{y} = (a_x.\exp(j\delta_x)\hat{x} + a_y.\exp(j\delta_y)\hat{y}).\exp(j(\omega t - kz) \qquad \textbf{(2.1)}$$

The tip of electric field vector forms an ellipse called polarization ellipse shown in figure-2.1. The polarization state also called Jones vector, is related to the shape and orientation of the ellipse together with the rotation sense of the field vector when looking along the direction of propagation [46].

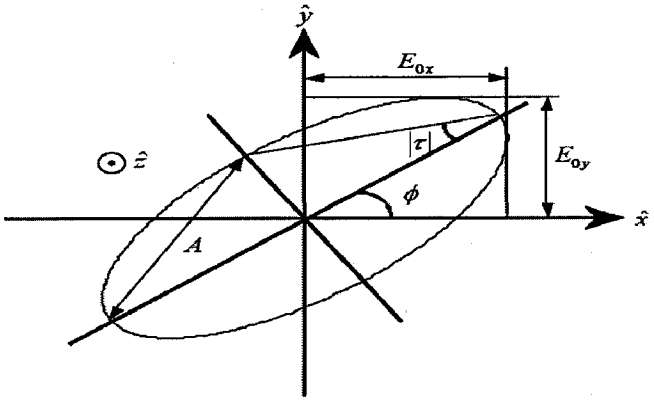

Figure - 2.1: Polarization ellipse[45]

There are two parameters which define the polarization state. They are described as follows:

- The orientation angle Φ defined as the angle between the major axis of the ellipse and the x- axis, expresses the inclination of the ellipse and is limited between 0° and 180°.
- The tilt angle τ , defined as the ratio between two minor semi-axes of the ellipse (a, and *b* axis), describes the shape of the ellipse.

$$\tan\tau = \pm\frac{b}{a} \qquad (2.2)$$

- The polarisation sense; given by the sign of τ (the positive value applies for right-handed polarizations)

There are three types of polarizations : linear , circular and elliptical depending on the values of above parameters. They are summerized in following table:

Table -2.1

Polarization descriptors for characteristic polarization states

	Horizontal	Vertical	Linear 45°	Linear 135°	Left circular	Right circular
Orientation Φ	90	0	45	135	0 to 180	0 to 180
Tilt angle τ	0	0	0	0	45	-45
Complex ratio ρ	0	∞	1	-1	i	-i

2.1.2 Characterization of polarization state

2.1.2.1 Jones vector

Jones vector E_{xy} may be defined as

$$E_{xy} = \begin{bmatrix} E_x \\ E_y \end{bmatrix} = \begin{bmatrix} |E_x| \exp(j\delta_x) \\ |E_y| \exp(j\delta_y) \end{bmatrix} = E_x \begin{bmatrix} 1 \\ \rho \end{bmatrix} \tag{2.3}$$

where ρ is called polarization ratio, defined by [47]

$$\rho = \frac{E_y}{E_x} = \frac{|E_y|}{|E_x|} \exp(j\{\delta_n - \delta_m\}) \tag{2.4}$$

2.1.2.2 Stokes vector

For a quasi monochromatic wave the Stokes vector formulation is used, which is defined by

$$g = \begin{bmatrix} g_0 \\ g_1 \\ g_2 \\ g_3 \end{bmatrix} = \begin{bmatrix} e^2 \\ e^2 \sin 2\phi \cos 2\tau \\ e^2 \cos 2\phi \sin 2\tau \\ e^2 \sin 2\tau \end{bmatrix} \tag{2.5}$$

g_0 is the total intensity, g_1 is the difference of the intensities in both polarizations, while g_2 and g_3 contain the phase information [6]. These four parameters are not independent for a fully polarized wave, since in that case the following identity holds:

$$g_0^{\,2} = g_1^{\,2} + g_2^{\,2} + g_3^{\,2} \tag{2.6}$$

2.1.3 Characterization of partially polarized wave

2.1.3.1 Coherency matrix

To advance the analysis of partially polarized waves, the concept of a wave coherency matrix was introduced by BORN & WOLF 1985. This matrix is defined, using the outer product of the corresponding Jones vector averaged over a coherency time [46].

$$[J] = \left\langle E(E^*)^T \right\rangle = \begin{bmatrix} \left\langle E_H E_H^{\,*} \right\rangle & \left\langle E_H E_V^{\,*} \right\rangle \\ \left\langle E_V E_H^{\,*} \right\rangle & \left\langle E_V E_V^{\,*} \right\rangle \end{bmatrix} = \begin{bmatrix} J_{HH} & J_{HV} \\ J_{VH} & J_{VV} \end{bmatrix} \tag{2.7}$$

2.1.3.2 Stokes vector

A partially polarized wave can also be characterized by the four time-averaged Stokes parameters of Equation (2.8), since they are simply related to the elements of the coherency matrix by

$$g = \begin{bmatrix} J_{HH} + J_{VV} \\ J_{HH} - J_{VV} \\ J_{HV} + J_{VH} \\ i(J_{HV} - J_{VH}) \end{bmatrix} \tag{2.8}$$

The partially polarized wave is expressed in terms of the 'degree of coherency and the 'degree of polarization' D_P [6].Degree of polarization is defined as the ratio of the completely polarized power to the total power and can be written as

$$D_P = \sqrt{1 - \frac{4(\det(J))}{(tarce(J))^2}} = \frac{\sqrt{g_1^{\,2} + g_2^{\,2} + g_3^{\,2}}}{g_0} \tag{2.9}$$

And the degree of coherency can be written as

$$\mu_{mn} = |\mu_{mn}| \exp(j\beta_{mn}) = \frac{J_{mn}}{\sqrt{J_{mn} J_{nm}}} \tag{2.10}$$

where, D_P=0: for totally depolarized and D_P=1: for fully polarized waves, respectively.

2.1.4 Mathematical representation of target scattering

2.1.4.1 Sinclair matrix

If the target is deterministic and time-invariant, then this target can be characterised by a 2 x 2 coherent scattering matrix *[S]*, also known as the Sinclair matrix for the back scatter case and Jones matrix for the forward scatter case. The normalized scattering matrix *[S(HV)]* is the orthogonal linear polarization basis (HV) is given by,

$$E^S(HV) = [S(HV]E^T(HV) \tag{2.11}$$

where $E^S(HV)$ and $E^T(HV)$ denote incident and scattered fields, respectively, and

$$[S(HV)] = \begin{bmatrix} S_{HH} & S_{HV} \\ S_{VH} & S_{VV} \end{bmatrix} \tag{2.12}$$

For monostatic case $S_{HV} = S_{HV}$.

2.1.4.2 Kennaugh matrix

In radar application BSA convention is used and the Stokes vector of the backscattered wave is related to the incident-wave Stokes vector through the Kennaugh matrix by [47] [48]

$$g^T = [K] g^S \tag{2.13}$$

The 4x4 Kennaugh matrix is defined in terms of Sinclair matrix as follows

$$[K] = 2[A]^*.[W].[A]^{-1} \tag{2.14}$$

where $[W] = [S] \otimes [S]^*$ is a standard tensorial Kronecker Matrix product.

and

$$[A] = \begin{bmatrix} 1 & 0 & 0 & 1 \\ 1 & 0 & 0 & -1 \\ 0 & 1 & 1 & 0 \\ 0 & j & -j & 0 \end{bmatrix} \tag{2.15}$$

2.1.4.3 Muller matrix

In optical or transmission polarimetry, the FSA convention is used and the Stokes vector of the scattered wave is related to the incident-wave Stokes vector through the Mueller matrix [M] by [48]

$$g^T = [M] g^S \tag{2.16}$$

Muller matrix is related to Kennaugh matrix by

$$[M] = diag[1 \quad 1 \quad 1 \quad -1].[K] \tag{2.17}$$

2.1.4.4 Coherency and covariance matrices

The 4X4 polarimetric covariance matrix [C] is ensemble average of outer product of the 4 dimensional lexicographic scattering vectors with its conjugate transpose [49].

$$[C] = \langle \bar{S}.\bar{S}^* \rangle \tag{2.18}$$

where $\bar{S}$ is called lexicographic scattering vector defined by

$$\bar{S} = [S_{HH}, S_{HV}, S_{VH}, S_{VV}]^T \tag{2.19}$$

and covariance matrix

$$[C] = \begin{bmatrix} \langle |S_{HH}|^2 \rangle & \langle S_{HH}S_{HV}^* \rangle & \langle S_{HH}S_{VH}^* \rangle & \langle S_{HH}S_{VV}^* \rangle \\ \langle S_{HV}S_{HH}^* \rangle & \langle |S_{HV}|^2 \rangle & \langle S_{HV}S_{VH}^* \rangle & \langle S_{HV}S_{VV}^* \rangle \\ \langle S_{VH}S_{HH}^* \rangle & \langle S_{VH}S_{HV}^* \rangle & \langle |S_{VH}|^2 \rangle & \langle S_{VH}S_{VV}^* \rangle \\ \langle S_{VV}S_{HH}^* \rangle & \langle S_{VV}S_{VH}^* \rangle & \langle S_{VV}S_{VH}^* \rangle & \langle |S_{VV}|^2 \rangle \end{bmatrix} \tag{2.20}$$

where <...> indicates spatial averaging, assuming homogeneity of the random scattering medium.

The 4X4 polarimetric coherency matrix [T] is ensemble average of outer product of the 4 dimensional Pauli scattering vectors with its conjugate transpose.

$$[C] = \langle \bar{k}.\bar{k}^* \rangle = \begin{bmatrix} \langle |k_0|^2 \rangle & \langle k_0k_1^* \rangle & \langle k_0k_2^* \rangle & \langle k_0k_3^* \rangle \\ \langle k_1k_0^* \rangle & \langle |k_1|^2 \rangle & \langle k_1k_2^* \rangle & \langle k_1k_3^* \rangle \\ \langle k_2k_0^* \rangle & \langle k_2k_1^* \rangle & \langle |k_2|^2 \rangle & \langle k_2k_3^* \rangle \\ \langle k_3k_0^* \rangle & \langle k_3k_1^* \rangle & \langle k_3k_2^* \rangle & \langle |k_3|^2 \rangle \end{bmatrix} \tag{2.21}$$

where $\bar{k}$ is Pauli scattering vector , defined by

$$\bar{k} = [S_{HH} + S_{VV}, S_{HH} - S_{VV}, S_{HV} + S_{VH}, j(S_{HV} - S_{VH})]^T \tag{2.22}$$

Both the above matrices are hermitian positive semi definite and have the same eigen values. *The coherency matrix is closely related to the physical and geometric properties of the scattering process, and thus allows better and direct physical interpretation. The covariance matrix is directly related to the system measurable.*

Due to ensemble averaging needed for the formation of coherency and covariance matrices resolution is reduced. Low resolution is not a problem with distributed scatterers

because this loss is compensated by reduced speckle noise due to multilooking, but for point scatterers loss of resolution is very critical. This trade-off between high resolution required for point scatterers and reduced speckle noise over distributed scatterers can be resolved by applying an adaptive polarimetric speckle filter instead of other filters [43] for the formation of the coherency (or covariance) matrix, which was first introduced by J.-S. Lee [38]. MAP filter can also perform well in this situation [42]. Such filters perform a multilooking filtering process on distributed scatterers, leading to a matrix with rank greater than one, while point scatterers or edges remain unfiltered leading thus, as expected, to a rank one matrix.

2.2 Target decomposition theorem

The decomposition in radar polarimetry provides a way for interpretation and optimum utilization of polarimetric scattering data by expressing the average mechanisms as the sum of independent elements. This leads to association of physical mechanism with each independent component having physical constraints such as the average target being invariant to changes in wave polarization basis. [16]. Thus, any decomposition technique manipulates the scattering matrix elements with the objective to provide more descriptive and discriminative target parameters, which have influential significance in various applications of radar polarimetry [17].

Target Decomposition theorems were first formalized by J.R. Huynen but have their origin in the research work of Chandrasekhar on light scattering by small anisotropic particles [16]. Since this original work, there have been several other proposed decompositions. At present, two theories of target decomposition can be distinguished: coherent target decomposition (CTD) and incoherent target decomposition (ICTD).

2.2.1 Coherent target decomposition (CTD)

CTD deals with decomposition of scattering matrix, which characterizes the scattering process from the target itself. This can happen only when incident and scattering waves are fully polarized. Consequently, CTD can only be employed to study coherent targets or point targets.

2.2.1.1 Pauli decomposition

The most common known and applied coherent decomposition is Pauli decomposition. The Pauli decomposition expresses the measured scattering matrix [S] in the so-called Pauli basis

[20]. The vectorization of [S] carried out by using the Pauli matrices basis set, leads to the Pauli scattering vector or Pauli feature vector f

or the bi-static case with the explicit form

$$\vec{k}_{4P} = [k_0, k_1, k_3, k_4]_P^T = [S_{HH} + S_{VV}, S_{HH} - S_{VV}, S_{HV} + S_{VH}, j(S_{HV} - S_{HV})]^T \quad \textbf{(2.23)}$$

In backscattering scenario, the target scattering matrix is symmetric if the medium between radar and target does not exhibit Faraday rotation. In this case the above scattering vector is reduced to three-component scattering vector due to presence of redundancy in one of the elements of the target vector. Consequently the Pauli scattering vector is given by

$$\vec{k}_{3P} = [S_{HH} + S_{VV}, S_{HH} - S_{VV}, 2S_{HV}]^T \quad \textbf{(2.24)}$$

The advantage of using the Pauli matrix basis lies in the straightforward physical interpretation of the Pauli matrices in terms of elementary scattering mechanisms as well as relative polarization plane preservation.

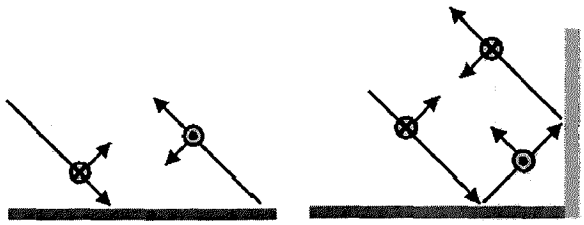

(a) (b)

Figure-2.2: Sketch of scattering mechanisms; (a) odd-bounce scattering, (b) even bounce scattering [53]

- The first Pauli matrix can be interpreted as the scattering matrix of an isotropic **"odd"**-bounce scatter. Such scatterers are characterized by $S_{HH} = S_{VV}$ and $S_{HV} = S_{VH} = 0$. **Spheres, flat surfaces or trihedral corner reflectors** represent this type of scattering.
- The second Pauli matrix is also diagonal but generates a π phase difference between the diagonal elements. It indicates isotropic **"even"**-bounce scattering which is characterized by $S_{HH} = -S_{VV}$ and $S_{HV} = S_{VH} = 0$.**Dihedral corner reflectors oriented at 0** □ represent this type of scattering behavior , in which reflected wave is mirrored version of incident wave.

- The third Pauli matrix can be interpreted as the scattering matrix of an isotropic **"even"**-bounce scattering objects with a **relative orientation of $\pi/4$** with respect to the horizontal, because it may be obtained from the second Pauli matrix by rotation of the reference basis by π /4. From a qualitative point of view, the scattering mechanism represented by is represented by those scattering objects that are able to return the orthogonal polarization, from which, one of the best examples is the **volume scattering produced by the forest canopy.**

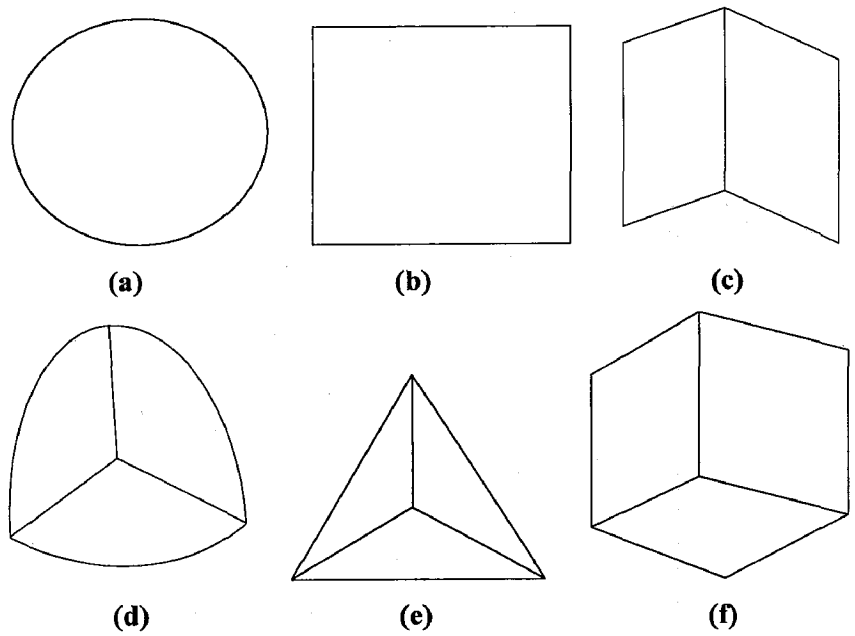

Figure 2.3: Types of theoretical scatterers defined by Pauli;(a)sphere,(b)flat square plate,(c)dihedral corner reflector, trihedral with (d) quarter circular sides,(e) triangular sides ,(f) square sides.

2.2.2 Incoherent target decomposition (ICTD)

The CTD approach shows inability in decomposing distributed targets. This type of scatterers can only be characterized, statistically, due to the presence of speckle noise. To reduce speckle noise only second order polarimetric representations are required to analyze distributed scatterers. These second order descriptors are the 3×3, Hermitian average covariance and the coherency matrices. ICTD deals with decomposition of these matrices. These matrices characterize the scattering process from distributed targets. Consequently, ICTD also deals with partial polarized case.

2.2.2.1 Eigen value decomposition

The eigenvector decomposition states that the target coherency written in the form:

$$<[T]>=[U_3][\Sigma][U_3]^{-1} \tag{2.25}$$

The 3x3 real diagonal matrix $[\Sigma]$contains the eigen values of < [T] > is a 3x3 diagonal matrix with non-negative real elements, $\lambda_1 \geq \lambda_2 \geq \lambda_3 \geq 0$.

$$[\Sigma]=\begin{bmatrix} \lambda_1 & 0 & 0 \\ 0 & \lambda_2 & 0 \\ 0 & 0 & \lambda_3 \end{bmatrix} \tag{2.26}$$

The 3x3 unitary matrix$[U_3]$, contains the eigenvector $\bar{u}_i$ for i= 1, 2, 3 of < [T] >

$$[U_3]=[\bar{u}_1,\bar{u}_2,\bar{u}_3] \tag{2.27}$$

Where

$$\bar{u}_i=[u_{i1} \quad u_{i2} \quad u_{i3}]=[\cos\alpha_i \quad \sin\alpha_i\cos\beta_i e^{j\delta_i} \quad \sin\alpha_i\cos\beta_i e^{j\gamma_i}]^T \tag{2.28}$$

The eigenvector approach leads to diagonalization of coherency matrix $[T]$ of a distributed scatterer by decomposing it into the non-coherent sum of three independent coherency matrices [52]. Equivalently, we can express coherency matrix as linear combination of outer products of eigenvectors.

$$[T]=\sum \lambda_i u_i u_i^{*T}=[T_1]+[T_2]+[T_3] \tag{2.29}$$

This decomposition has the intrinsic characteristics of every eigen value decomposition, namely:

i. The decomposition is basis invariant, i.e. the same result can be obtained for any basis that can be employed in polarization definition.
ii. The three scattering mechanisms are statistically independent.
iii. The eigenvalues are the weights of decomposition, so they indicate which scattering mechanism is dominant one, and quantify in what proportion they dominate.

The eigenvalues and the eigenvectors are considered as the primary parameters of the eigen decomposition of < [T] >. In order to simplify the analysis of the physical information

provided by this eigen decomposition, three secondary parameters are defined as a function of the eigenvalues and the eigenvectors of < [T] >.

2.2.2.1.1 Parameters derived from eigen values

a) Entropy

It is the measure of randomness of scattering, which can also be interpreted as degree of statistical disorder and can be defined by

$$H = -\sum_{i=1}^{3} p_i \log_n p_i \quad , \qquad p_i = \frac{\lambda_i}{\sum_{i=1}^{3} \lambda_i} \tag{2.30}$$

where n=3 , for backscatter and n=4 , for bi-static problems. p_i is the probability of each eigenvalue λ_i (in the Von Neumann sense). It represents the relative importance of this eigenvalue with respect to the total scattered power. It expresses the number of effective scattering processes occurring [17].

- ***H = 0**, indicates a rank 1 [T] matrix with only one nonzero eigenvalue, i.e.* $\lambda_2 = \lambda_3 = 0$. *This corresponds to pure target and implies a non-depolarizing scattering process described by a single scattering matrix.*
- ***H = 1**, indicates the presence of three equal nonzero eigenvalues, i.e.* $\lambda_1 = \lambda_2 = \lambda_3$. *It characterizes a random noise scattering process, which depolarizes completely the incident wave regardless of its polarization.*

However, most distributed natural scatterers (partial targets) lie in between these two extreme cases, having intermediate entropy values with non-zero and non-equal eigenvalues [18].

b) Anisotropy

It can be defined as the normalized difference between the appearance probabilities of the second and the third scattering component

$$A = \frac{\lambda_2 - \lambda_3}{\lambda_2 + \lambda_3} \tag{2.31}$$

From a practical point of view, the anisotropy can be employed as a source of discrimination only when H>0.7. The reason is that for lower entropies, the second and third eigenvalues are highly affected by noise. Consequently, the anisotropy is also very noisy [52].

- *A = 0, implies azimuthal symmetry and represents the appearance of two equally strong scattering mechanisms.*
- *A =1, implies asymmetric depolarization situation and represents the presence of only one strong secondary scattering process.*

2.2.2.1.2 Parameters derived from eigen vectors

They are four angles used to define eigenvector. Among them δ and γ are the phase terms without any straightforward interpretation. Only α and β give useful interpretation of scattering mechanisms present in the target. All possible target vectors can be mapped into (α, β) pairs by using the following effective range of validity of angles [53]:

$$0° \le \alpha \le 90° \qquad 0° \le \beta \le 360° \tag{2.32}$$

The parameter α is an indicator of type of scattering and is called scattering mechanism. In the general case it is often better to form a weighted average of the α parameters from the eigenvectors to obtain an average scattering mechanism Such an average has been used for the interpretation of scattering by random particle volumes [54].

$$\overline{\alpha} = \sum_{i=1}^{3} \alpha_i p_i, \text{ where } \alpha_i = \arccos(|u_{ii}|) \tag{2.33}$$

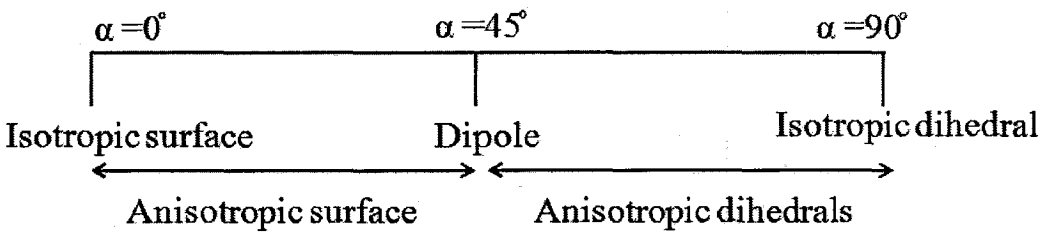

Figure – 2.4: Schematic representation of the range of α

Mean roll angle α possesses useful polarimetric scattering characteristics especially applicable to rough surface scattering [52]:

- *$\alpha=0$: The scattering corresponds to single-bounce scattering produced by a rough surface (isotropic surface scattering).*
- *$\alpha=\pi/4$: The scattering mechanism corresponds to volume scattering (dipole like scattering).*
- *$\alpha=\pi/2$: The scattering mechanism is due to double-bounce scattering (dihedral / helix type scattering).*

The parameter β is just the physical orientation of the object about the line of sight [22].

$$\overline{\beta} = \beta_i \text{ , where } \beta_i = \arctan\left(\frac{|u_{i3}|}{|u_{i2}|}\right) \quad \textbf{(2.34)}$$

The eigen decomposition of the coherency matrix is also referred as the H/A/$\underline{\alpha}$ decomposition.

2.2.2.2 Model based decomposition

2.2.2.2.1 Three component scattering model

FREEMAN developed from 1992 to 1998 a three-component scattering model suited for classification and inversion of air- and space-borne polarimetric SAR image data. The Freeman decomposition models the covariance matrix as the contribution of three scattering mechanisms [30]:

- **Volume scattering:** Modelled by a set of randomly oriented dipoles.
- **Double-bounce scattering:** Modelled by scattering from a dihedral corner reflector.
- **Single-bounce scattering**: Modelled by a first-order Bragg surface scatterer.

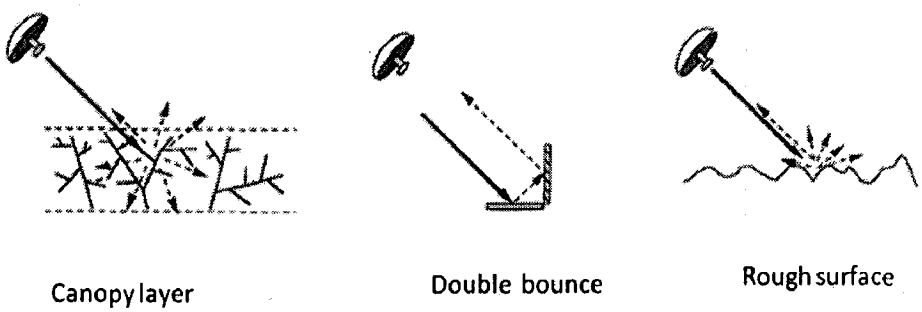

Figure- 2.5: Sketch of three scattering mechanisms used in the model [30]

Assuming the three processes to be independent from one another, each contributes to the total observed coherency matrix [T] as

$$[T]=[T_S]+[T_D]+[T_V] \tag{2.35}$$

where, $[T_S],[T_D]$ and $[T_V]$ are the coherency matrices for the surface, dihedral and volume scattering respectively.

a) Surface Scattering Contribution

$$[T_S]=f_S\begin{bmatrix}\beta^2 & \beta & 0\\ \beta & 1 & 0\\ 0 & 0 & 0\end{bmatrix} \tag{2.36}$$

b) Dihedral Scattering Contribution

In this case, the scattering is completely described by the Fresnel reflection coefficients of each reflection plane.

For example, the scattering matrix of a soil-trunk dihedral interaction is obtained as

$$[T_D]=f_D\begin{bmatrix}\alpha^2 & -\alpha & 0\\ -\alpha & 1 & 0\\ 0 & 0 & 0\end{bmatrix} \tag{2.37}$$

c) Volume scattering

For volume scattering, it is assumed that the radar return is from a cloud of randomly oriented, very thin, cylinder-like scatterers.

$$[T_V]=f_V\begin{bmatrix}1 & 0 & 0\\ 0 & \delta & 0\\ 0 & 0 & \delta\end{bmatrix} \tag{2.38}$$

where, f_V is the backscattering amplitude and δ depends upon the shape and the dielectric constant of the scatter. It value between 0 and 0.5, where the value 0 correspondences to spheres and 0.5 to dipoles.

The Freeman decomposition presents 5 independent parameters $\{f_v, f_d, f_s, \alpha, \beta\}$ and only 4 equations. Consequently, some hypothesis must be considered in order to find the values of $\{f_v, f_d, f_s, \alpha, \beta\}$.

- If $f_S\beta > f_D\alpha \rightarrow \beta = 1$: Dominant Surface Scattering

- If $f_S\beta < f_D\alpha \rightarrow \alpha = -1$: Dominant Dihedral Scattering

The scattering powers corresponding to surface, double and volume scattering component is given by

$$P_S = f_S(1+|\beta|^2) \quad \textbf{(2.39)}$$

$$P_D = f_D(1+|\alpha|^2) \quad \textbf{(2.40)}$$

$$P_V = 8 * f_V / 3 \quad \textbf{(2.41)}$$

Merits:

- Simplicity
- Easy to implement
- Suitable for decomposing natural targets

Demerits:

- Unable to decompose man-made targets (e.g. urban area)

2.2.2.2.2 Four component scattering model

The four component scattering model is proposed by Yamaguchi, which decomposes covariance matrix [31] or coherency matrix [32] into four scattering components namely surface, double, volume and helix scattering components.

$$[C] = [C_S] + [C_D] + [C_V] + [C_C] \quad \textbf{(2.42)}$$

where, $[C_S], [C_D], [C_V]$ and $[C_C]$ are the covariance matrices for the surface, dihedral, volume and helix scattering respectively(see figure-2.6).

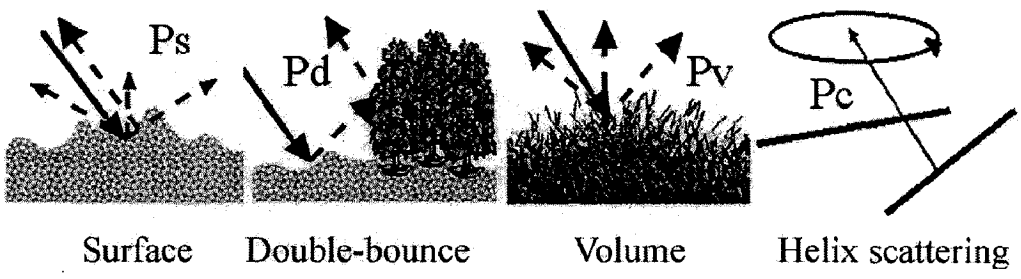

Figure -2.6: Sketch of four scattering mechanisms used in the model [31]

Unlike three component scattering model, this model deals with non-symmetric cases $< S_{HH} S_{HV}^{*} > \neq 0$ and $< S_{HH} S_{HV}^{*} > \neq 0$. This condition introduces fourth term, called Helix scattering component, which is essentially caused by the scattering matrix of helices (or equivalently, left or right circular polarization states). It is relevant for the complicated shapes of man-made structures, which are predominant in urban areas [31]. Single bounce and double bounce have same interpretation as in three component scattering model. The volume scattering components is modified by change of probability density function for associated characteristic angle distribution, which is responsible for scattering from vegetated areas, especially by trunk and tree branches. The choice between symmetric and asymmetric cases is made by $10\log_{10} \langle |S_{HH}|^2 \rangle / \langle |S_{VV}|^2 \rangle$. The power scattering matrices for single, double, volume and helix scattering component is given by

$$P_S = f_S(1 + |\beta|^2) \tag{2.43}$$

$$P_D = f_D(1 + |\alpha|^2) \tag{2.44}$$

$$P_V = f_V \tag{2.45}$$

$$P_C = f_C \tag{2.46}$$

2.2.2.2.3 Modified four component scattering model

Yamaguchi introduced the modified four component scattering model in 2008. This model removes negative powers produced in image analysis of previous models [31] [32]. This negative power is inconsistent with physical conditions. Therefore, previous decomposition model was modified to produce all positive powers [33].

2.3 Classification schemes

Quantitative assessment of land cover is required for every country in order to make proper planning against earth surface alteration, since land cover change is related to global change due to its interaction with climate, eco system process, bio-geochemical cycles, biodiversity and human activity. Classification of SAR images is important for environmental and socioeconomic applications like agriculture monitoring, flood mapping, oil spill detection etc. Remote sensing plays an important role in land cover classification due to availability of various SAR images through ENVISAT, ALOS PALSAR, and RADARSAT etc.

Classification is the task in which set of given data elements (pixels) are assigned to some classes such that cost of assigning data elements is minimum [55]. The intent of the classification process is to categorize all pixels in image into one of several land cover classes, or *"themes"*. This categorized data may then be used to produce thematic maps of the land cover present in an image. Land cover classification through remotely sensed data is very challenging because more or less classification is related to various factors like selected remotely sensed data, image processing , classification approaches etc. The major steps of classification are as follows [56]:

i. Determination of suitable classification system.
ii. Image pre-processing and feature extraction.
iii. Selection of training samples.
iv. Selection of suitable classification approach.
v. Post classification and accuracy assessment.

There are two main types of classification techniques: supervised and unsupervised. Supervised methods require the user to collect samples to "train" or teach the classifier to determine the decision boundaries in feature space, and such decision boundaries are significantly affected by the properties and the size of the samples used to train the classifier. On the other hand, unsupervised classifiers "learn" the characteristics of each class (and possibly even the number of classes directly from the input data.

2.3.1 Supervised classification

Supervised classification involves using a priori knowledge of data to "train" computer software to identify categories in an image [57]. The supervised approach to pixel labeling requires the user to select representative training data for each of a predefined number of classes [58]. It is assumed that the classification (the definition of the groups and their characteristics) has been defined before any previously unknown objects were identified. The supervised classification is carried out in following steps:

i. Decide the set of ground cover types into which image is to be segmented. These are called information class. The information classes are determined by ground truth survey, maps or personal experience,
ii. Chose representative pixels on image from each of the desired set of classes. These pixels are called training samples.

iii. Estimate the statistical parameters for each required class using training samples.

iv. Select proper decision rule for classification.

v. Select the classifier, which classify every pixel in the image into one of the desired ground cover types (information class).

The main supervised classification techniques are defined below:

2.3.1.1 Parallelepiped classification

It uses simple decision rule for classifying remotely sensed data. It characterizes each class by range of expected values on each band. The range is defined by maximum and minimum pixel value in given class or alternatively by a certain number of standard deviations on either side of mean of training data for a given class as illustrated in figure-2.6. These decision boundaries form n- dimensional parallelepiped. If a pixel value lies above the low threshold and below the high threshold for all n- bands being classified, it is assigned to that class. If the pixel value falls in multiple classes, pixel is assigned to the last class matched or to overlap class. If the pixel does not fall within any of the parallelepiped classes it is designated as unclassified or null class [56] [58].

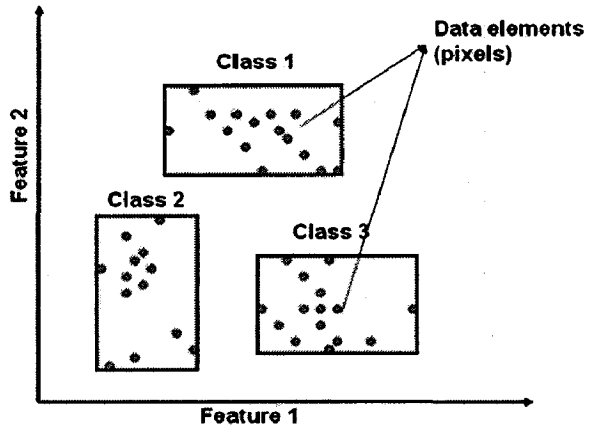

Figure-2.6: Illustration of parallelepiped classification with parallelepipeds bound maximum and minimum value of data elements.

Merits:

a. Technique is very simple.

b. Easy to implement.

Demerits:

a. Performance is very poor.

b. For correlated data there can be overlap of the parallelepipeds since their sides are parallel to the spectral axes. Consequently there is some data that cannot be separated (ref. figure-2.7) [58].

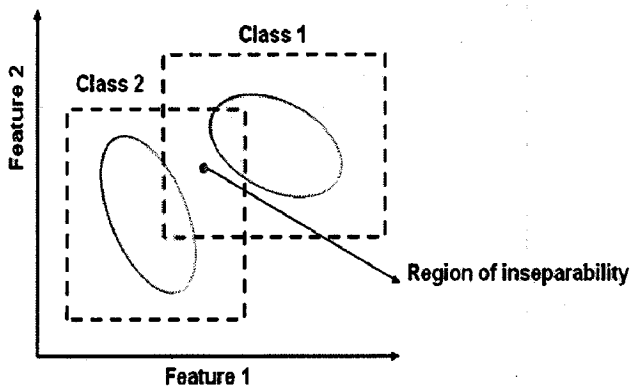

Figure-2.7: Parallelepiped classification for correlated data showing region of inseparability.

2.3.1.2 Minimum distance classification

With this classifier, mean vector of each class is calculated from training data. The decision rule adopted by the Minimum distance classifier to determine a pixel's label is the minimum distance between the pixel and the class centres (mean), measured either by the Euclidean distance or the Mahalanobis generalized distance. Classification is then performed by placing a pixel in the class of the nearest mean [58]. This is illustrated in figure-2.8 in which data pixel 'a' is closest to class 3, hence classified as class 3.

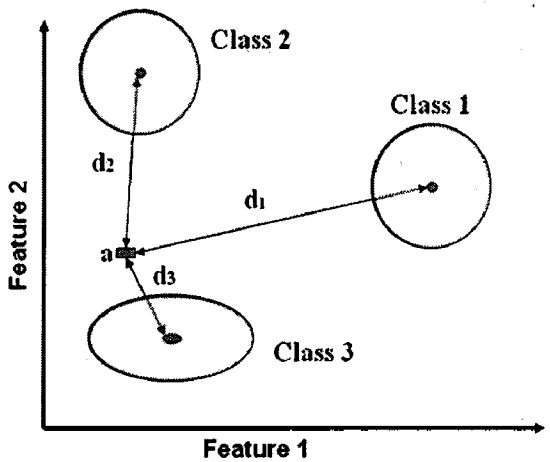

Figure-2.8: An example of minimum distance classification.

Merits:

a. Mathematically simple and computationally efficient technique.
b. Provides better accuracies than the maximum likelihood procedure in the case when the number of training samples is limited.

Demerits:

a. By characterizing each class by its mean band reflectance only, it has no knowledge of the fact that some classes are inherently more variable than others, which in turn can lead to misclassification.

2.3.1.3 Maximum likelihood classification

Maximum Likelihood Classification is one of the most widely used methods in classifying remotely sensed data. The MLC procedure is based on Bayesian probability theory. This classification is based on probability density function associated with a particular training site. Decision rule is to calculate mean and standard deviation of each training set and derive probability density function from mean and standard deviation for computing probability of each pixel belonging to each class. The classifier then assigns pixel to the class for which the probability is the highest [58].

Merits:

a. Yields higher accuracies than other hard classifiers.

Demerits:

a. Computationally intensive and time consuming technique.
b. Each data sample has to be tested against all classes in a classification, which leads to a relative degree of inefficiency.
c. With a fixed relatively small size training set the classification accuracy may actually decrease when the number of features is increased.

2.3.2 Unsupervised classification

Unsupervised classification is the process in which clusters are generated automatically based on natural grouping found in data. This is because this technique is commonly referred to as clustering. Unlike supervised classifier, it does not require the selection of training data in order to train the classifier. This classifier operates independently and does not require intervention of user. Therefore sometimes it may happen that results are unaccepted on the basis of failure of user's expectations. The steps carried by unsupervised classifier are as follows [56]:

i. Classify image into number of clusters or group.
ii. Indentify clusters and assign name to each group.
iii. Merge classes (if required).
iv. Post classification and accuracy assessment.

Unsupervised classification is of two types: K – mean and ISO data.

2.3.2.1 K-mean

K-Means unsupervised classification algorithm (see- figure-2.9) first assigns arbitrarily initial K- cluster vectors. The input cluster vectors are then iteratively assigned to closest cluster according to the square of the Euclidean distance from the clusters (as in minimum distance technique). Each iteration recalculates mean (centroid) of each cluster and reclassifies pixels with respect to the new means. All pixels are classified to the nearest class unless a standard deviation or distance threshold is specified, in which case some pixels may be unclassified if they do not meet the selected criteria. This process is repeated until no more "change" in the value of the means or the maximum number of iterations is reached. The "change" can be defined either by measuring the distances the mean cluster vector have changed from one iteration to another or by the percentage of pixels that have changed between iterations [59].

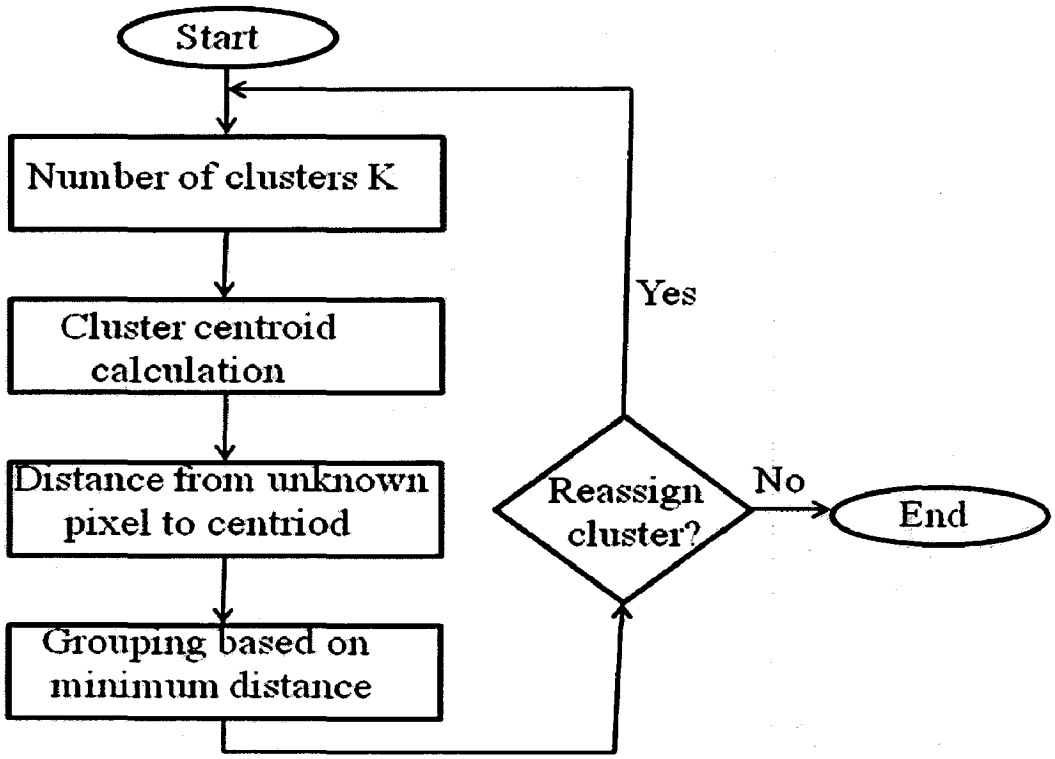

Figure - 2.9: K-mean algorithm

Merits:

a. With a large number of variables, K-Means may be computationally faster than hierarchical clustering (if K is small).
b. K-Means may produce tighter clusters than hierarchical clustering, especially if the clusters are globular.

Demerits [60]:

a. K- mean is very sensitive to initial starting value of cluster centre.
b. K-means assumes that the number of clusters is known a priori, which is not true for real world situation.
c. Does not work well with non-globular clusters.

2.3.2.2 ISODATA

The iterative self organizing data (ISODATA) algorithm represents a comprehensive set of heuristic (rule of thumb) procedures that have been incorporated into an iterative classification algorithm. ISODATA is a nearest-centroid, non-hierarchical, clustering algorithm. It performs in the same manner as K-mean but with further refinements by splitting and merging of clusters [61]. Iterative class splitting, merging, and deleting are done based on input threshold parameters. Clusters are merged if either the number of members (pixel) in a cluster is less than a certain threshold or if the centers of two clusters are closer than a certain threshold. Clusters are split into two different clusters if the cluster standard deviation exceeds a predefined value and the number of members (pixels) is twice the threshold for the minimum number of members.

Merits:

a. More robust.
b. User specific.
c. ISODATA is self-organizing because it requires relatively little human input.
d. Clustering is not geographically biased to the top or bottom pixels, since it is iterative.

Demerits:

a. The clustering process is time-consuming, because it can repeat many times.

2.3.3 Non – parametric classifiers

The classifiers which do not involve estimation of statistical parameters before classification are referred to as non parametric classifiers [56]. Decision trees, artificial neural networks, or

support vector machines, are nonparametric and require that training data sets are large enough to represent the characteristics of each class.

2.3.3.1 Decision tree classifier

Decision tree classification, a machine learning algorithm, is a knowledge based data mining technique. It is an efficient tool for land cover classification. It is a hierarchal top- down approach, in which a decision rules defined by combination of several features and a set of linear discriminate functions are applied at each test node, where a binary decision is made for splitting a complex decision into several simpler decisions in order to separate either one class or some of the classes from remaining classes [62]. In this approach, feature of data (i.e. bands) are predictor variables whereas the class to be mapped is referred to as target variable [63].

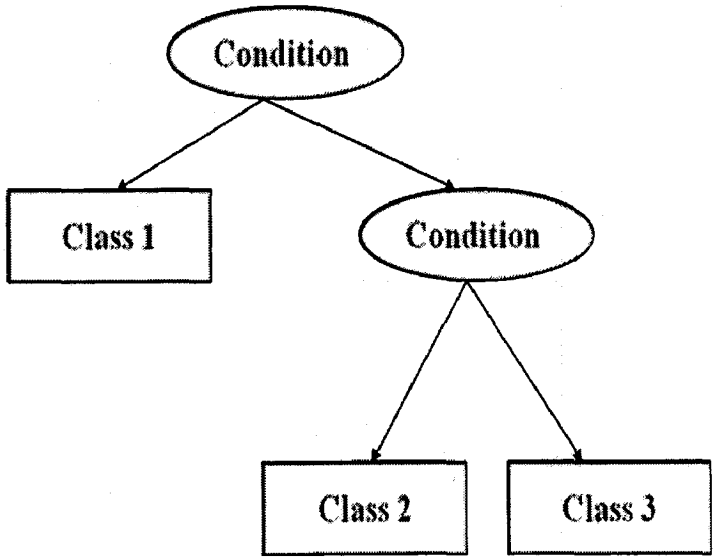

Figure-2.10. Decision tree classification technique.

A tree generally consists of a root node, a number of non terminal nodes or decision stages and a number of terminal nodes (final classifications). It performs binary recursive partitioning to assign automatically maximum information carrying feature for the classification and rejects remaining features at that intermediate stage, thereby increases computational efficiency [64]. The main issues in this approach are [65]:

- Choice of splitting criterion;
- Stopping rules ;
- Labeling the terminal nodes.

Merits:

a. This method is easier to interpret and understand the relation between the inputs and outputs.
b. It can differentiate classes with similar spectral feature.

Demerits:

a. It requires large number of training data, which is time consuming task.

2.4 Accuracy assessment

The most common way of evaluating the effectiveness of classification of remotely sensed data is preparation of so-called error matrix also known as *confusion matrix* or *contingency matrix* [66]. The columns in a confusion matrix represent test data, while rows represent the labels assigned by the classifier. The main diagonal of the matrix lists the correctly classified pixels. There are several measures of agreement derived from error matrix. They are described as follows:

2.4.1 Kappa coefficient

The calculations of kappa coefficient takes into account all of the elements of the error matrix, not just the diagonals of the matrix. This has the effect of taking into account chance agreement in the classification [66]. The resulting Kappa measure compensates for chance agreement in the classification and provides a measure of how much better the classification performed in comparison to the probability of random assigning of pixels to their correct categories. It is defined as

$$\hat{K} = \frac{N\sum_{i=1}^{r} x_{ii} - \sum_{i=1}^{r} x_{i+} * x_{+i}}{N^2 - \sum_{i=1}^{r} x_{i+} * x_{+i}} \tag{2.47}$$

where,

N = total no. of observations

r = the no. of rows in error matrix

x_{ii} =the no. of observations in row i and column i

x_{i+}=the marginal totals of row i

x_{+i}=the marginal totals of column i

Kappa ranges from 0 to 1. *The higher the value of kappa, the better will be the performance of classification* [67].

2.4.2 Overall accuracy

The overall accuracy is computed by dividing the total of correctly assigned pixels (i.e. the sum of the major diagonal), by the total number of pixels in the error matrix.

2.4.3 Producer's accuracy

The producer's accuracy is a measure indicating the probability that the classifier has labelled an image pixel into Class. The producer's accuracy is calculated by dividing the entry (*i*, *i*) by the sum of column *i*. Thus, the producer's accuracy tells us the proportion of pixels in the test data set that are correctly recognized by the classifier. It includes the *error of omission* which refers to the proportion of observed features on the ground that are not classified in the map [66]. The more errors of omission exist, the lower the producer's accuracy.

$$\text{Producer's accuracy} = 100\% - \text{error of omission (\%)} \tag{2.48}$$

2.4.4 User's accuracy

The total number of 'correct pixels' in a category is divided by the total number of pixels classified in that category, then this result gives a measure of the commissions. This measure, the user's accuracy (UA), is indicative of the probability that a pixel on the image actually represents that category on the ground [67]. User accuracy, or reliability, is actually the equivalent of percentage correct for an individual category and is calculated as

$$\text{User's accuracy} = 100\% - \text{error on commission (\%)} \tag{2.49}$$

CHAPTER 3. METHODOLOGY

In this chapter methodology adopted for polarimetric analysis of SAR images for land cover classification is discussed. Starting with the discussion of study site used in our dissertation work, we have discussed about the SAR images used for land cover classification. Target decomposition theorems which form the basis for classification are discussed next followed by various classification techniques.

3.1 Materials used

3.1.1 Study area

The study area has centre latitude 29.61380° and longitude 78.0086730°. It is shown on map in figure -3.1. It covers Roorkee, Laksar, Bijnor regions.

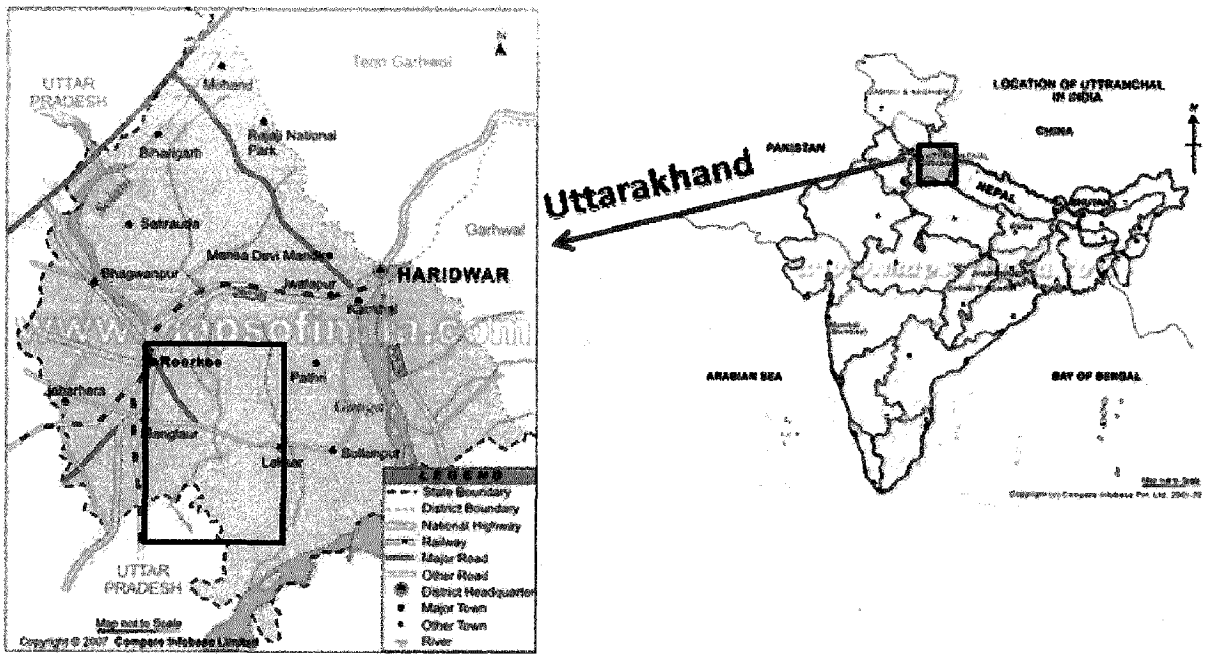

Figure-3.1: Location of study area

Roorkee, a city in the state of Uttarakhand within India is located at 29° 51' N, 77° 53' E on the south bank of Solani River. The Upper Ganga Canal which runs from north to south adds beauty to the city and divides the city in two distinct parts. Laksar is one of the three tehsils in Haridwar district in the state of Uttarkhand. Bijnor is a small town in the state of Uttar Pradesh.

This study area is chosen for its varied landscapes: water (source: Ganga canal, river Ganges), urban (source: Roorkee, Laksar, Bijnor), tall vegetation (source: dense tree cover in city Roorkee), bare soil, short vegetation (source: crop land and grass land).

3.1.2 Data sets used

Advanced Land Observatory Satellite (ALOS) PALSAR polarimetric data taken on date 6th April 2009 was used in the study. The data has four different modes: HH, HV, VH and VV polarization (ref. table-3.1). The ALOS PALSAR product is level 1.1 data in VEXCEL format, which is single look complex data on slant range. The product has single number of looks on range and azimuth. The default off nadir angle for polarimetric acquisition mode is 21.5°. The product has resolution on ground of 30m (range) x 20 m (azimuth) [68] .The product description is given in table-3.2 and table 3.3.

Table -3.1

Polarization description of polarimetric data

Polarization	Explanation
HH	• Horizontally polarized transmission • Horizontally polarized reception only
HV	• Horizontally polarized transmission • Vertically polarized reception only
VH	• Vertically polarized transmission • Horizontally polarized reception only
VV	• Vertically polarized transmission • Vertically polarized reception only

Table- 3.2

File description of ALOS PALSAR L-1.1 data sets

File extension	Numbers	Description
_.slc	4	Single look complex image files for each polarization
_.par	4	Parameter files for all polarizations
_.meta	1	Meta file containing general information about product

Table-3.3

Product description

Source	ALOS
Sensor	PALSAR
Instrument mode	PLR (Polarimetric)(HH,HV,VH,VV)
Product	L-1.1
Product type	Single look complex (SLC)
Pixel spacing	9.368514 (m)
Bytes per pixel	8
PRF	1.93 GHz
Look angle	21.5^0
Incidence angle	24^0
Range resolution	11.094462(m)
Azimuth resolution	4.892375(m)

3.1.3 Software used

In the whole study three software were used:

- **ENVI 4.3** - *Environment* for Visualizing Images (ENVI) was for processing SAR images.
- **SARSCAPE 4.1**- SARSCAPE data analysis module allows image processing with ENVI. This software perfectly complements ENVI's functionality for analyzing and visualizing remote sensing data of any kind.
- **MATLAB 2007**- This software was used for developing algorithms of various decompositions and for plotting various graphs.

3.2 Pre-classification technique: a general overview

Before actually performing decomposition and classification some pre-processing of SAR image is required due to several reasons. There is no particular chain of procedure for pre-processing, but following procedures are required before classification:

3.2.1 Data import

As mentioned earlier, the data provided by ERSDAC is single look slant range fully polarimetric complex data (HH, HV, VH, and VV). Since this is already focused; therefore it is just imported through SARSCAPE using ENVI-4.3 software. This provides four -slc (single look complex files (HH.slc, HV.slc, VH.slc and VV.slc).

3.2.2 Polarimetric calibration

Polarimetric calibration minimizes the impact of non ideal behavior of a full-polarimetric SAR acquisition system in order to obtain an estimate of the scattering matrix of the imaged objects as accurate as possible from their available measurement.

3.2.3 Speckle filtering

Speckle noise is generated due to coherent interference of electromagnetic waves reflected from many randomly distributed elementary scatterers within a resolution cell. *Speckle has the characteristics of a random multiplicative noise (defined below) in the sense that as the average*

grey level of a local area increases, the noise level increases [69]. Speckle removal is required in order to improve classification results. Two procedures can be adopted for speckle reduction:

3.2.3.1 Multilooking

Radar speckle can be suppressed by averaging several looks (images) to reduce the noise variance. This procedure is called *multilook processing*. Multiple looks are generated by averaging azimuth or range resolution cell. The goal of multilooking is to obtain approximately squared pixels. In order to avoid oversampling effect in geocoding, multillooked image should have same spatial resolution as recommended for geocoded product. Numbers of looks are calculated by following procedure:

$$\text{Ground range resolution} = \frac{\text{pixel spacing range}}{\sin(\text{incidence angle})} \tag{3.1}$$

From table 3.2 after putting value in above equation ground range resolution is obtained as 23.0145 m.

$$\text{Number of looks} \approx \frac{\text{Ground range resolution}}{\text{line spacing (azimuth)}} \tag{3.2}$$

In our case multi-look factor is obtained as 7 [70].

3.2.3.2 Filtering

The second method of speckle suppression uses filtering methods, which fall into two main categories, namely, adaptive and non-adaptive filters. *Adaptive filters* use weights that are dependent on the degree of speckle in the image, whereas *non-adaptive* filters use the same set of weights over the entire image. **A speckle suppression filter is expected to filter the homogeneous areas with reasonable speckle reduction capability, retain edges, and preserve features (linear features and point features) [38].**

In this study Wishart Gamma map filter is used. It is a polarimetric filter which is suitable for polarimetric data. It performs well in the presence of regular texture and moderate relief. The filter operates under the assumption of target reciprocity (i.e. HV=VH) [70]. Thus only three filtered images are produced (HH, HV, VV).

The output speckle filtered Covariance Matrix terms ($S_{HH}.S_{HH}^{*}$, $S_{VV}.S_{VV}^{*}$, $S_{HV}.S_{HV}^{*}$, $\mathrm{Re}\{S_{HH}.S_{VV}^{*}\}$, $\mathrm{Im}\{S_{HH}.S_{VV}^{*}\}$, $\mathrm{Re}\{S_{HH}.S_{HV}^{*}\}$, $\mathrm{Im}\{S_{HH}.S_{HV}^{*}\}$, $\mathrm{Re}\{S_{VV}.S_{HV}^{*}\}$, $\mathrm{Im}\{S_{VV}.S_{HV}^{*}\}$ contains all the polarimetric information required for further computation.

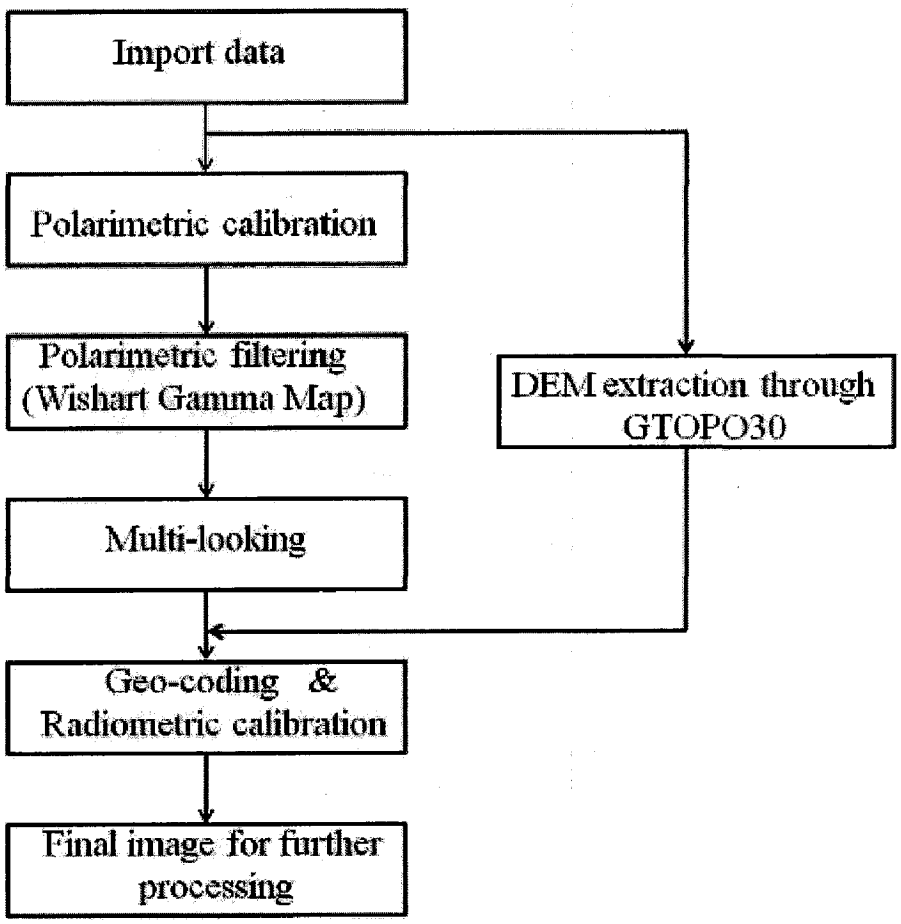

Figure -3.2: Flow chart for pre-classification procedure

3.2.4 DEM extraction

It is digital representation of ground surface topography or terrain. In this study digital elevation model (DEM) was extracted by technique GTOPO30. It is a global digital elevation model (DEM) with a horizontal grid spacing of 30 arc seconds (approximately 1 km). Datum selected was WGS-84.

3.2.5 Geocoding and radiometric calibration

Geocoding is the process of transforming remote sensing image from slant range projection to a cartographic reference system considering ellipsoidal height or a Digital Elevation Model. Here in this study UTM global is chosen as cartographic reference system with WGS-84 as datum.

The radiometric calibration, which is performed during the geocoding, is based on the exploitation of the radar equation.

3.3 Used target decomposition methods

Target decomposition forms the basis of classification procedure. The decomposition theorems manipulate the scattering matrix elements in order to provide more elaborated and descriptive polarimetric observables, which can be used further for classification.

In the following sections we have presented three decomposition methods. In sec- 3.3.3 three D decomposition technique is discussed, which can be used further for studying the effect of window size and filtering. Two other decomposition techniques are presented in the following sections -3.3.1 and 3.3.2. They are discussed below:

3.3.1 Pauli decomposition

The method discussed in section-2.2.1.1. is presented here. The procedure to obtain Pauli decomposed image is described below (also refer figure- 3.3):

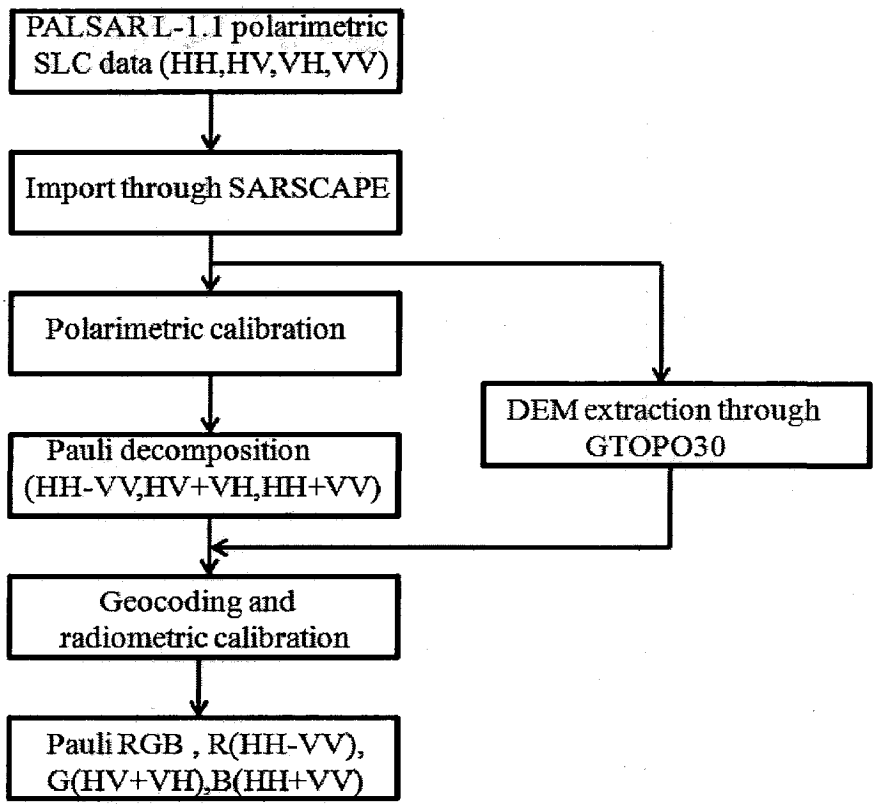

Figure -3.3: Flow chart of Pauli decomposition

The PALSAR data sets were first imported through software SARSCAPE using ENVI 4.3. These –slc (single look complex) files were calibrated using defined polarimetric calibration matrices. Then Pauli decomposition was performed on calibrated data using SARSCAPE. Three files were generated as a result of decomposition corresponding to HH-VV, HV+VH, HH+VV representing even-bounce scattering, scattering from 45° tilted dihedral and odd- bounce scattering respectively. The digital elevation model was extracted using technique GTOPO30 for terrain correction prior to geocoding. Then nearest neighbor resampling method was applied to data for radiometric calibration. These geocoded and radiometrically calibrated files were used to produce final RGB decomposed image taking HH-VV as red, HV+VH as green and HH+VV as blue.

3.3.2 Eigen value decomposition

The eigen value decomposition has already been discussed in section-2.2.2.2. The procedure adopted for eigen value decomposition is described in figure-3.4.

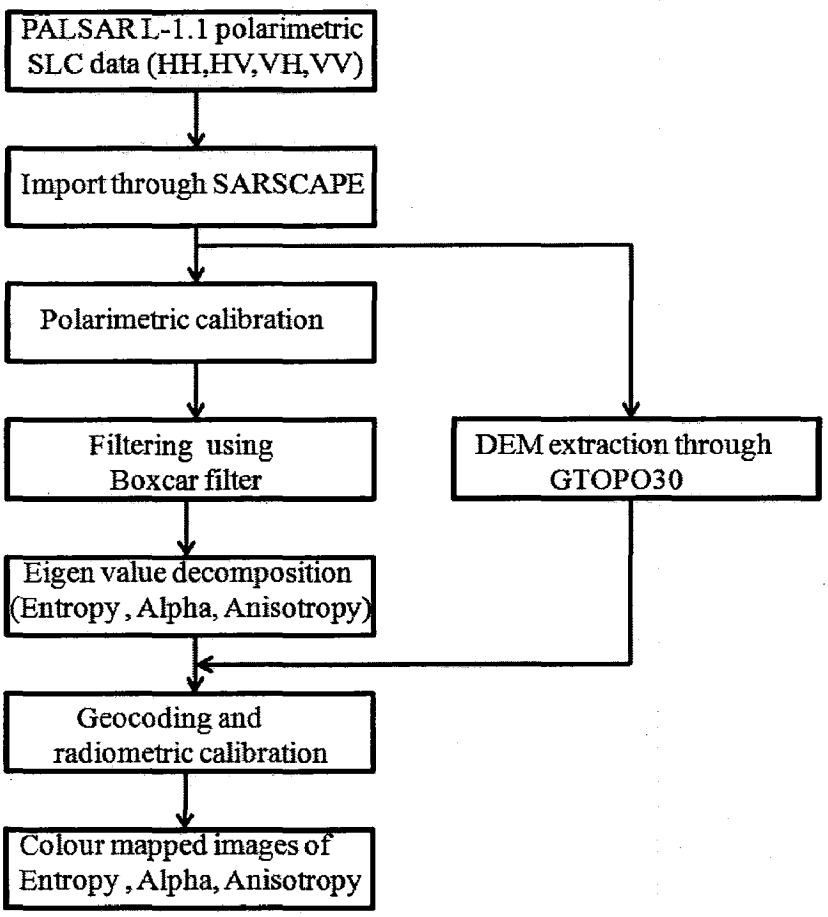

Figure- 3.4: Flow chart of eigen value decomposition

The PALSAR data sets were first imported through software SARSCAPE using ENVI 4.3. These –slc (single look complex) files were calibrated using defined polarimetric calibration matrices. For speckle suppression box-filter was used. This is a non- adaptive filter. Only this preprocessing step is required for the decomposition. The eigen value decomposition was performed on filtered data, as a result of which three files (entropy {eq-2.30}, alpha {eq-2.33} and anisotropy {eq-2.31}) were generated. The description of these parameters is given in sections 2.2.2.1.1 and 2.2.2.1.2. The digital elevation model was extracted using technique GTOPO30 for terrain correction prior to geocoding. Then nearest neighbor re-sampling method was applied to data for radiometric calibration. After geocoding color coded images of all three images were obtained.

3.3.3 Three D decomposition

The three D decomposition method (see section 2.2.2.2.1) is discussed in following section. We are using this technique to study the effect of ensemble averaging on classification and filtering on flat terrain. Therefore we are adopting two procedures for performing three D decomposition

(a) Without polarimetric filtering

The data were first imported through software SARSCAPE using ENVI 4.3 in order to obtain SLC files. These are complex files containing both real and imaginary part. Since we do not want to lose phase information after multilooking (which produces intensity data), we adopted method for pre-processing shown in figure-3.5.After importing data sets through SARSCAPE, they were converted into mod-phase form. It generated two files for each polarization. In order to improve radiometric resolution, each mod – phase file was multilooked by factor 7. Each multilooked mod- phase file was geocoded using DEM file extracted by GTOPO30 technique. The geocoded mod – phase files were combined together to obtain complex files. Then these files were calibrated using defined polarimetric calibration matrices in order to obtain scattering terms as accurate as possible.

After pre- processing image of size 400x400 was obtained by resizing whole image in order to crop Roorkee region only. This data was converted into ASCII in order to be processed through MATLAB. A MATLAB code was written for 3 D decomposition based on the algorithm [21] (see Appendix-B.1 (a)). The results of MATLAB code were saved in -.dat file format so that they can be further processed through software ENVI 4.3. As a result of 3 D decomposition three images P_d, P_V and P_S were obtained corresponding to double bounce scattering, volume scattering and single bounce scattering respectively (see eqs. 2.39, 2.40 and

2.41). Then co-registration of these images was done by image to image registration using the original resized image as base image Input image was warped using one degree polynomial and nearest neighbor resampling technique. This whole process was repeated using different window size (3x3, 5x5, 7x7, 9x9, 11x11, 15x15) while formulation of covariance matrix terms in MATLAB code.

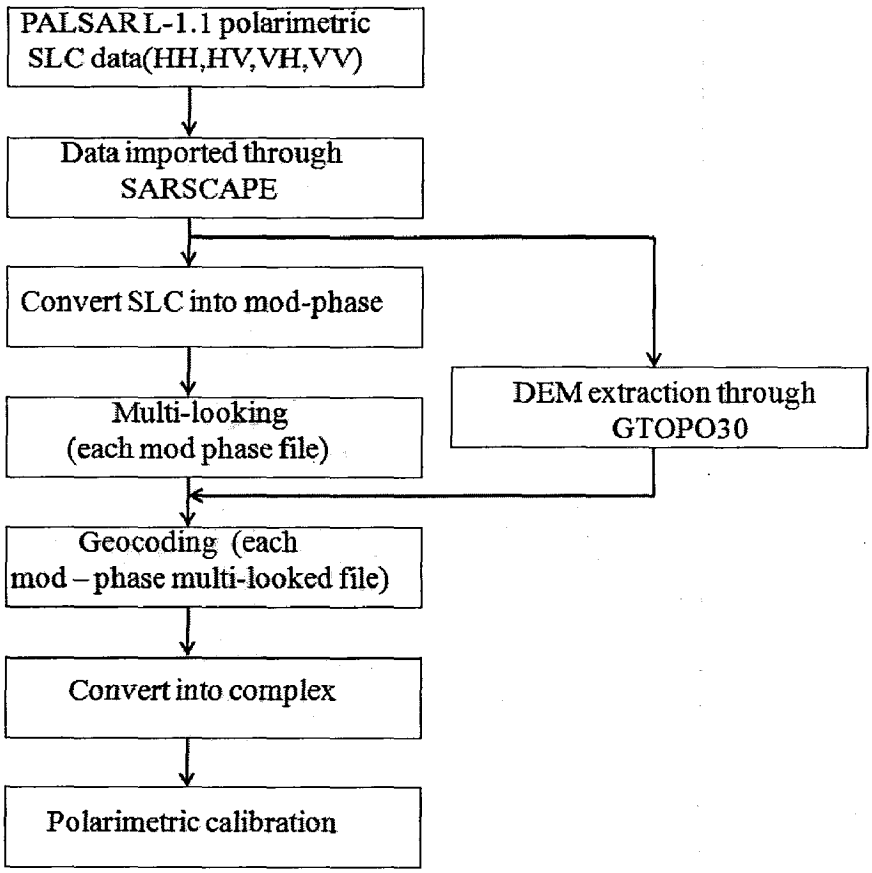

Figure-3.5: Flow chart of data pre-processing before 3-D decomposition (without polarimetric filtering)

(b) With polarimetric filtering

The data sets were first imported through SARSCAPE using ENVI 4.3.The SLC data so obtained were given as input to Wishart Gamma Map filter, which is a polarimetric filter. The size of processing window is another important factor for decomposition of SAR images. *For very large processing window, resolution of image is very low due to amalgamation of various textural features. On the other hand, for very small processing window second order statistics do follow by second – order statistics. So for our site we chose 5x5 processing window.* Due to

different resolution in range and azimuth direction multilooking (with multi-look factor 7) was performed to improve the radiometric resolution. Then these images were geocoded and radiometrically calibrated. Geocoding was done using DEM file extracted through technique GTOPO30 for terrain correction and radiometric calibration was done using nearest neighbor technique.

After this preprocessing (see figure-3.6), images were resized in order to obtain images of size 400x400 containing region Roorkee only. These files were converted into ASCII form so that they can further be processes using MATLAB. A MATLAB code was written for 3 D decomposition proposed by Freeman et. al. [23] (see- Appendix-B-1 (b)) and resultant images of P_d, P_v and P_s were saved in .dat format. These files P_d, P_v and P_s were imported into ENVI 4.3. Then co-registration of these images was done by image to image registration using the original resized image as base image Input image was warped using one degree polynomial and nearest neighbor resampling technique. Then decomposed image was obtained by taking P_d as red , P_s as blue and P_v as green.

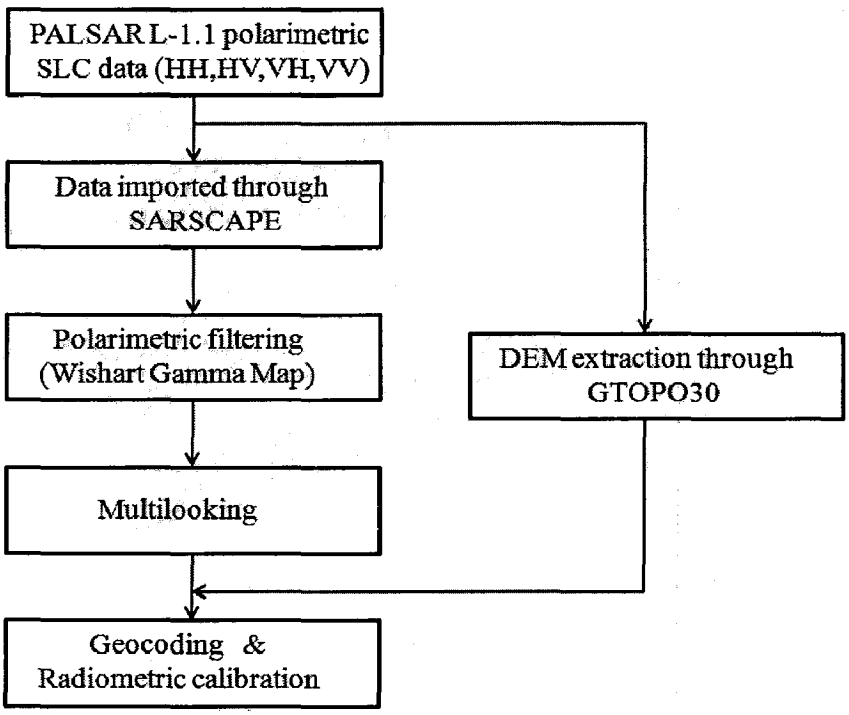

Figure-3.6. Flow chart of data pre-processing before 3-D decomposition (with polarimetric filtering)

3.4 Classification techniques adopted

In the following sections the classification techniques are discussed. In section- 3.4.1, the decision tree classification algorithm is proposed. This classification algorithm is based on the knowledge acquired by backscattering coefficients. In the rest of the sections three supervised classification algorithms (Parallelepiped, Minimum distance, and Maximum likelihood) are applied over polarimetric observables obtained by decomposition techniques. The classification tests based on the parameters obtained by three D decomposition are applied over resized image of region Roorkee of size 400 x 400 (sec-3.4.2). This classification is used for studying the effect of window size on classification. Through this technique we are also trying to see the effect of filtering over filtering over flat terrain like Roorkee. Rest of the two classification tests based on Pauli decomposition and Eigen value decomposition are performed over whole data.

3.4.1 Decision tree classification

Decision rule

Decision tree approach requires thorough knowledge of information bearing features and their physical understanding. It is already known that backscattering is function of the electromagnetic wave parameters such as wave frequency, its polarization and its incidence angle and it depends on the target characteristics such as surface geometry and dielectric characteristics of the medium. **Our objective is to extract physical information from backscattering behavior of various objects.** The analysis is based on polarized backscattering coefficients measured at HH-,VV-,HV-, RR-(circular copular), RL- (circular cross polar),45C-(45° co-polar) , 45X- (45° cross polar) and cross-pol ratios $\sigma^{\circ}_{HV}/\sigma^{\circ}_{VV}$ and $\sigma^{\circ}_{RR}/\sigma^{\circ}_{RL}$. These standard polarimetric features act as our information bearing features.

Extensive ground truth survey was performed over the whole region. Around 211 Ground truth points (GCP) were collected for training and 840 for testing the accuracy of classification map. Table 3.4 presents the training and control samples number made with the ground truth data. Based on ground truth information five classes were identified: water (includes wetland also), urban, short vegetation (cropland, grass land, shrubs etc.), tall vegetation and bare soil surface. Then in order to obtain decision rule rigorous experiment was done over whole 211 training ROI's. Since each class represents specific scattering property so decision boundaries are made based on knowledge acquired experimentally by the analysis of scattering behavior of each surface types. For each aforementioned class backscattering

coefficients described above were calculated. Then based on the experimental procedure and previous research validation decision rule for classifying each land cover type was decided.

Table -3.4

Ground trouth survey points

Sort	Training	Test sample
Water	64	302
Tall vegetation	19	70
Urban	67	265
Short vegetation	37	137
Bare soil	24	66

Data pre-processing for decision tree classification technique was same as described in fig 3.5. Above mentioned all polarized backscatter coefficients were calculated for each class like urban, water, short vegetation, tall vegetation and bare soil covered by GCPs. Decision tree was implemented by ENVI 4.3 software.

Classification scheme

The classification scheme for ALOS-PALSAR data is shown in figure-3.7.Our classification scheme is very much inspired by [71, 72, 76].The algorithm starts with discrimination between water and other classes. Based on empirical evidence and experimental validation, decision boundaries are created. Water bodies can be separated from other classes on the basis of σ°_{HV} and σ°_{xy}. For our site σ°_{HV} is less than -30 db and σ°_{xy} is less than -25 db. All the areas with σ°_{HV} less than -18 db [73] and $\sigma^\circ_{HV}/\sigma^\circ_{VV}$ greater than -11 db [74] are classified as tall vegetation. But similar scattering behavior is represented by both forest and urban area due to their geometrical structure, so they are separated on the basis of cross pol ratio of circular polarization which is negative for urban and positive for tall vegetation. It has been verified that for bare soil, σ°_{RR} is appreciably less than σ°_{RL} [75] and $\sigma^\circ_{HH} < \sigma^\circ_{VV}$ (which is the case of surface scattering) [71] .In our site, $\sigma^\circ_{RR}/\sigma^\circ_{RL}$ is less than -12db and σ°_{HV} is less than -25 db

for bare soil surface. This allows the segregation of bare soil surface from other classes. As we already know that for vegetation $\sigma^{\circ}_{HV}/\sigma^{\circ}_{VV}$ is less than -11 db. Also we have found that σ°_{HH} is greater than -18 db for short vegetation. The pixels that do not satisfy above criteria are termed as unclassified.

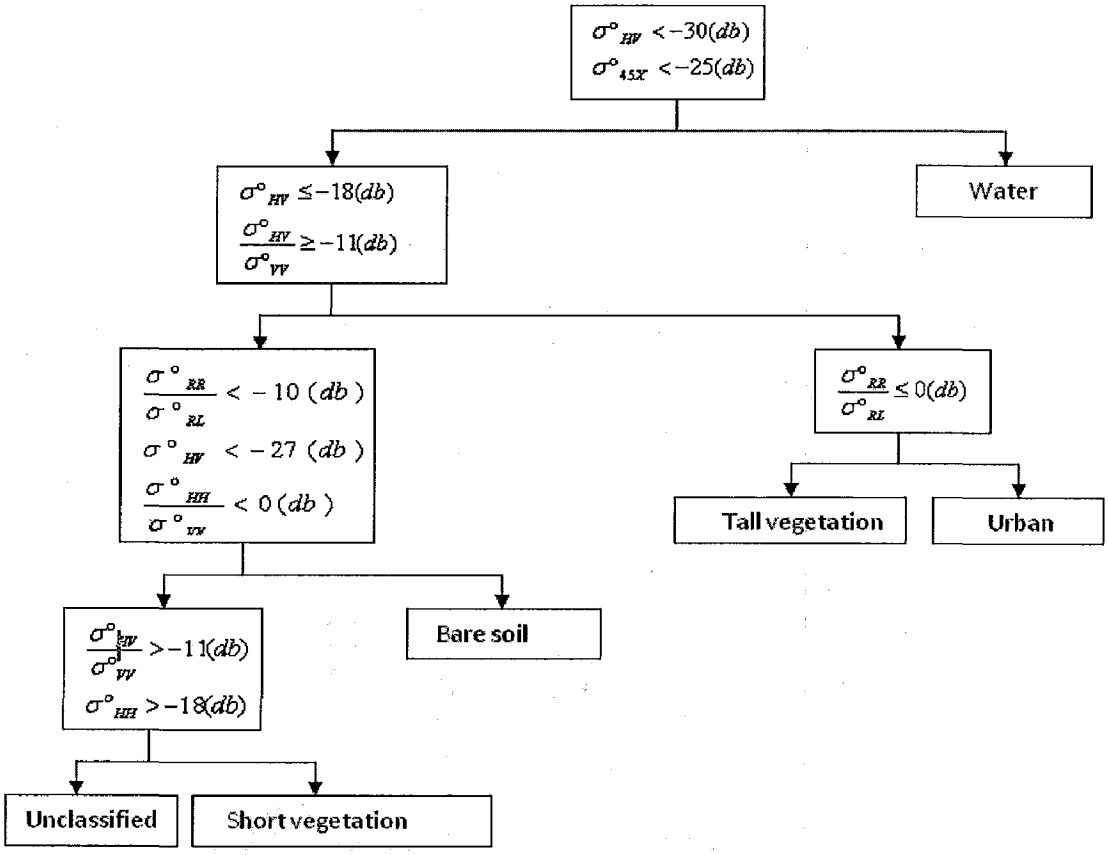

Figure-3.7: Algorithm for decision tree classification

The result of classification algorithm was calculated using confusion matrix (or error matrix), which compares the classification result with ground truth information and reports overall accuracy, kappa coefficient, producer accuracy and user accuracy.

3.4.2 Classification based on 3 D decomposition

The decomposed image obtained as a result of 3 D decomposition from sec -3.2.3 (b) was used for classification here.

Extensive ground truth survey was performed over the whole region. Around 133 Ground truth points (GCP) were collected for training and 726 for testing the accuracy of

classification map shown in table- 3.5. Based on ground truth survey three classes were defined: water (includes wetland also), urban, vegetation

Table 3.5

Ground truth survey points for region Roorkee

Sort	Training sample	Test sample
Water	51	272
Urban	44	304
Vegetation	38	150

We used three supervised classification techniques: minimum distance, parallelepiped and maximum likelihood. We trained these classifiers through 133 ROI's. The result of classification algorithm was calculated using confusion matrix (or error matrix), which compares the classification result with ground truth information and reports overall accuracy, kappa coefficient, producer accuracy and user accuracy. We repeated this procedure for all decomposed images obtained by taking various window sizes in formulation of covariance matrix terms while writing MATLAB code. Then the effect of window size on all the classifications was also seen.

3.4.3 Classification based on Pauli decomposition

The decomposed image obtained as a result of Pauli decomposition from sec -3.2.1 was used for classification here. We used the same ground truth survey points for training and testing control points as in table-3.4. We classified decomposed image by three supervised classification techniques: minimum distance, parallelepiped and maximum likelihood. The classification result was obtained for each classification technique by generating confusion matrix in order to determine the agreement between the selected reference ground controls points (840 ROI's) and classified data.

3.4.4 Classification based on Eigen value decomposition

This classification procedure is based on the parameters obtained by eigen value decomposition as discussed in section 3.3.2.We performed two sets of classification tests: first by taking entropy and alpha as input to classifier and then by taking entropy, alpha and anisotropy. Three supervised classification techniques: minimum distance, parallelepiped and maximum likelihood were applied to each decomposed image. In order to train these classifiers we use 211 ground truth points (GCP's) as shown in table- 3.4. The classification map so obtained was compared with 840 GCP's by calculating confusion matrix which reports overall accuracy, kappa coefficient, producer accuracy and user accuracy as an indicator of classification result.

3.4.5 Classification by combining intensities of various polarizations

This classification technique is very much inspired by [77],[78].The data pre-processing was performed in the same manner as shown in fig- 3.5 of sec -3.2.3(b).The same procedure was adopted for circularly polarized images. Thus we obtained six intensity images: HH, HV, VV, LL, LR and RR. Images were obtained in following manner:

1. Form images by combining pair of intensities (HH-HV, HH-VV, HV-VV, LL-RR, LL-LR, and LR-RR).
2. Form images by combining set of three intensities (HH-HV-VV, and LL-LR-RR).
3. Form image by combining set of four intensities (HH-HV-VV-LL)
4. Form image by combining of five intensities (HH-HV-VV-LL-LR).
5. Form image by combining set of all six intensities (HH-HV-VV-LL-LR-RR).

In order to train the classifier we used 211 ground control points as in table -3.4. The above images were classified by ML classifier and minimum distance classifier, we performed post classification by using 840 GCP's in order to calculate confusion matrix.

CHAPTER 4. RESULTS AND DISCUSSION

4.1 Decomposition results

4.1.1 Results of three D decomposition

The results of three D decomposition discussed in section-3.3.3 are presented in following sections.

4.1.1.1 Without polarimetric filtering

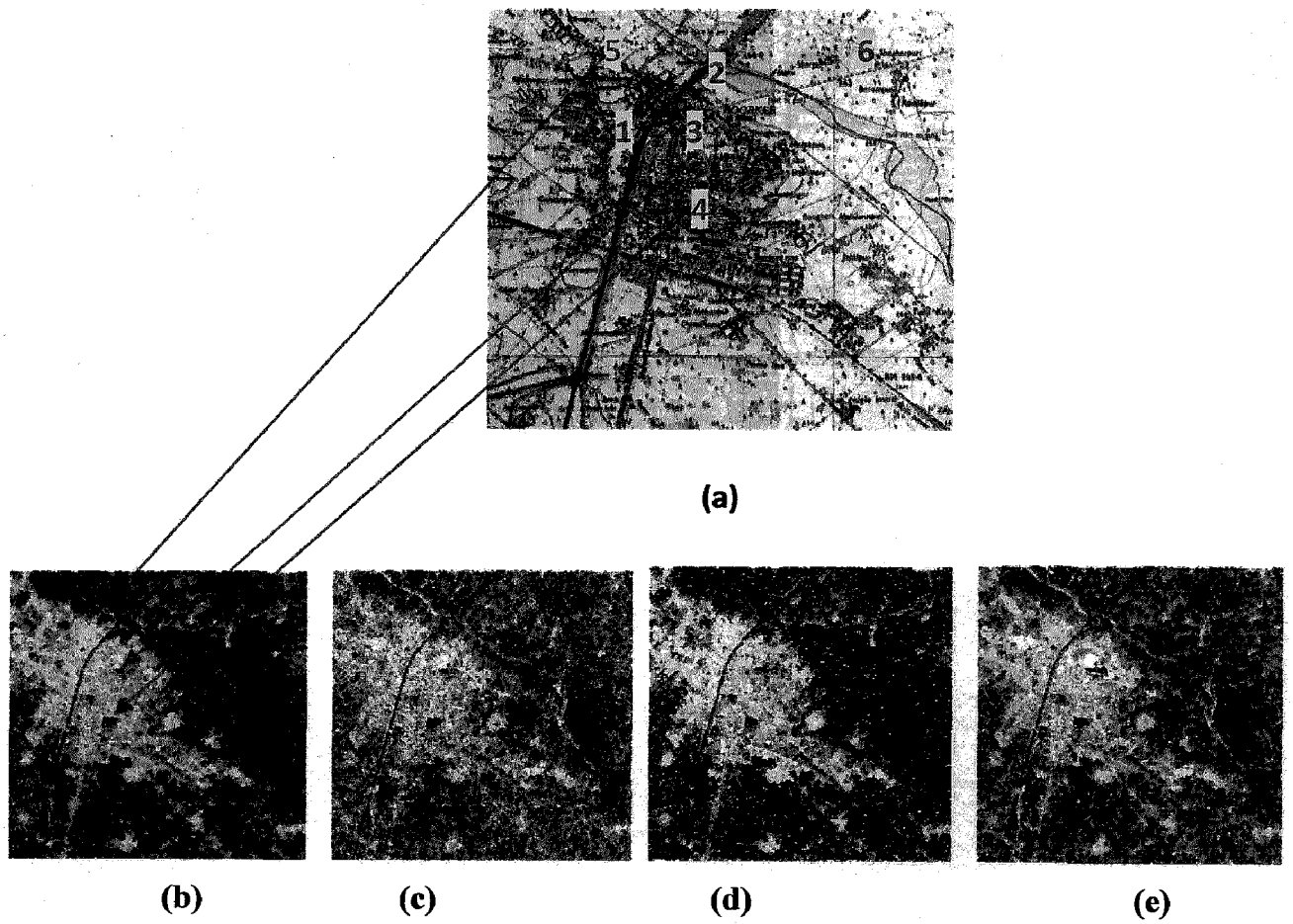

Figure 4.1.(a) Toposheet Roorkee, (b) Decomposed image with Pd (red), Pv (green), Ps (blue) using 15x15 averaging window, (c) P_d (d) Pv (e) Ps.

The results of three D decomposition as discussed in sec-3.3.3 (a) are shown in figure 4.1. The colour coded decomposed image was obtained by taking ***Pd as red, Pv as gree),and Ps as***

blue.the decomposed image shows that in urban area (1 in toposheet) most of the region shows volumetric scattering , only some part shows a mixture of double –bounce and single bounce. There are also some white pixels in the image which reveals the amalgamation of all three scattering mechanisms.

The black pixels shows specular scattering. In this image of region Roorkee specular scattering is obatined by Ganga canal (2 in toposheet), grass land (mostly wet:3 in topsheet) ahead of main building of Indian institute of technology Roorkee and in cantonment area(4:in toposheet).

The river which crosses solani acquiduct (5: in toposheet) shows single bounce scattering with a some double bounce because this river is dried in its most of the course in month April. Rest of the part which is short vegetation (including cropland ,grass land, shrubs etc.:6 in topsheet) shows a mixture of double bounce scattering and single bounce scattering. Only some part shows volume scattering.

4.1.1.2 With polarimetric filtering

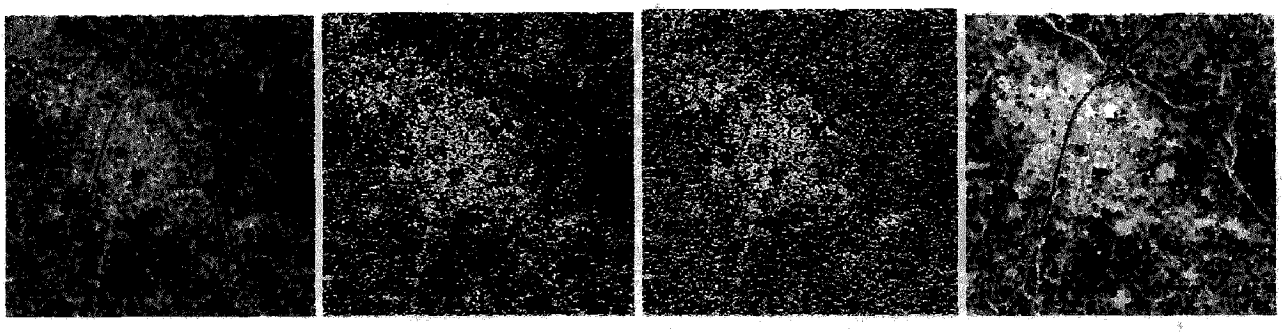

(a) (b) (c) (d)

Figure 4.2.(a) Decomposed image with Pd(red), Pv(green), Ps(blue) using 5x5 averaging window, (b) P_d ,(c) Ps, (d) Pv.

The results of three D decomposition discussed in section-3.3.3 (b) are shown in figure-4.2. The covariance terms produced as a result of polarimetric filtering were used in developing algorithm. The MATLAB code of this algorithm produces three images $\mathbf{P_d}$, **Ps** and **Pv.** For refernce with toposheet refer figure-4.1(a).As seen in figre -4.2(a) most of the region appears green which shows volume scattering. In urban area small amount of double bounce and single bounce components appears. In urban area white colour appears due to presence of all three componets.In decomposed image black colour appears due to specular scattering either from water or wet grass land. In figure-4.2 (b) and (c) most of the part appears black due to some constraints of Wisharat Gamma map polarimetric filter.

The filter does not perform well since Roorkee is a flat terrain. The decomposition results show that filtering does not improve decomposition results, rather degrades the results by not preserving linear features of terrain.

4.1.2 Results of Pauli decomposition

The results of Pauli decomposition discussed in section 2.2.1.1 (also ref. figure-3.3) are shown in figure 4.3. Figure-4.3(a) is color coded decomposed image by taking **HH-VV** as **red** channel, **2HV** as **green** channel and **HH+VV** as **blue** channel. Figure-4.3(b) (highlighted part of figure 4.2(a)) is resized image of region Roorkee of size 400x400 for clear elaboration of results.

Bare soil surface appears blue in image which indicate that the third polarimetric clannel HH+VV has larger magnitude than others. This is the case of single bounce scattering.River channel , wet grass land appears black due to specular scattering from the surfcae.

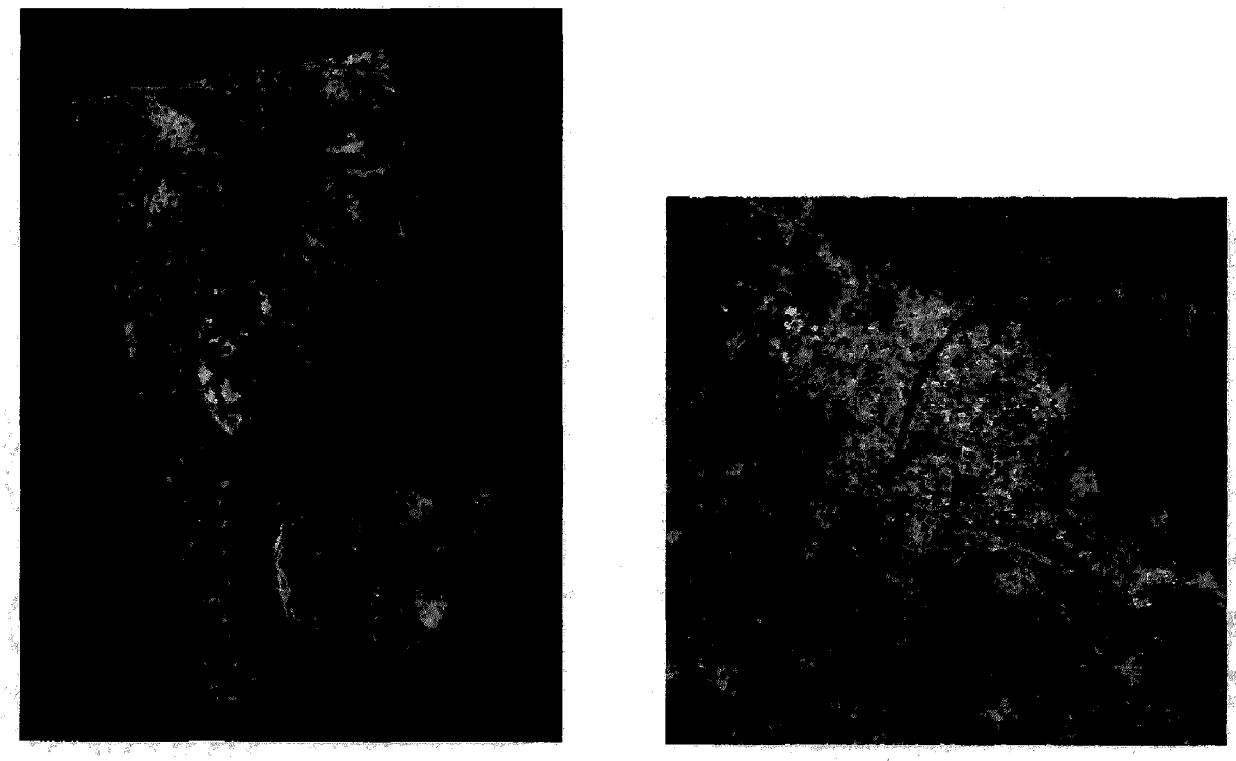

Figure 4.3. (a) Colour coded pauli decomposed image having HH-VV(red) , 2HV(green), HH+VV(blue), (b) decomposed image of region Roorkee of size 400x400.

Green colour is shown by classes "urban" and "tall vegetation". This indicates dominant HV component which is the characteristics of vegetated fields, but due to structural similarity some part of urban area shows same characteristics as tall vegetation.

Over some part of urban area dominant colour is pink and white.Pink colour shows combination of single bounce (blue) and double bounce scatterinng (red).White pixels correspond to equal amplitude over all polarimetric channels.

The class "short vegetation" does not show any specific scattering type. In most of the part it shows single bounce scattering (blue). Some double bounce also appears in this region.

The advantage of this decomposition lies in the fact that it can clearly distinguishes natural targets, roads and even railway track, which reamins invisible in almost all decompositions. The drawback of this decomposition is that it can not distinguish man made targets well.

4.1.3 Results of eigen value decomposition

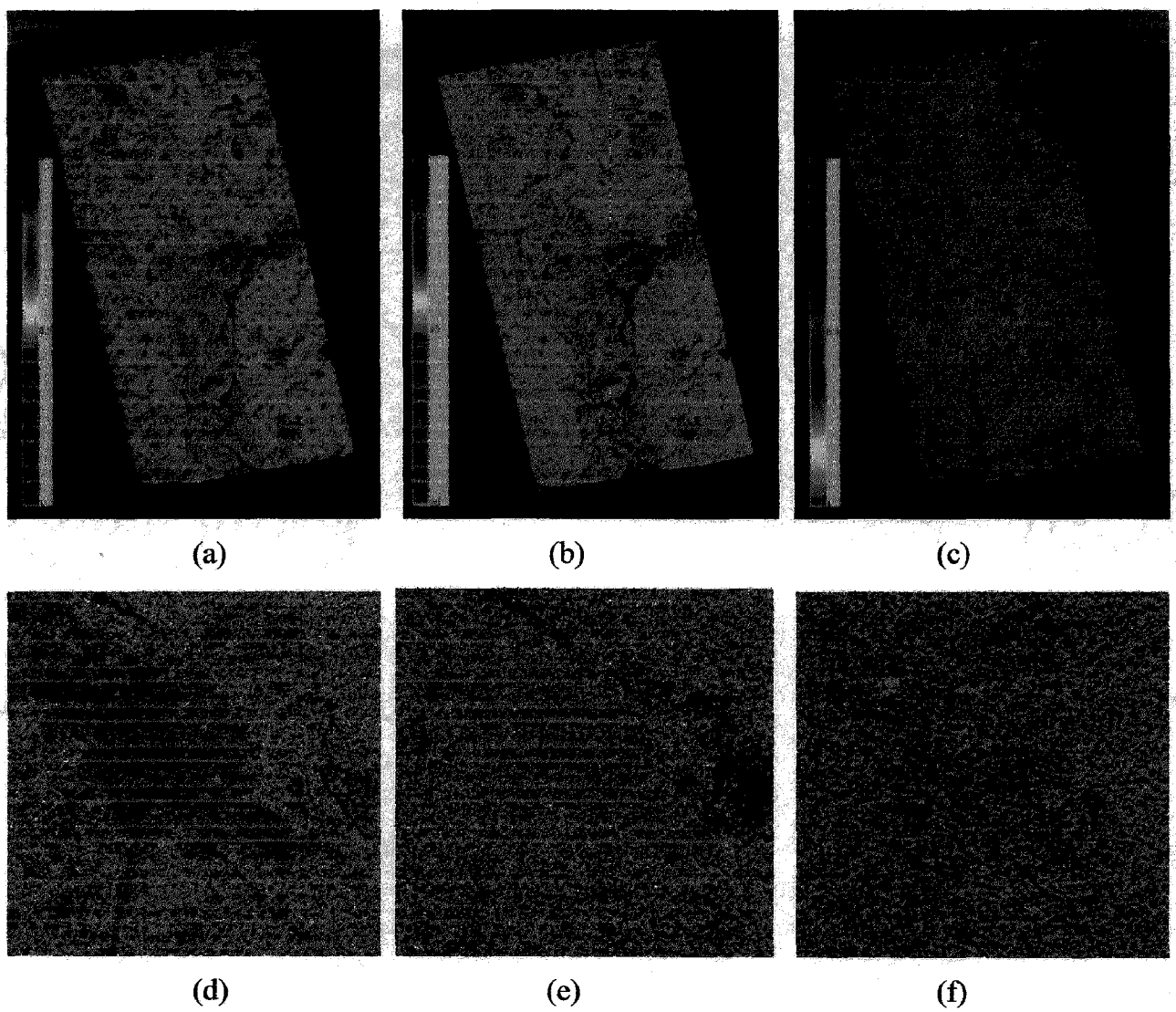

Figure -4.4:Images of eigen value parameters:(a) & (d) Entropy image with (d) of region Roorkee, (b) & (e) Alpha image with (e) of region Roorkee , (c) & (f) Anisotropy image with (f) of region Roorkee.

In figure-4.4 images of parameters obtained by eigen value decomposition (ref. figure-3.4) are shown. In entropy image (eq-2.30) it is clearly seen that many features have high entropy so they have reduced polarimetric information. Tall vegetation and urban area shows high entropy ranges from 0.6 to 1. This high value of entropy indicates the superposition of three scattering mechanisms. The Bare surface and river show low entropy ranging from 0 to 0.4.Short vegetation shows medium entropy ranging from 0.5 to 0.6.

The averaged alpha (eq. 2.33) image is shown in figure-4.4(b). This alpha image depicts the scattering mechanisms. The high alpha values ranging from 55° up to 90° indicate dominant dihedral scattering. Urban area and tall vegetation fall within this range. River and bare surface have low value of alpha (below 35°), which indicate anisotropic surface scattering. The areas having short vegetation have alpha value around 40°.

The anisotropy eq. (2.31) varies over its whole definition range from 0 to 1, from low values over high roughness areas for which the presence of secondary scattering effects is expected, to high values over small roughness areas for which the scattering process becomes quasi-deterministic. High anisotropy values indicate the presence of two main scattering mechanisms, while low anisotropy values indicate three scattering mechanisms.

4.2 Effect of ensemble averaging on classification

The size of processing window or the number of averaging window is one of the important factor for accurate decomposition and hence classification of SAR images. Analyzing classification behavior based on the selection of processing window size is one of the major issues; therefore in this section the effect of window size or ensemble averaging on decomposition and various classification techniques for land cover classification was studied. For very large processing window, resolution of image is very low due to amalgamation of various textural features. On the other hand, for very small processing window second order statistics do not abide by averaged quantities of coherency matrix used in decomposition [79]. Our work is focused on varying the size of processing window and visualizing its effect on classification by calculating overall classification accuracy.

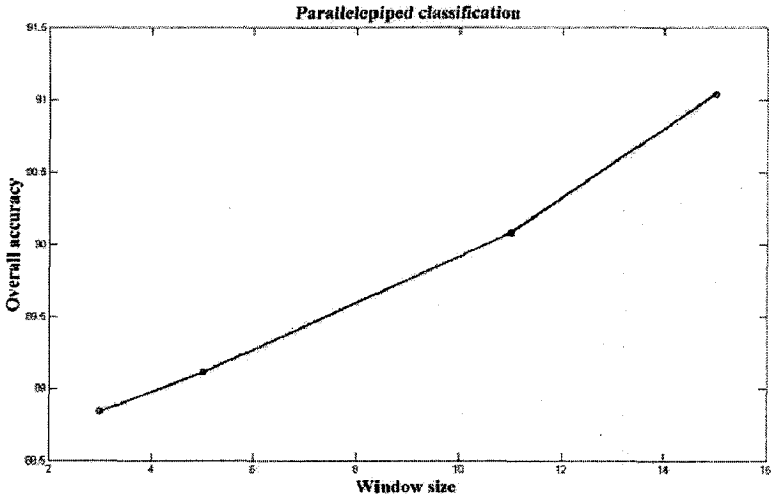

(a)

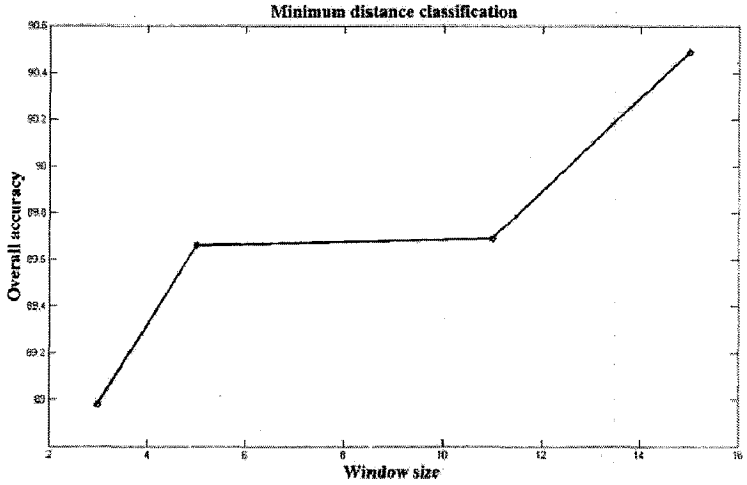

(b)

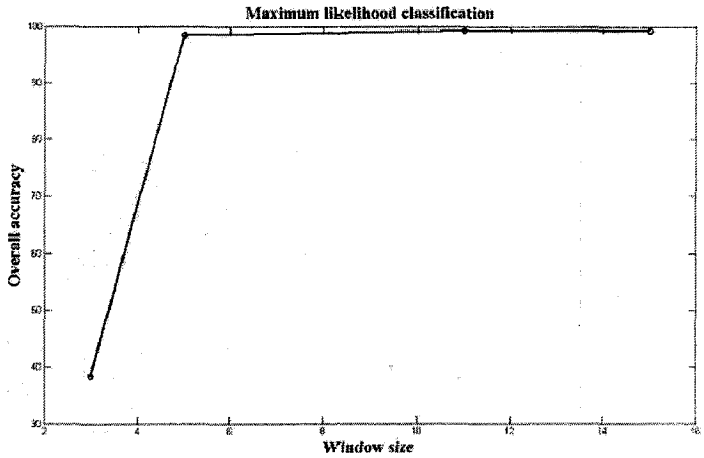

(c)

Figure-4.23: Accuracy estimation of classification tests based on three D decomposition: (a) Parallelepiped, (b) Minimum distance, (c) Maximum Likelihood.

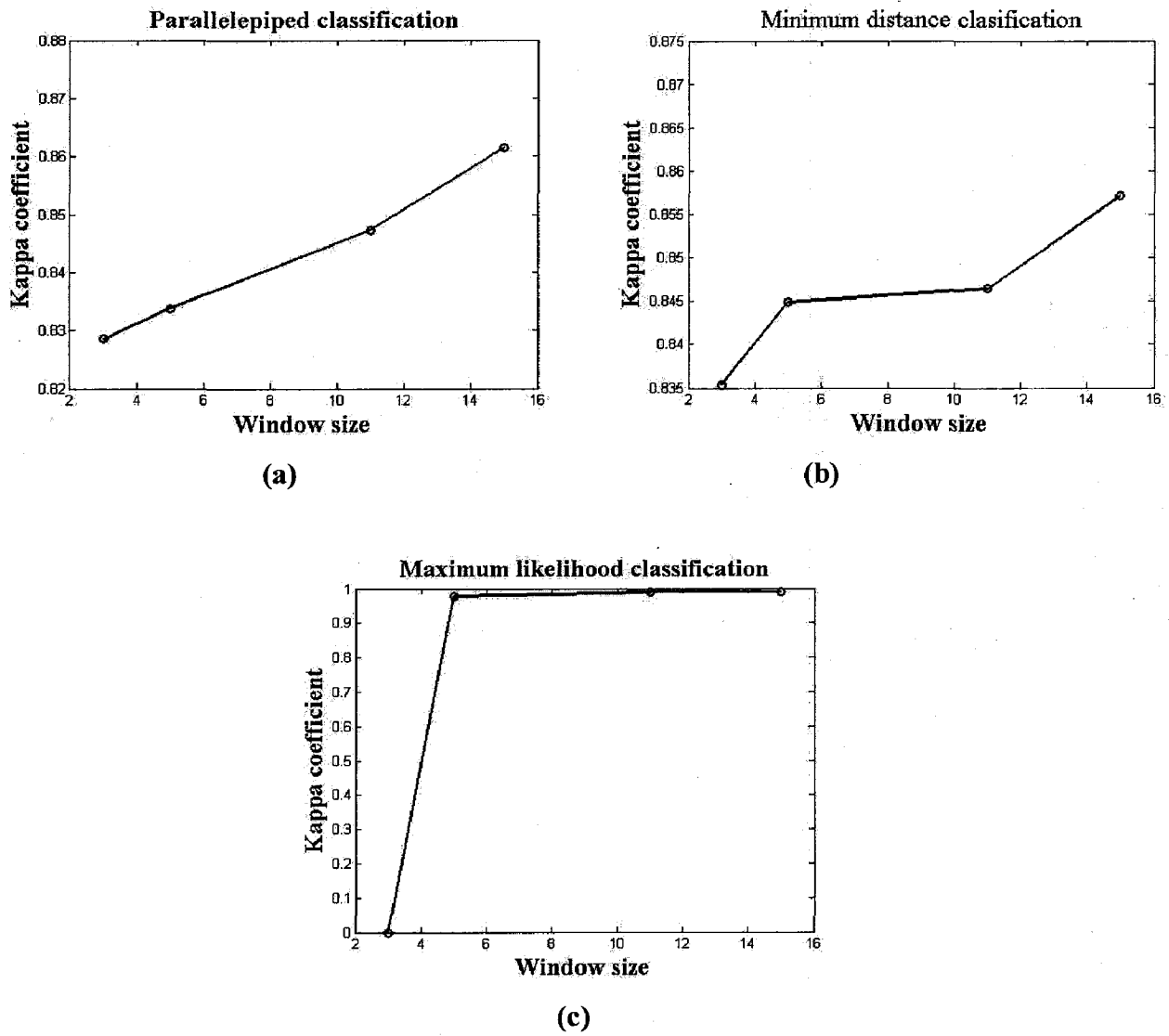

Figure–4.24: Kappa coefficient estimation of classification tests based on three D decomposition related to, (a) Parallelepiped, (b) Minimum distance, (c) Maximum Likelihood.

Overall accuracy is consistently high for averaging window 15x15 for all the classification techniques (ref. tables A-10, A-11 and A-12 of appendix-A). For minimum distance and parallelepiped classifiers overall accuracy increases monotonically, while for maximum likelihood classifier the classification accuracy rapidly increase at smaller window size and then becomes constant. The results verified previous works by Alberga [80] and Hodgson [81].Thus it is concluded that for ALOS PALSAR data 15x15 window size is suitable for classification.

4.3 Classification results

4.3.1 Results of decision tree classifier

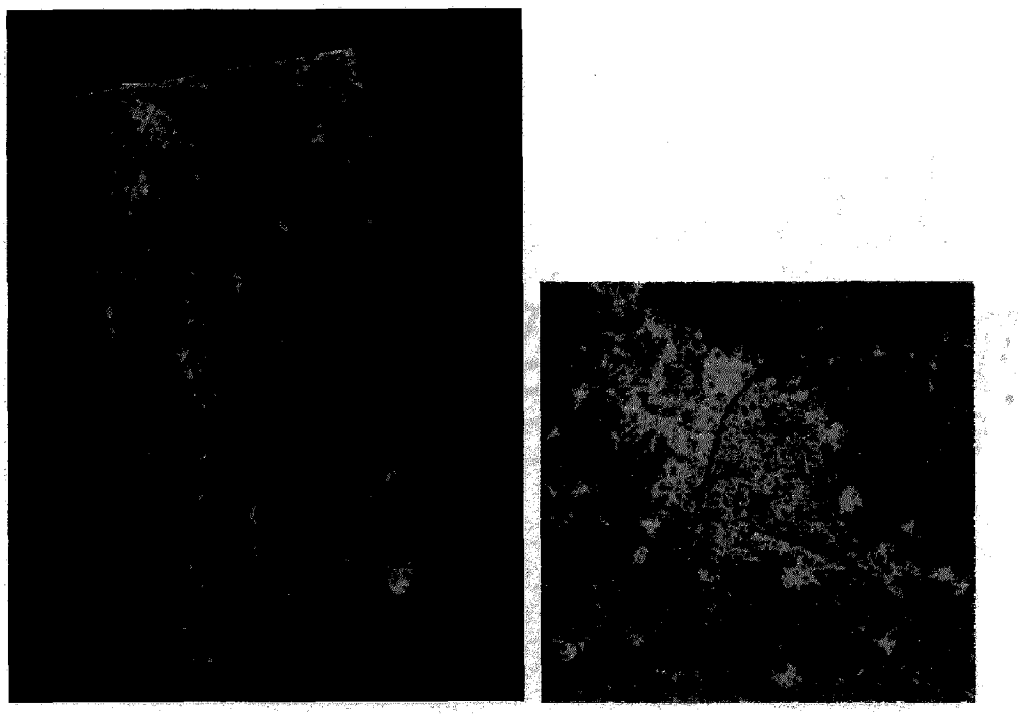

(a) (b)

Figure - 4.7: (a) Classification map based on decision tree classifier of test site, (b) Resized image showing region Roorkee (water-blue, urban-pink, baresoil-red, short vegetation-green, tall vegetation-cyan)

According to the classification scheme as described in section-3.4.1 (figure-3.7), the algorithm developed by ENVI 4.3 was run on pixel by pixel basis. The result of this classification scheme is shown in figure - 4.7(a) and 4.7(b) in which classification result can clearly be visualized. These figures show that most of the pixels belonging to specific field are classified as same category. We observe very coherent result for each of the individual fields.

The result of classification algorithm is calculated using confusion matrix (or error matrix), which compares the classification result with ground truth information and reports overall accuracy, kappa coefficient, producer accuracy and user accuracy. The confusion matrix for accuracy assessment is shown in table -4.1 (ref. table-3.4 for ROI's). The results in terms of producer's accuracy and user's accuracy is given in table A-1 of appendix –A. The overall classification accuracy is estimated as **88.0208%**and kappa coefficient as **0.8313**. The greatest error of commission occurs on short vegetation for which user accuracy is about 44.75 % because some of the pixels of class urban are misclassified as short vegetation as shown in table – 4.1.

Table -4.1

Confusion matrix for decision tree classification

Classes	Water	Tall veg.	Urban	Short veg.	Bare soil	Total
Water	298	0	0	17	20	335
Tall vegetation	0	67	2	0	0	69
Urban	0	2	208	0	0	210
Short vegetation	1	1	49	63	0	114
Bare soil	0	0	0	0	40	40

4.3.2 Results of classification based on three D decomposition

The results of classification tests based on three D decomposition are shown in figure-4.8. The accuracy estimate and kappa coefficient estimate for all three classification algorithms (parallelepiped, minimum distance and maximum likelihood) are shown in figure-4.9 (ref.-table- A-8,A-9 and A-10 for results using all window size).

The classification results based on 3 D decomposition are acceptable because kappa coefficient which describes the perfectness of classification is greater than 0.4.It is also worth mentioning it that kappa coefficient is greater than 0.75 for all the classification techniques, which shows excellent performance. The overall accuracy for all the classification tests is greater than 85%.

Maximum likelihood classifier performs best with maximum overall accuracy of about 99%. Maximum likelihood classifier performs best in classifying "water" and "vegetation" with 100% producer's accuracy. "Urban" is classified with maximum 99.34% producer's accuracy by parallelepiped classifier.

Note that the producer's accuracy for all the land cover type is greater than 32% (33.3% denotes perfect classification).

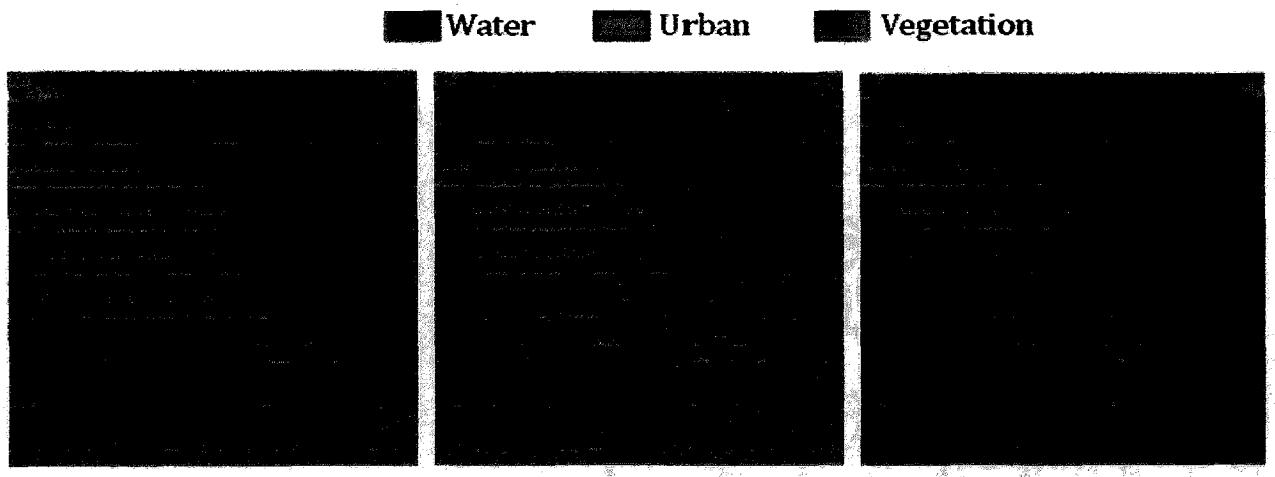

(a) (b) (c)

Figure - 4.8: Classification map based on 3 D decomposition (15x15- pixel averaging window): (a) Parallelepiped , (b) Minimum distance, (c) Maximum likelihood .

Table –4.2

Confusion matrix of classification based on three D decomposition (for 15x15 window size)

Classification	Water		Urban		Vegetation	
	P.A.	U.A.	P.A.	U.A.	P.A.	U.A.
Parallelepiped	84.19	100.00	99.34	93.50	86.67	75.58
Minimum distance	80.15	100.00	97.04	99.66	96.00	79.12
Maximum likelihood	100	100	97.73	100	100	97.44

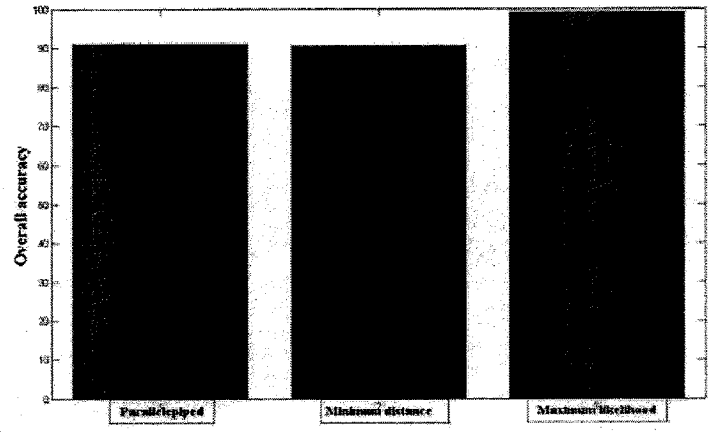

(a)

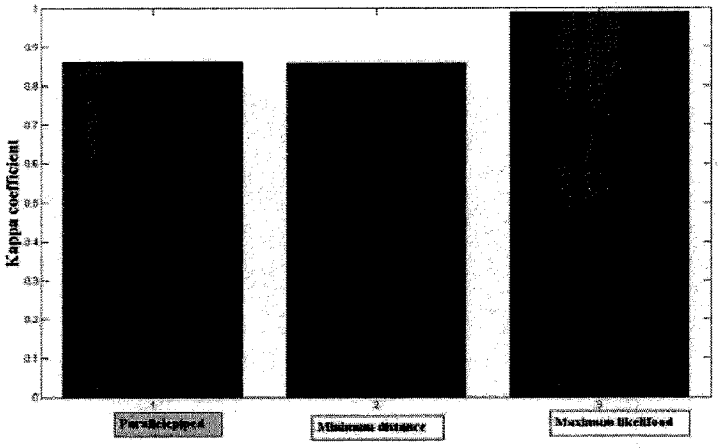

(b)

Figure-4.9: (a) Accuracy estimate, (b) Kappa coefficient estimate of classifications based on three D decomposition (15x15- pixel averaging window).

4.3.3 Results of classification based on Pauli decomposition

The classification map based on Pauli decomposition (ref. section-4.1.2) is shown in figure-4.10. The accuracy estimate and kappa coefficient estimate for all three classification algorithms (parallelepiped, minimum distance and maximum likelihood) are shown in figure-4.11. The confusion matrix which exhibits producer's accuracy in percent for classification tests based on Pauli decomposition is shown in table-4.3.

Maximum likelihood classifier gives maximum overall accuracy which is 71.54% while minimum classification accuracy is shown by Parallelepiped classifier. The kappa value is near 0.2 for parallelepiped classifier and greater than 0.4 for minimum distance and maximum likelihood classifiers.

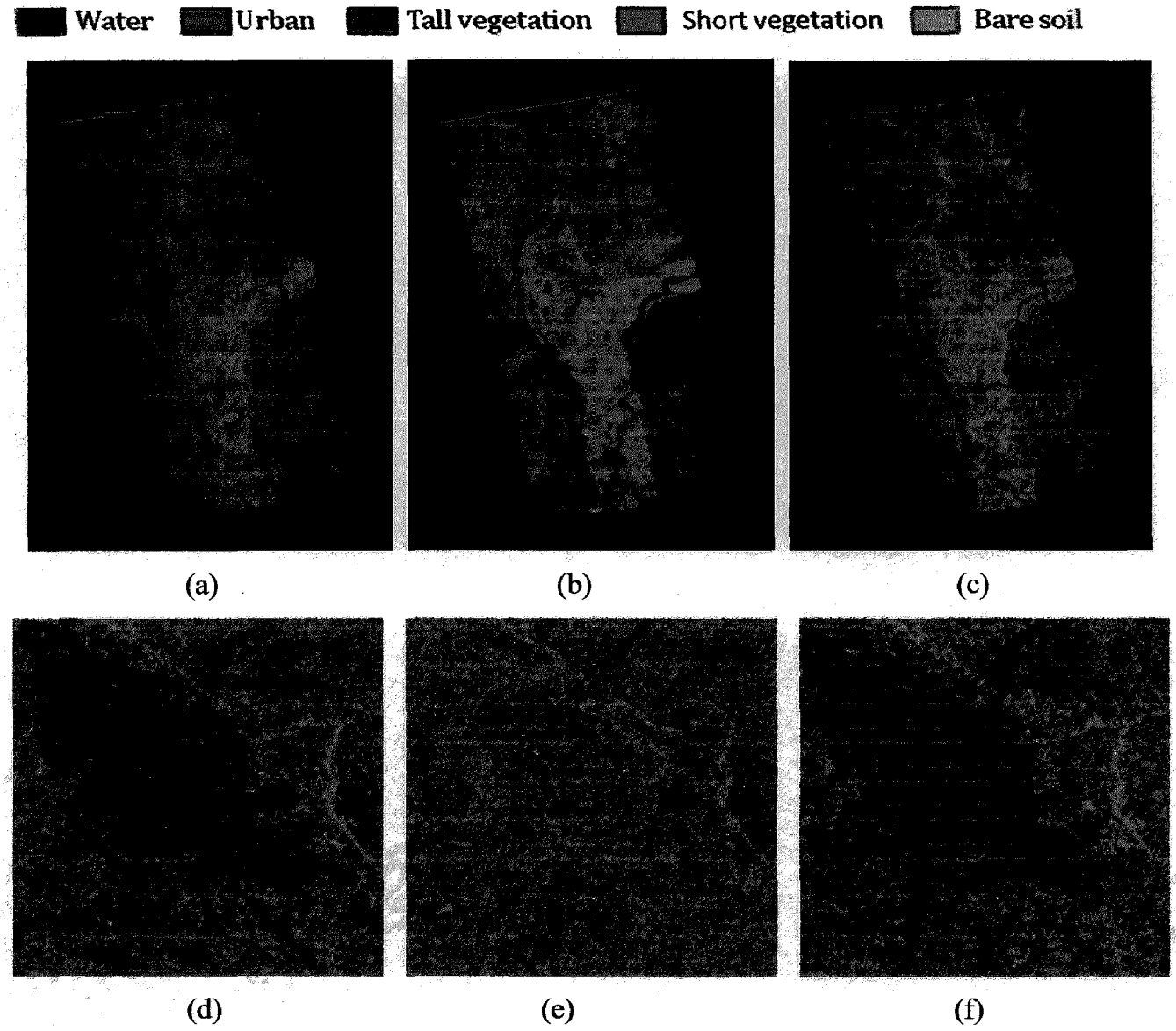

Figure - 4.8 : Classification map based on Pauli decomposition with (a) & (d) Parallelepiped with (d) resized image of region Roorkee, (b) & (e) Minimum distance with (e) resized image of region Roorkee , (c) & (f) Maximum likelihood with (f) resized image of region Roorkee.

Some limits are shown by parallelepiped classifier in classifying classes "water" and "urban". This classification technique completely fails in recognizing training pixels related to classes "water" and classifies class "urban" with producer's accuracy 3.77% only because the class "tall vegetation" is misclassified.

Maximum likelihood classifier identifies all the training pixels more accurately than others and classifies all land cover types with satisfactory performance indices, since each class

has producer's accuracy greater than 33.33%(table-A-4 of appendix). Minimum distance also shows almost same results. It classifies class "water" more accurately than maximum likelihood classifier, which somewhere is misclassified by maximum likelihood classifier (table-A-3 of app.).

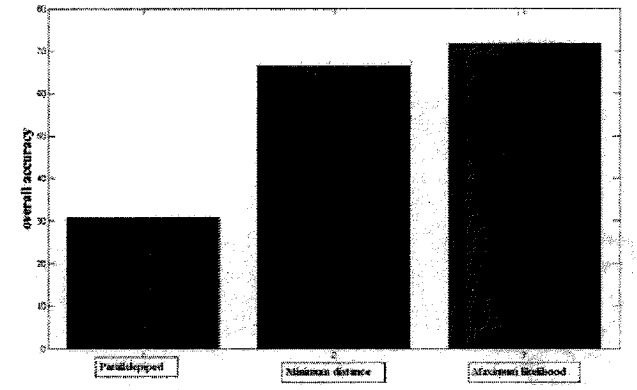

(a)

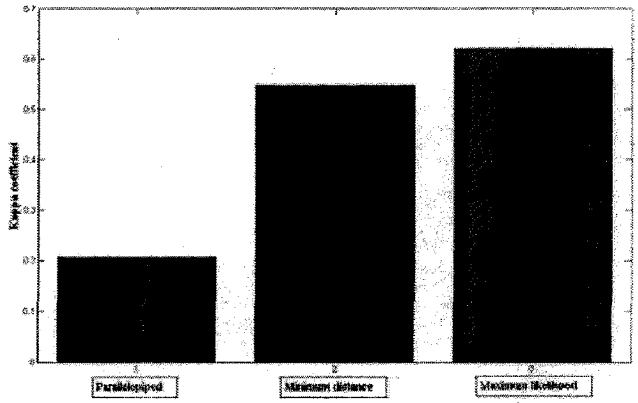

(b)

Figure -4.9: (a) Accuracy estimate and (b) Kappa coefficient estimate of classifications based on Pauli decomposition.

Table -4.3

Confusion matrix showing producer's accuracy in percent for classifications based on Pauli decomposition

Classification	Water	Tall veg.	Short veg.	Urban	Bare soil
Parallelepiped	0	98.57	93.43	3.77	75.76
Minimum distance	78.81	48.57	54.01	68.30	46.97
Maximum likelihood	59.60	34.29	73.72	91.32	81.82

4.3.4 Results of classification based on eigen value decomposition

The classification tests based on eigen value decomposition were performed in two series of experiments (ref. section-4.1.3). First series of experiment was performed using entropy (H) and alpha (α) as an input to classifier. The results of all three classification methods in terms of overall accuracy and kappa coefficient are shown in figure-4.13. The classification maps for this series of experiments are shown in figure-4.12. The confusion matrix is shown in table-4.4.

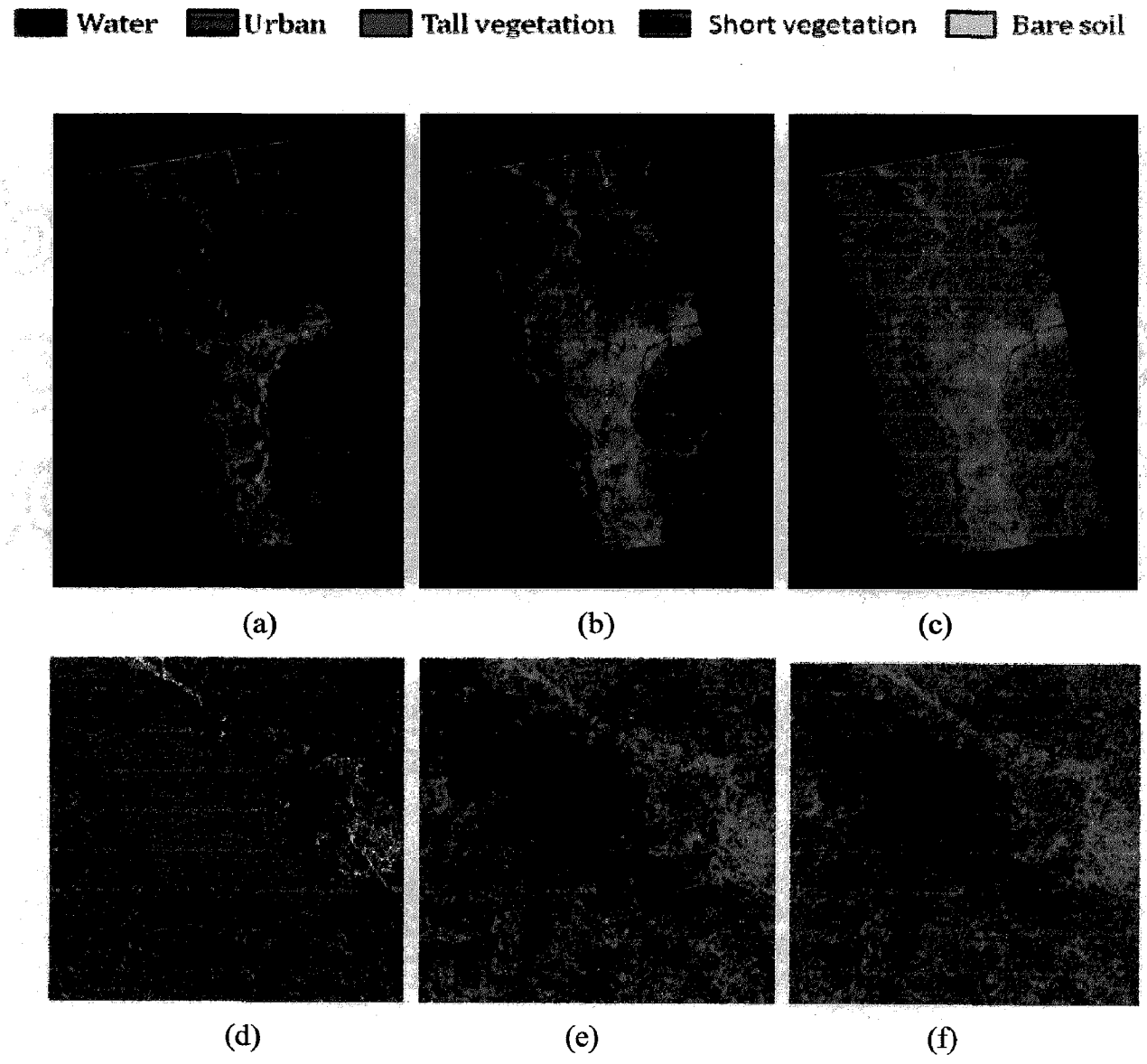

Figure -4.12 : Classification map based on eigen value decomposition (using parameters H/α): (a) & (d) Parallelepiped with (d) resized image of region Roorkee, (b) & (e) Minimum distance with (e) resized image of region Roorkee , (c) & (f) Maximum likelihood with (f) resized image of region Roorkee.

Table –4.4

Confusion matrix showing producer's accuracy for classification tests based on H/α

Classification	Water	Tall veg.	Short veg.	Urban	Bare soil
Parallelepiped	0	30.00	78.10	53.96	86.36
Minimum distance	17.88	80.00	37.96	43.02	93.94
Max. likelihood	11.26	55.71	52.55	56.98	93.94

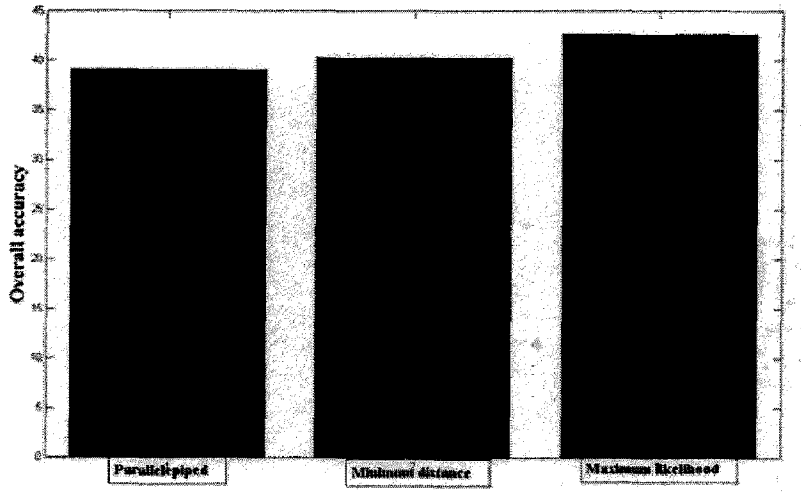

(a)

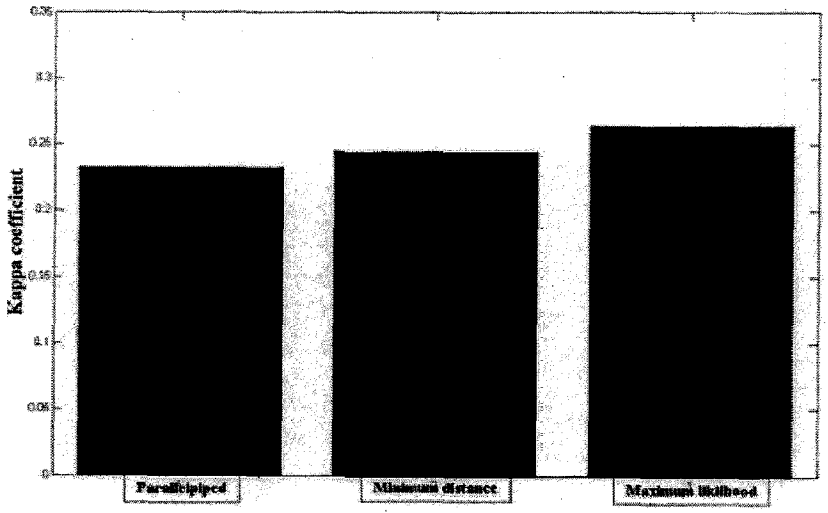

(b)

Figure – 4.13: (a) Accuracy estimate, and, (b) Kappa coefficient of classifications based on eigen value decomposition (using parameters H/α).

The second series of experiment was performed using all three eigen value parameters i.e. entropy (H) ,alpha (α) and anisotropy (A).Same procedure was adopted for this series and results of all the classifications in terms of overall accuracy and kappa coefficient are shown in figure 4.15.

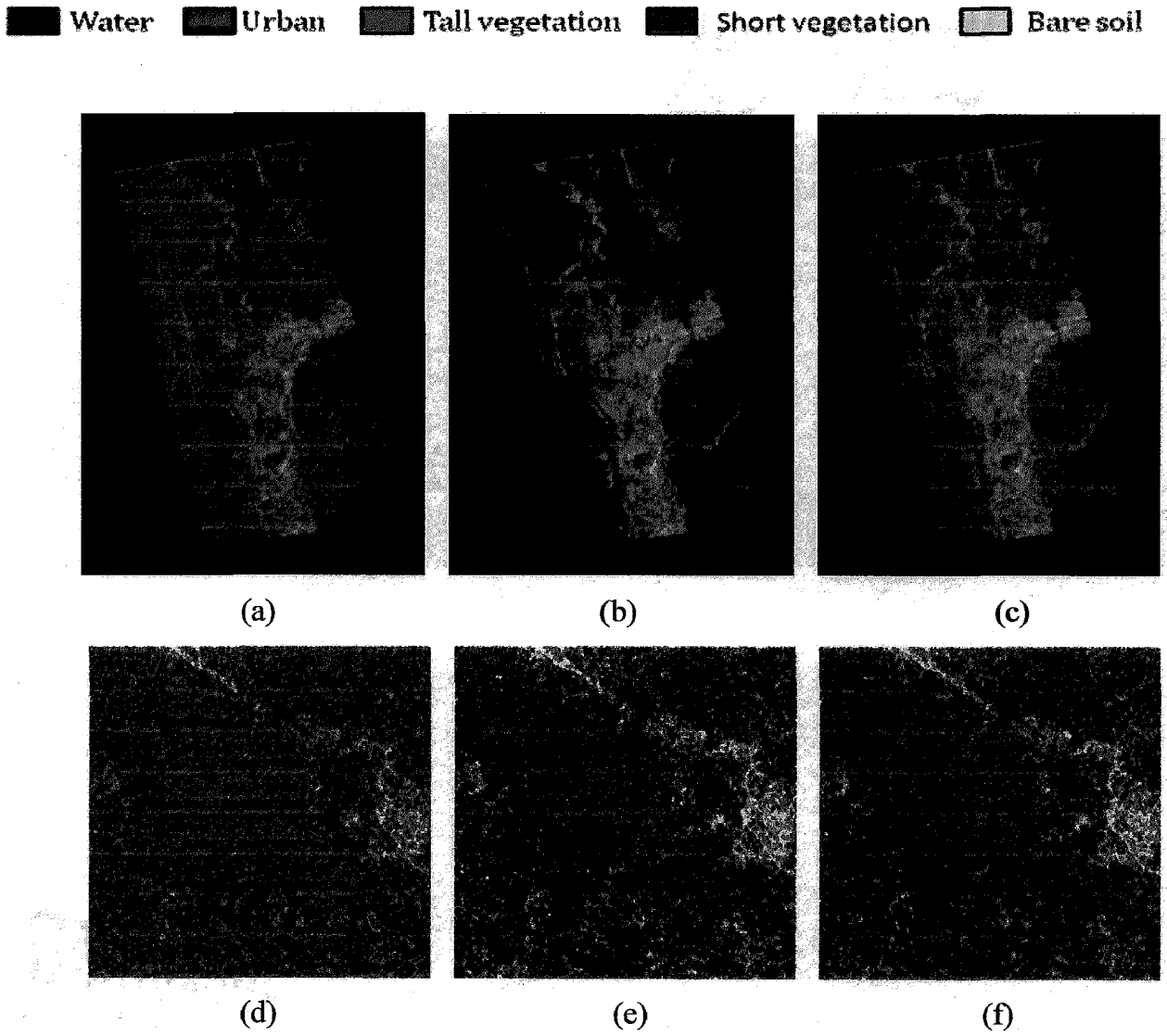

Figure–4.14:Classification map based on eigen value decomposition (using parameters H/A/α) related to (a) & (d) Parallelepiped with (d) resized image of region Roorkee, (b) & (e) Minimum distance with (e) resized image of region Roorkee , (c) & (f) Maximum likelihood with (f) resized image of region Roorkee.

In both the series of tests, overall accuracy remains low (around 40 %). The kappa coefficient, which is an indicator of performance of classification lies below 0.4 in all the cases. The classifications are not sensitive to additional anisotropy information. Rather, after including anisotropy as a parameter to classifiers, overall accuracy decreases slightly.

The parallelepiped classification based on parameters **H and α** fails to recognize "water" from training pixels. Class **"water"** is also poorly classified by minimum distance and maximum likelihood classifier with producer's accuracy of 17.88% and 11.26 % respectively. "Bare soil" is classified perfectly by all the classifiers.

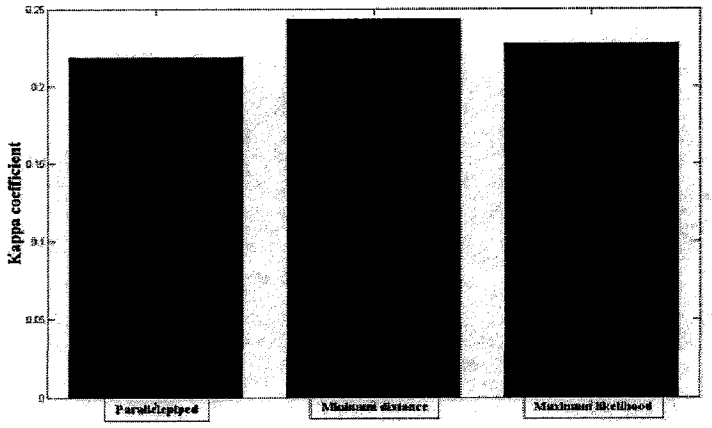

(a)

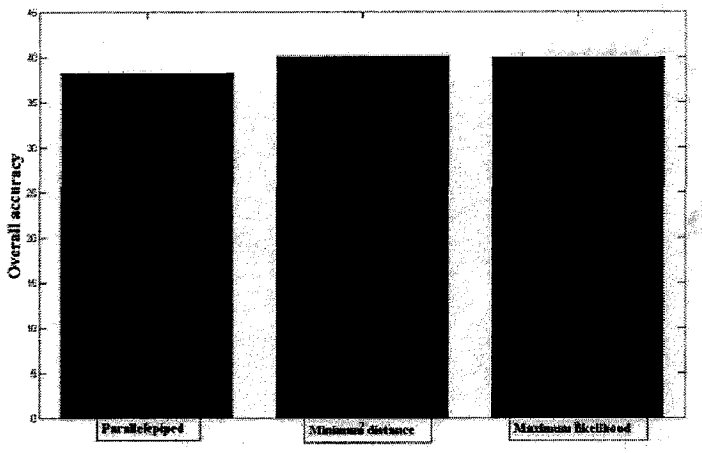

(b)

Figure – 4.15: (a) Accuracy estimate, and, (b) Kappa coefficient of classifications based on eigen value decomposition (using parameters H/A/α).

The visual analysis of classification maps reveals the fact that class "water" is either poorly classified or inseparable from other classes. Class "urban" is well defined in parallelepiped classification for both series of tests. In minimum distance classification "urban" and "tall vegetation" classes are mingled with each other.

For second series of test based on parameters **H, A and α,** parallelepiped classifier again performs poorly in classifying "water". The producer's accuracy for class water by

parallelepiped classification is only 0.33%.Class "bare soil" again classified correctly by all three classifiers. The confusion matrix for second series of tests is shown in table-4.5.

Table –4.5

Confusion matrix showing producer's accuracy for classification based on H/A/α

Classification	Water	Tall veg.	Short veg.	Urban	Bare soil
Parallelepiped	0.33	20.00	69.34	56.98	90.91
Minimum distance	17.88	80.00	37.96	43.02	92.42
Maximum likelihood	11.92	45.71	46.72	55.09	87.08

4.3.4.1 Results of classification of fused intensity images of various polarizations

4.3.4.2 Parallelepiped classification

The classification maps based on fusion of intensity images are shown in figure-4.16. Figure-4.17 is more elaborated version of figure -4.16, which is resized image of region Roorkee of size 400x400. The classification results in terms of overall accuracy and kappa coefficient are shown in figure-4.18. The overall accuracy for all the features greater than 40 % except the feature HH-VV for which the overall accuracy is about 20%. The kappa coefficient, which exhibits perfect classification performance for its value greater than 0.4, is less than 0.4 for most of the features except for the features LR-RR, LL-LR-RR, HH-HV-VV-LL-LR and HH-HV-VV-LL-LR-RR.

The parallelepiped classifier completely fails in recognizing class "water" from training pixels for all the features without any exception. The class "tall vegetation" is poorly classified for almost all the features except for the feature HH-HV for which the producer's accuracy is 40%.The class "bare soil" is classified satisfactorily by almost all the features except HH-VV, in which "bare soil" is misclassified due to wrong pixel assignment.

The classes "urban" and "short vegetation" show satisfactory classification performance. The feature HH-VV poorly classifies class "urban" with producer's accuracy of only 0.38%.

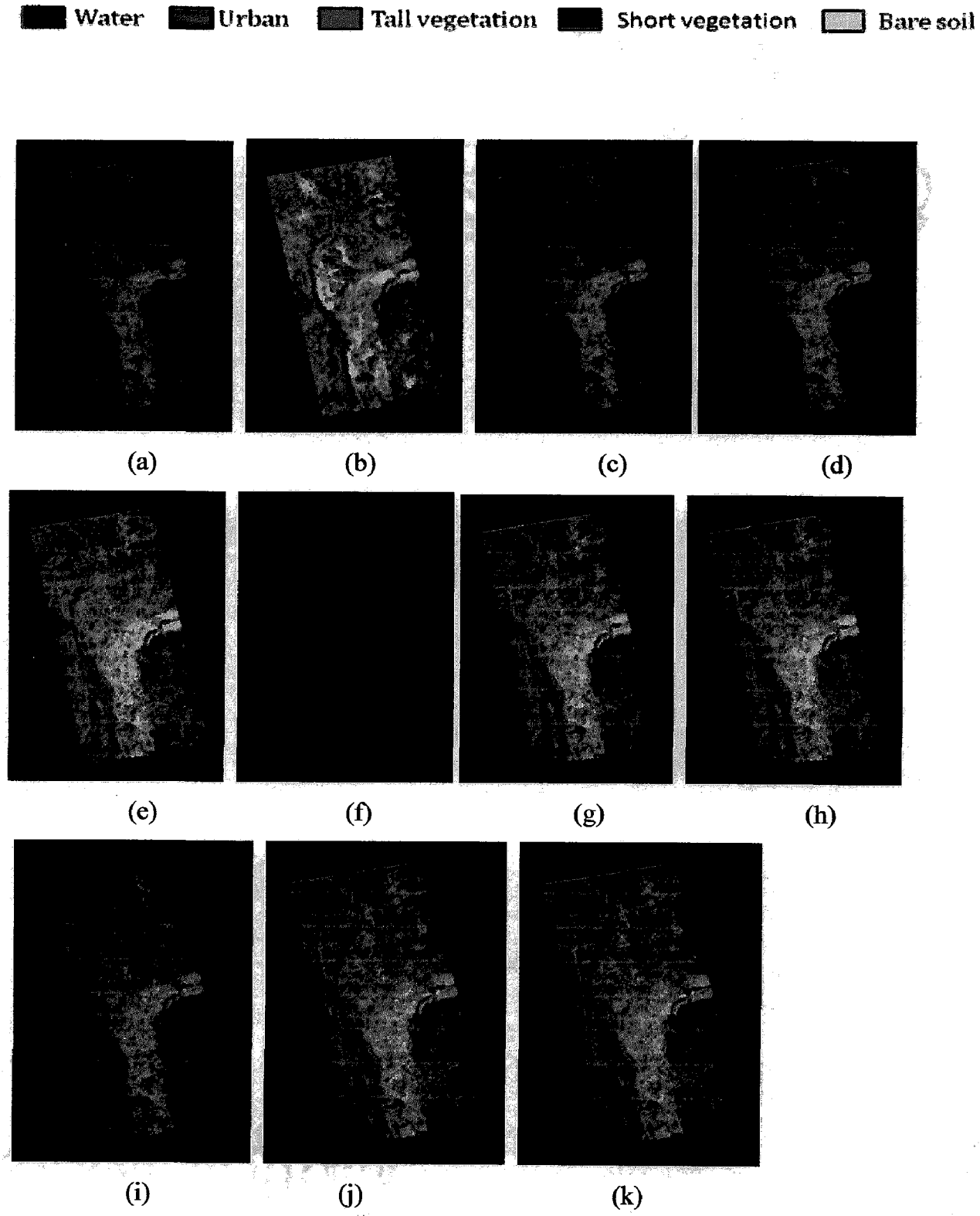

Figure -4.16 : Classification map based on fusion of intensity image of various polarizations by parallelepiped classification : (a)HH-HV,(b) HH-VV,(c)HV-VV,(d)HH-HV-VV,(e)LL-LR,(f)LL-RR,(g)LR-RR,(h)LL-LR-RR,(i)HH-HV-VV-LL,(j)HH-HV-VV-LL-LR,(k)HH-HV-VV-LL-LR-RR.

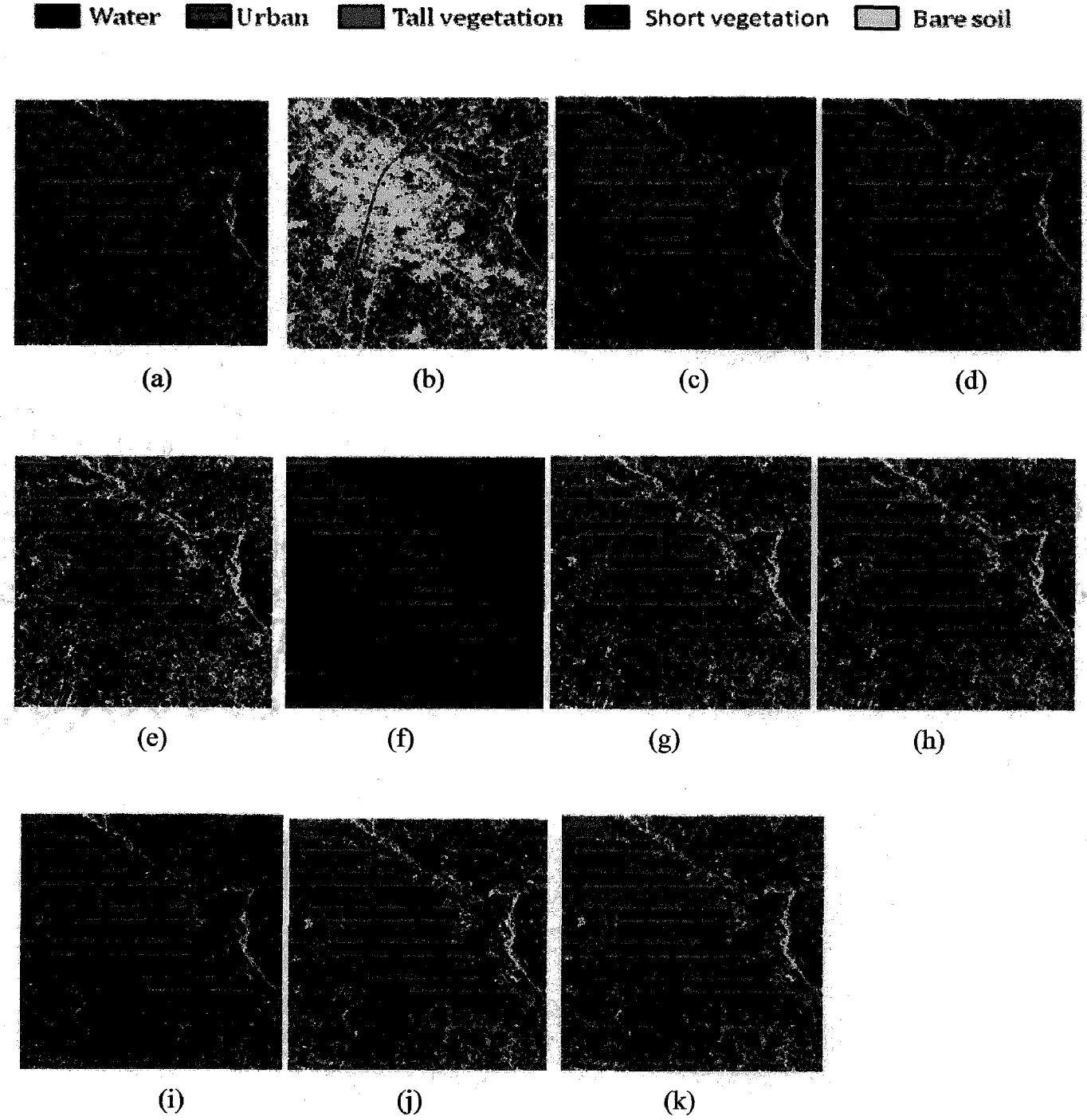

Figure -4.17: Classification map of resized images of region Roorkee based on fusion of intensity image of various polarizations by parallelepiped classification : (a)HH-HV, (b)HH-VV,(c)HV-VV, (d)HH-HV-VV, (e)LL-LR, (f)LL-RR, (g)LR-RR, (h)LL-LR-RR, (i)HH-HV-VV-LL,(j)HH-HV-VV-LL-LR,(k)HH-HV-VV-LL-LR-RR.

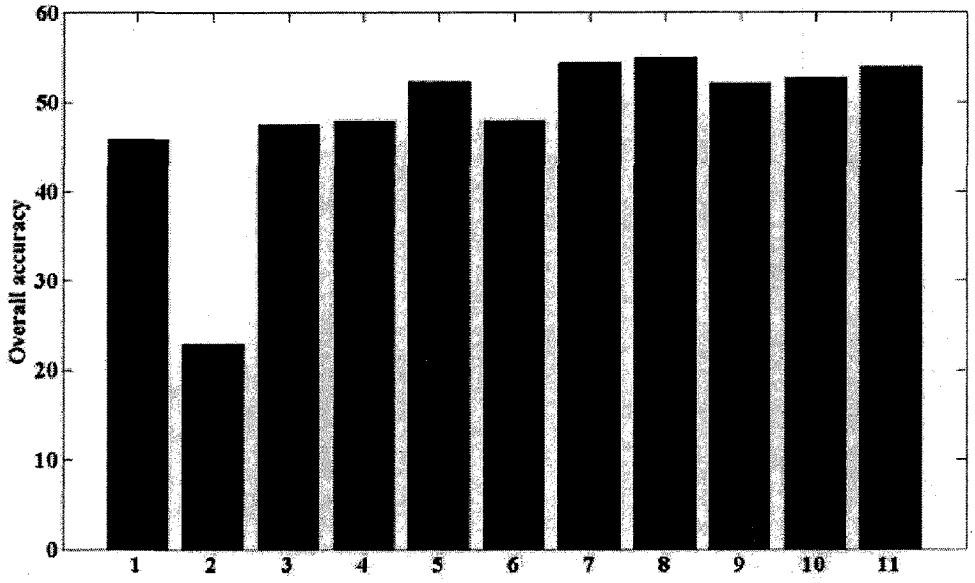

(a)

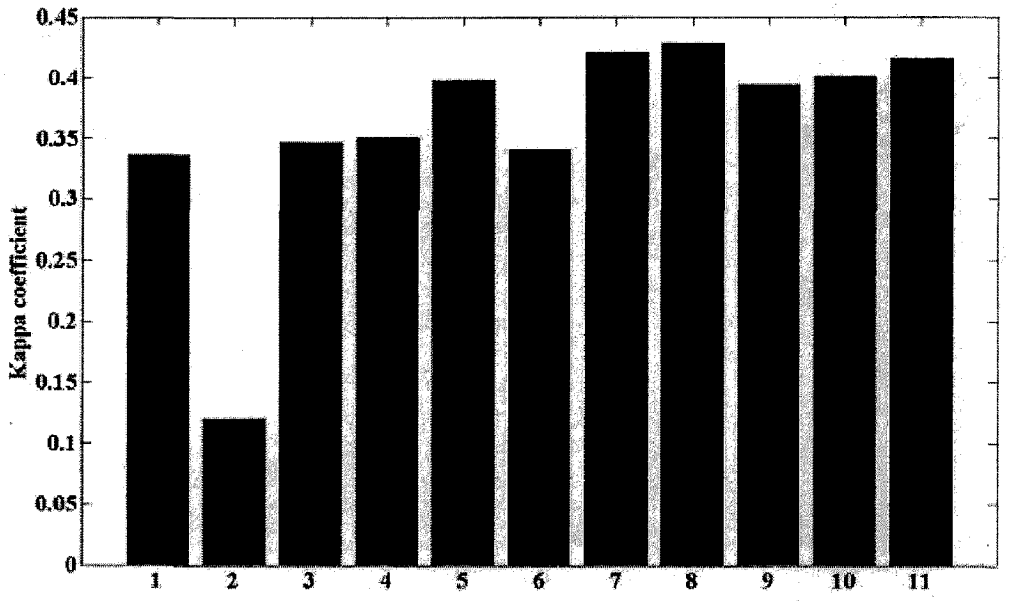

(b)

Figure – 4.18: (a) Accuracy estimate, (b) Kappa coefficient related to parallelepiped classifications based on fusion of intensity images of various polarizations:(1)HH-HV, (2)HH-VV,(3)HV-VV, (4)HH-HV-VV, (5)LL-LR, (6)LL-RR, (7)LR-RR, (8)LL-LR-RR, (9)HH-HV-VV-LL,(10)HH-HV-VV-LL-LR,(11)HH-HV-VV-

Table -4.6

Confusion matrix showing producer's accuracy for parallelepiped classification based on fusion of intensity images

Features	Water	Urban	Short veg.	Tall veg.	Bare soil
HH-HV	N.S.	64.91	99.27	40.00	74.24
HH-VV	N.S.	0.38	99.27	0.00	83.33
HV-VV	N.S.	74.34	99.27	15.71	83.33
LL-LR	N.S.	90.57	97.81	5.71	92.42
LL-RR	N.S.	90.19	100	37.14	0.00
LR-RR	N.S.	96.23	97.81	8.57	92.42
HH-HV-VV	N.S.	76.23	99.27	12.86	83.33
LL-LR-RR	N.S.	99.25	97.81	5.71	92.42
HH-HV-VV-LL	N.S.	90.57	99.27	8.57	83.33
HH-HV-VV-LL-LR	N.S.	92.83	97.81	1.43	92.42
HH-HV-VV-LL-LR-RR	N.S.	96.98	97.81	1.43	92.42

N.S.- not significant

4.3.4.3 Minimum distance classification

The classification maps based on fused intensity images by minimum distance classifier are shown in figure-4.19.The classification results in terms of overall accuracy and kappa coefficient are shown in figure-4.21.The classification results for minimum distance classifier are better than parallelepiped classifier. For almost all of the features the overall accuracy is greater than 70%, which is quiet satisfactory. The kappa coefficient is greater than 0.4 for all the features, which also exhibits good classification performance. The maximum overall accuracy of about 76% is obtained by feature HH-HV-VV-LL.

The class "water" is misclassified by features LL-LR, LL-LR-RR and LR-RR. These features recognize this class incorrectly from training pixels. This class is accurately classified

by features HH-VV and HV-VV. The class "water" has maximum producer's accuracy of about 92% for feature HV-VV.

The class "urban" is best classified by feature LL-RR having producer's accuracy of 93.21%. This class is misclassified by features HH-HV-VV-LL, HH-HV-VV-LL-LR and HH-HV-VV-LL-LR-RR.

The class "short vegetation" has maximum producer's accuracy by feature HH-HV. The feature LL-RR causes very low producer's accuracy (37.96%) for this class.

The minimum distance classifier does not perfectly distinguish classes "bare soil" and "tall vegetation" by training pixels. The producer's accuracy for these classes is very low as compared to other classes.

Table -4.7 which is shown below gives a general overview about classification results. The values in the table exhibit producer's accuracy for each class classified by taking one of the eleven features as input to minimum distance classifier.

Table -4.7

Confusion matrix showing producer's accuracy for minimum distance classification based on fusion of intensity images

Features	Water	Urban	Short veg.	Tall veg.	Bare soil
HH-HV	89.74	52.83	**91.97**	12.86	54.55
HH-VV	91.39	48.68	86.86	12.86	57.58
HV-VV	**92.05**	67.17	77.37	37.14	45.45
LL-LR	86.42	83.40	55.47	30.00	22.73
LL-RR	81.79	**93.21**	37.96	24.29	15.15
LR-RR	87.09	88.68	56.20	28.57	22.73
HH-HV-VV	90.7	75.09	85.40	12.86	39.39
LL-LR-RR	87.09	88.68	56.20	28.57	22.73
HH-HV-VV-LL	90.07	87.17	84.67	12.86	25.67
HH-HV-VV-LL-LR	91.39	86.42	81.75	12.86	13.64
HH-HV-VV-LL-LR-RR	89.74	88.68	79.56	15.71	12.12

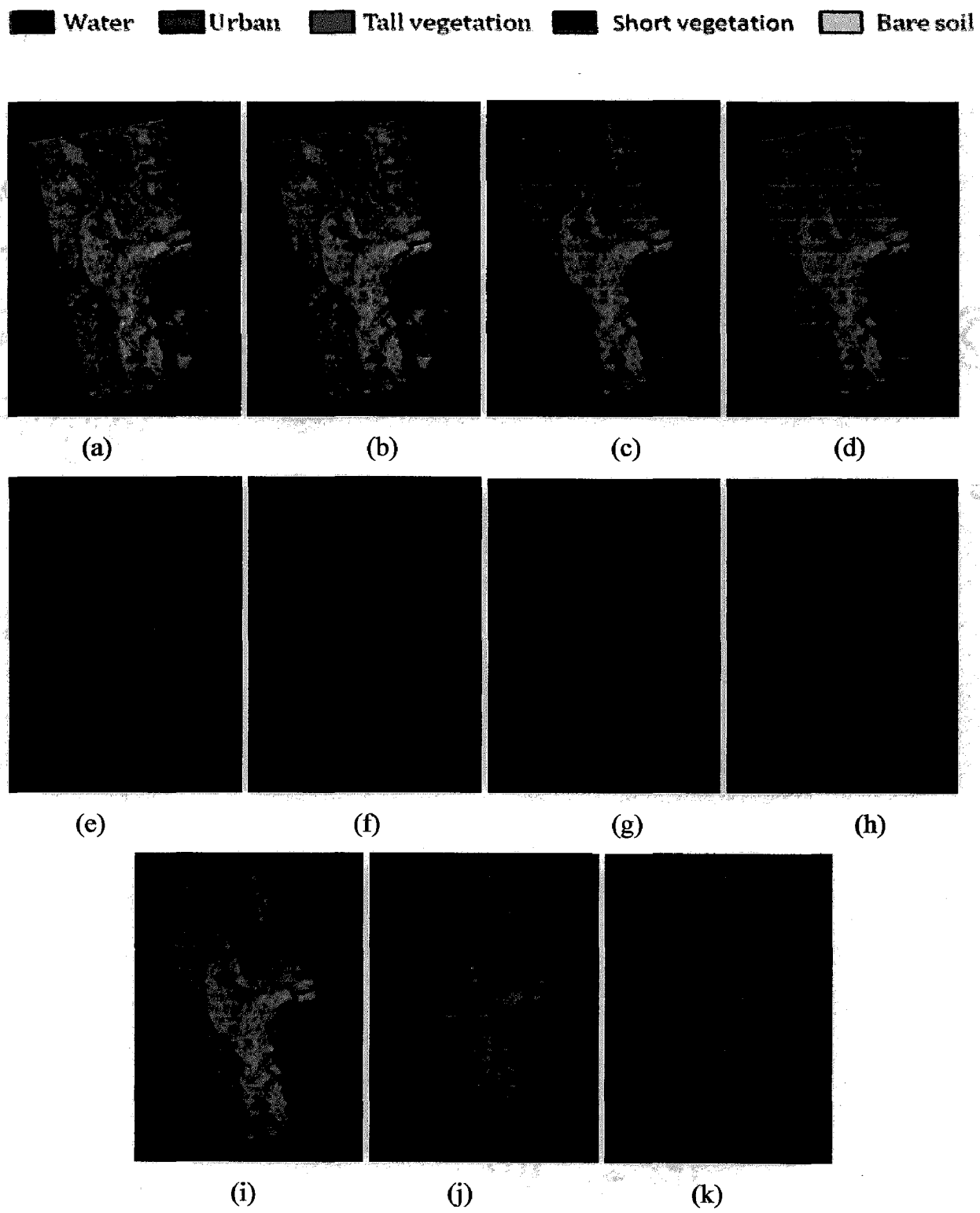

Figure -4.19 : Classification map based on fusion of intensity image of various polarizations by Minimum distance classification : (a)HH-HV,(b) HH-VV,(c)HV-VV,(d)HH-HV-VV,(e)LL-LR,(f)LL-RR,(g)LR-RR,(h)LL-LR-RR,(i)HH-HV-VV-LL,(j)HH-HV-VV-LL-LR,(k)HH-HV-VV-LL-LR-RR.

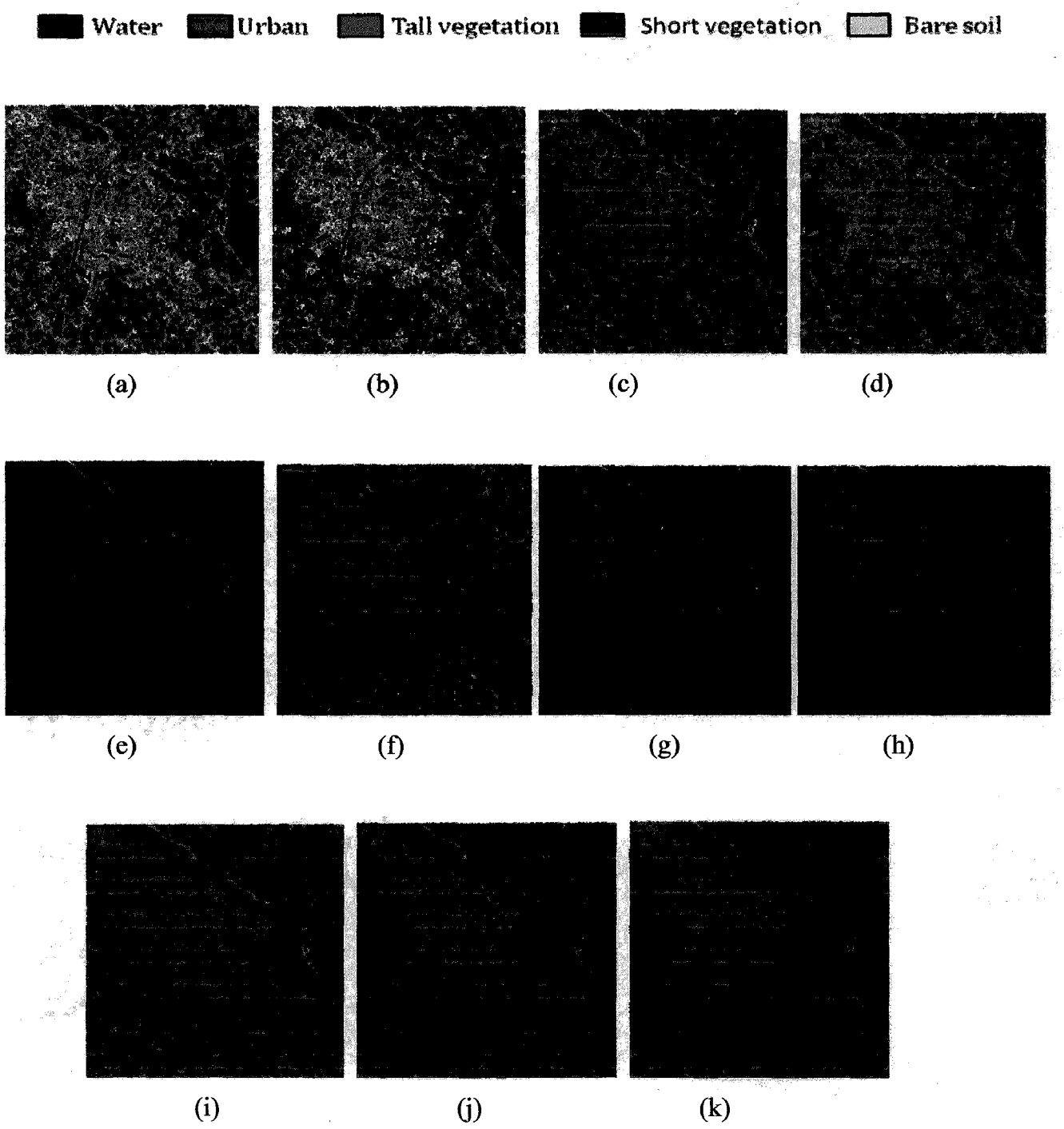

Figure -4.20 : Classification map of resized images of region Roorkee based on fusion of intensity image of various polarizations by Minimum distance classification : (a)HH-HV,(b)HH-VV,(c)HV-VV,(d)HH-HV-VV,(e)LL-LR,(f)LL-RR,(g)LR-RR,(h)LL-LR-RR, (i) HH-HV-VV-LL, (j)HH-HV-VV-LL-LR,(k)HH-HV-VV-LL-LR-RR.

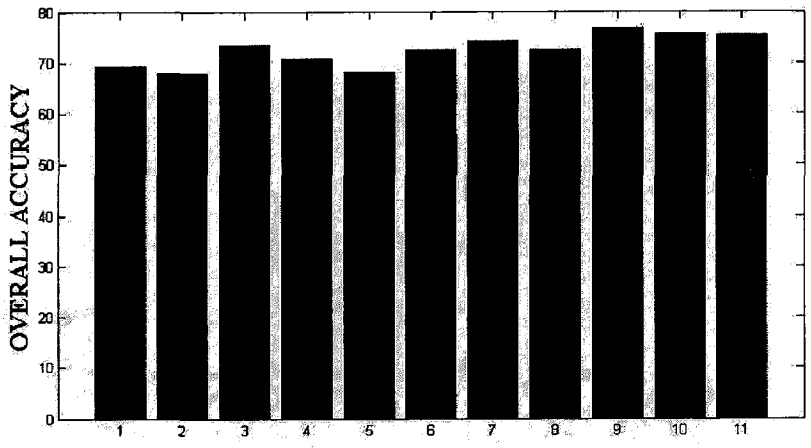

(a)

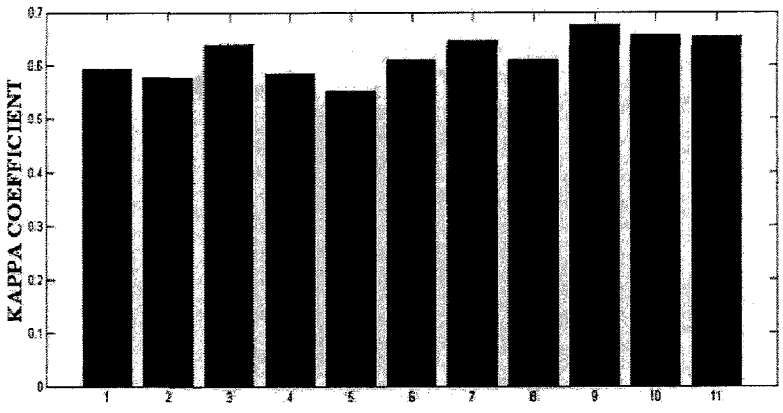

(b)

Figure – 4.21: (a) Accuracy estimate, (b) Kappa coefficient related to minimum distance classifications based on fusion of intensity images of various polarizations:(1)HH-HV, (2)HH-VV,(3)HV-VV, (4)HH-HV-VV, (5)LL-LR, (6)LL-RR, (7)LR-RR, (8)LL-LR-RR, (9)HH-HV-VV-LL,(10)HH-HV-VV-LL-LR,(11)HH-HV-VV-LL-LR-RR.

4.3.4.4 Maximum likelihood classification

The classification maps based on fused intensity images related to maximum likelihood classifier are shown in figure-4.22.The classification results in terms of overall accuracy and kappa coefficient are shown in figure-4.24 (ref. table-A-12). The classification results in terms of overall accuracy and kappa coefficient are better than minimum distance classification. For almost all of the features the overall accuracy is greater than 70%, except for feature LL-RR which has minimum overall accuracy of about 57%. The kappa coefficient is greater than 0.4

for all the features even for feature LL-RR. The maximum overall accuracy of about 86% is obtained by feature HH-HV-VV.

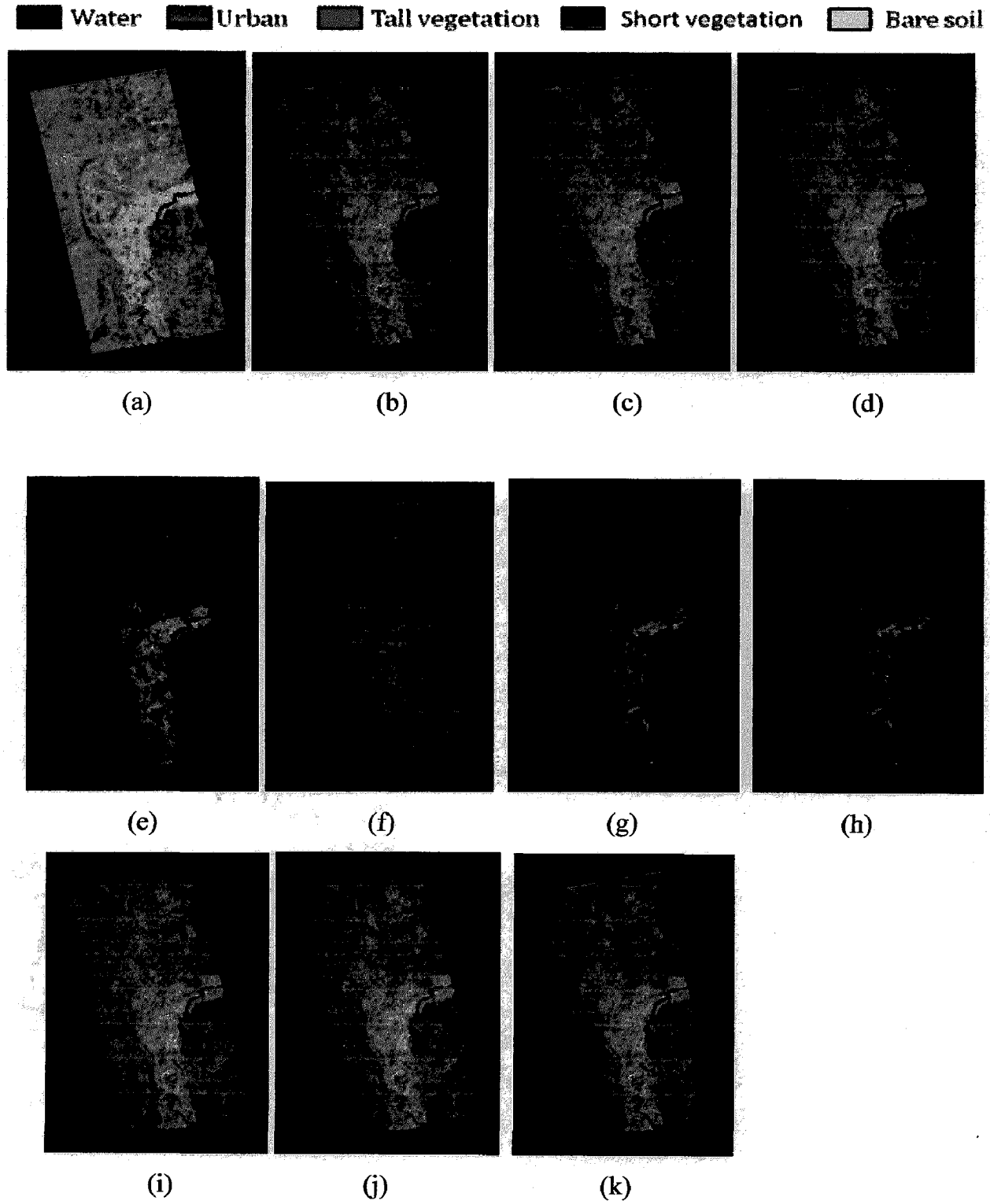

Figure -4.22 : Classification map based on fusion of intensity image of various polarizations by Maximum likelihood classification : (a)HH-HV,(b) HH-VV,(c)HV-VV,(d)HH-HV-VV,(e)LL-LR,(f)LL-RR,(g)LR-RR,(h)LL-LR-RR,(i)HH-HV-VV-LL,(j)HH-HV-VV-LL-LR,(k)HH-HV-VV-LL-LR-RR.

Table -4.8

Confusion matrix showing producer's accuracy for maximum likelihood classification based on fusion of intensity images

Features	Water	Urban	Short veg.	Tall veg.	Bare soil
HH-HV	90.07	75.09	86.13	4.29	80.30
HH-VV	**97.68**	90.94	82.48	27.14	**90.91**
HV-VV	95.36	82.64	**87.59**	35.71	89.39
LL-LR	72.85	91.70	81.02	51.43	87.88
LL-RR	32.12	95.09	67.88	31.43	30.30
LR-RR	7285	96.23	78.10	**64.29**	90.91
HH-HV-VV	96.36	90.94	85.40	20.00	90.91
LL-LR-RR	72.85	**96.60**	78.83	54.29	89.29
HH-HV-VV-LL	92.72	92.83	85.40	21.43	**90.91**
HH-HV-VV-LL-LR	91.39	92.83	81.02	41.43	89.39
HH-HV-VV-LL-LR-RR	89.40	95.85	81.75	31.43	92.42

The class "water" is misclassified by features LL-LR, LL-LR-RR and LR-RR, just like minimum distance classification. The producer's accuracy is maximum for class 'water" in feature HH-VV.

The class "urban" is best classified by feature LL-LR-RR having producer's accuracy of 96.60%. This class is misclassified by features HH-HV-VV-LL, HH-HV-VV-LL-LR and HH-HV-VV-LL-LR-RR.

The class "short vegetation" has maximum producer's accuracy by feature HV-VV. The maximum likelihood classifier does not perfectly distinguish class "tall vegetation" using feature HH-HV for which the producer's accuracy is only 4.29 %. The producer's accuracy for this class is below satisfactory level (< 33.33%) for various features, namely HH-HV, HH-VV,

HV-VV, HH-HV-VV, LL-RR, HH-HV-VV-LL and HH-HV-VV-LL-LR-RR. The maximum producer's accuracy for this class is obtained by feature LR-RR.

The maximum likelihood classifier fails to recognize class "bare soil" from its training pixels for feature LL-RR. The producer's accuracy for this feature is only 30.30%.

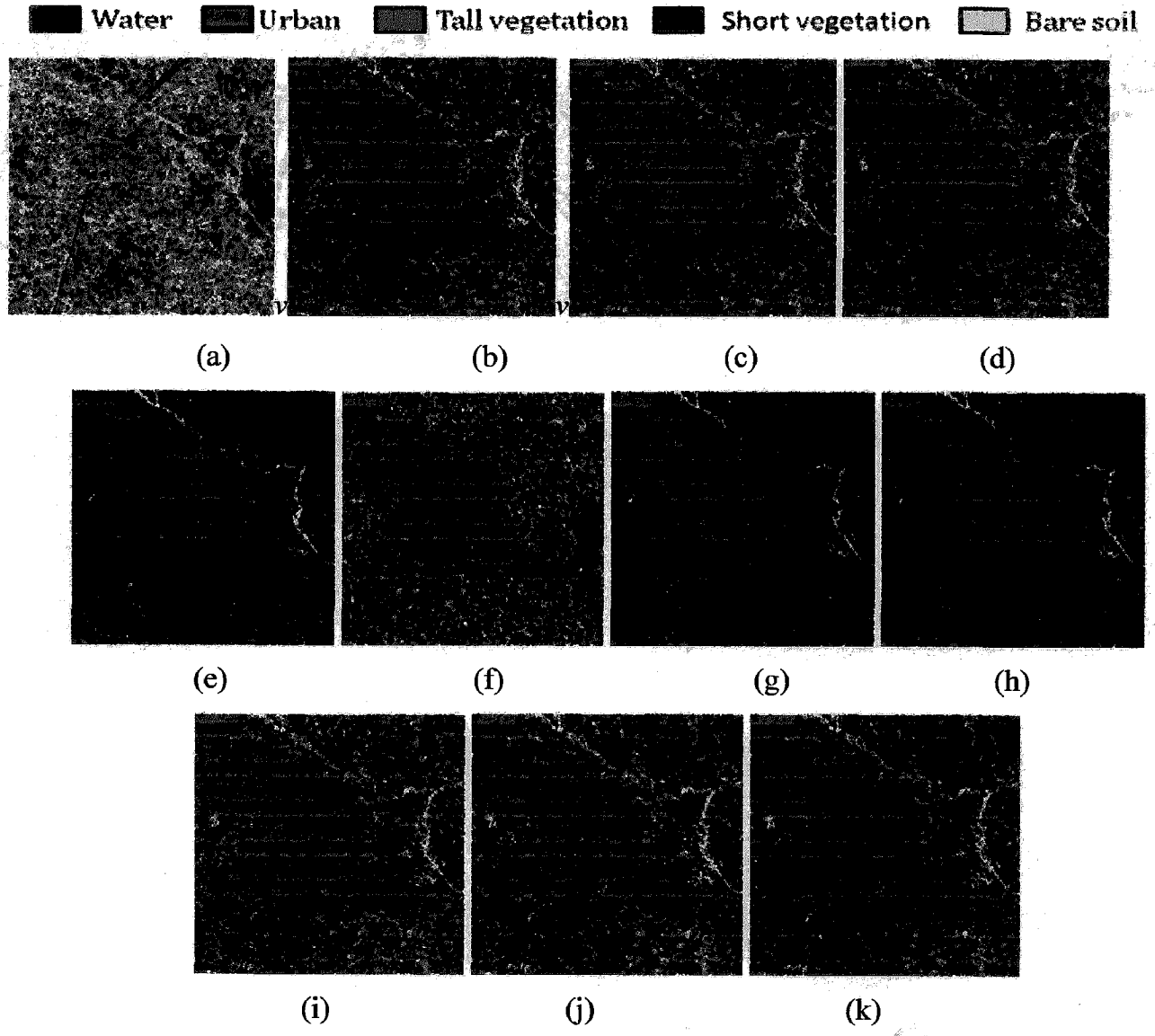

Figure -4.23: Classification map of resized images of region Roorkee based on fusion of intensity image of various polarizations by Maximum likelihood classification : (a)HH-HV, (b)HH-VV,(c)HV-VV, (d)HH-HV-VV, (e)LL-LR, (f)LL-RR, (g)LR-RR, (h)LL-LR-RR, (i)HH-HV-VV-LL,(j)HH-HV-VV-LL-LR,(k)HH-HV-VV-LL-LR-RR.

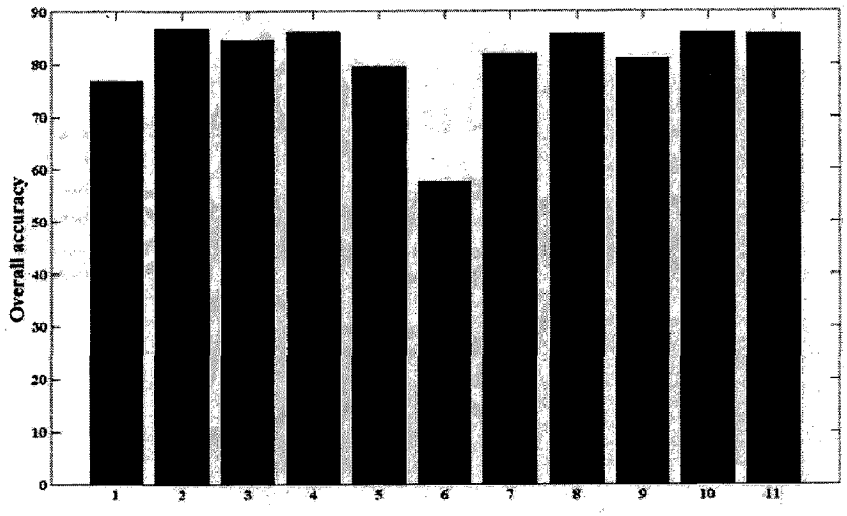

(a)

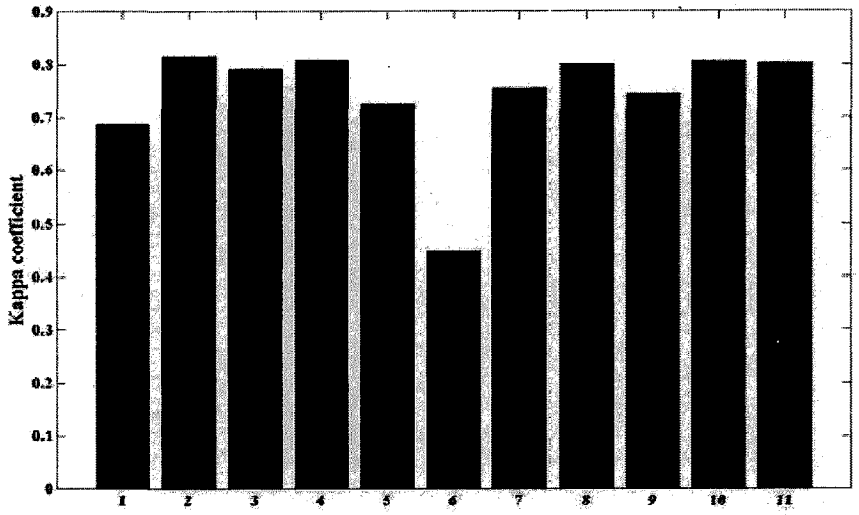

(b)

Figure-4.24: (a) Accuracy estimate, (b) Kappa coefficient related to maximum likelihood classifications based on fusion of intensity images of various polarizations: (1)HH-HV, (2)HH-VV,(3)HV-VV, (4)HH-HV-VV, (5)LL-LR, (6)LL-RR, (7)LR-RR, (8)LL-LR-RR, (9)HH-HV-VV-LL,(10)HH-HV-VV-LL-LR,(11)HH-HV-VV-LL-LR-RR.

CHAPTER 5. COMPARISON OF RESULTS

The results are summarized in table-5.1 giving general overview of results discussed in previous chapter. Since all the classifications were performed on single data set, therefore it is possible to compare all the results on common ground. The results indicate a trend that is reasonable to assume valid for similar data set. The results are compared in terms of overall accuracy and kappa coefficient of agreement. The classification is declared perfect if overall accuracy is greater than 33.33% and kappa coefficient is greater than 0.4.

Two classification techniques were adopted: parametric and non – parametric. Parametric classification were performed over various polarimetric features (here: Pauli coefficient, H/A/α H/α, and 11 backscattered intensities) using three supervised classification algorithms: parallelepiped, minimum distance and maximum likelihood. All the classification algorithms were performed using software ENVI.

The results show that non- parametric classifier i.e. decision tree classifier performs best as compared to others. This is due to the fact that this classifier is implemented with thorough knowledge of data obtained by empirical evidence and experimental validation which does not require any prior assumption to be made.

In non-parametric case, maximum likelihood classifier performs best as compared to minimum distance and parallelepiped classifiers. The possible reason is following: the maximum likelihood classifier is based on Bayesian probability theory which uses second order statistics unlike minimum distance and parallelepiped classifiers which adopt first order statistics. It also assumes that input data (training data) is normally distributed and independent. The classifications based on H/A/α and H/α give worst results for all three classification algorithms. The possible reason of the poor result is the use of boxcar filter for speckle removal. The boxcar filter causes sharp edges to be blurred and transforms point scatterer to spread target due to over-filtering.

The classification results also depend on choice of training data. Sometimes it may happen that some ground cover types are not well recognized by the classifier and cause bad classification accuracy.

Comparison between single pixel and averaged pixel shows that ensemble averaging of image pixels give improved classification result than single pixel. The classification accuracy

actually increases by increasing averaging window size. This means that PALSAR data is correlated and physical properties associated with data spread over neighbourhood pixel.

Table-5.1

Classification performance estimate in terms of overall accuracy and kappa coefficient

Class. algo. ⟶	Max. Likelihood		Min. Distance		Parallelepiped	
Pol. parameters ↓	O.A (%)	Kappa	O.A (%)	Kappa	O.A (%)	Kappa
Pauli coefficients	71.5476	0.6203	66.4286	0.5469	30.5952	0.2075
H/A/α	40.000	0.2772	40.1190	0.2431	38.2143	0.2186
H/α	42.6190	0.2643	40.238	0.2444	39.0476	0.2325
HH-HV	76.7857	0.6860	69.2857	0.5930	45.8333	0.3352
HH-VV	86.6667	0.8153	67.9762	0.5772	22.8571	0.1196
HV-VV	84.6429	0.7898	73.5714	0.6388	47.5000	0.3467
LL-LR	79.5238	0.7235	70.7143	0.5832	52.2619	0.3976
LL-RR	57.6190	0.4477	68.2143	0.5515	47.8571	0.3406
LR-RR	81.7857	0.7357	72.6190	0.6084	54.2857	0.4209
HH-HV-VV	86.0714	0.8071	74.1667	0.6441	47.8571	0.3499
LL-LR-RR	85.4762	0.7997	72.6190	0.6084	55.0000	0.4279
HH-HV-VV-LL	81.0714	0.7429	76.7857	0.6744	52.0238	0.3935
HH-HV-VV-LL-LR	85.8330	0.8054	75.5952	0.6552	52.6190	0.4005
HH-HV-VV-LL-LR-RR	85.5952	0.8015	75.4762	0.6527	53.9286	0.4152
DECISION TREE	O.A.- 88.0208%			Kappa -0.8313		

CHAPTER 6. CONCLUSIONS

6.1 Concluding remarks

This work started with the aim of gaining knowledge about SAR observables from PALSAR data. Therefore various classification algorithms were applied in order to see the possible differences among the SAR polarimetric observables in terms of amount of information they contain and their usefulness in classifying particular land cover type. The comparison among various classification techniques was done in terms of classification accuracy and kappa coefficient of agreement.

The non- parametric classifier give better classification results as compared to parallelepiped, minimum distance and maximum likelihood classifiers. The decision tree classifier recognizes all land cover types more accurately from training pixel than parallelepiped, minimum distance and maximum likelihood classifiers. For latter the classification depends on choice of training data and classification statistics, which sometimes causes poor result to occur. The bad performance of parametric classifiers occurs due to two reasons: when some land cover types are not recognized by the classifier or when wrong statistical parameters are given to classifier.

Thus in spite of using supervised classification algorithms (parallelepiped, minimum distance, and maximum likelihood), we can refer the proposed classification algorithms based on decomposition method as **semi-supervised**. The reason of referring these methods as semi-supervised is that segmentation of image was done by decomposition method (like unsupervised) and then class labeling was done by using training data (like supervised).

It is also seen that the classification efficiency of parametric classifiers is improved by ensemble averaging of image pixels. Larger window size produces better classification accuracy than smaller window size.

The effect of filtering was also seen by performing three D decomposition by using two data: non-filtered but multilooked and polarimetric filtered multilooked. It has been verified that polarimetric filtering is not fully capable of preserving linear features of flat terrain like Roorkee.

6.2 Future scope

Possible future research could include replicating the whole study by writing own codes for all classification algorithms because in this whole study the inbuilt algorithms of software ENVI and SARSCAPE were used for supervised classification techniques. Some constraints were found in eigen value decomposition method of inbuilt module of SARSCAPE; like it uses boxcar filter which loses some useful information about point scatterers due to over-filtering. It is expected that result may improve if all the classification algorithms are developed by own.

Another suggestion for future research is in the area of speckle filtering. Some limitations were found in filtering module of SARSCAPE. For speckle reduction wavelet filters and curvelet filters will be much effective because of their capability of edge preservation.
Future addition of this research will also involve collection of more ground truth survey points. The collected points would be used to increase both the number of training sample as well as number of points used for accuracy assessment. An increased number of training and testing ground truth sample points would improve classification accuracy.

REFERENCES:

[1] Floyed F. Sabins, *Remote Sensing Principles And Interpretation*, W.H. Freeman & Co., New York.

[2] H. Zebker, and VanZyl , "Imaging Radar Polarimetry: A Review", *Proceedings of the IEEE*, vol. 79, no. 11, 1991.

[3] Pottier et al., 'Bistatic radar polarimetry theory,' chapter 14 in James D. Taylor (ed.), *Ultra wideband radar technology*, CRC press, e-book ISBN-978-1-4200-3729-6, 2001.

[4] J. Fransis Reintjes et al., *Principles of Radar,* third edition, McGraw-Hill book company, Inc., New York, 1952.

[5] Parul Patel , H. S. Srivastava, and R. R. Navalgund, "Use of synthetic aperture radar polarimetry to characterize wetland targets of Keoladeo National Park, Bharatpur, India," Research article ,*Current Science*, vol. 97, no. 4,pp. 529-537, 2009.

[6] W. M. Boerner, E. Pottier, S. Cloude, "Extra-wide-band Polarimetry, Interferometry & Polarimetric Interferometry in Synthetic Aperture Remote Sensing", International Symposium on Antennas and Propagation, , ACROS Fukoka, Japan, 2000.

[7] E. Luneburg, "Aspects of radar polarimetry," *Turk J. Ele.c Engin*, vol.10, no.2, pp. 219-243, 2002.

[8] R. Touzi, W.M. Boerner, J.S. Lee, and E. Lueneburg, "A review of polarimetry in the context of synthetic aperture radar: concepts and information extraction," *Can. J. Remote Sensing*, vol. 30, no.3, pp. 380–407, 2004.

[9] Sinclair, "Transmission and reception of elliptically polarized waves," *Proceedings of the IRE*, vol. 38, pp. 148–151, 1950.

[10] Deschamps, "Part II- Geometrical representation of polarization of plane magnetic wave," *Proceedings of IRE*, vol. 39, pp. 540-544, 1951.

[11] Kennaugh, "Polarization properties of radar reflections," M. Sc. Thesis, The Ohio State university, Columbus, Ohio, 1952.

[12] C.D. Graves, "Radar polarization power scattering matrix," Proceedings of the IRE, vol. 44, pp. 248–256, 1956.

[13] Copeland, J. R., "Radar target classification by polarization properties," *Proceedings of the IRE*, vol. 48, pp.1290-1296, 1960.

[14] G.A. Ionnidis et al. "Optimum antenna polarizations for target discrimination in clutter," *IEEE Transactions on Antennas and Propagation*, vol. AP-27, pp. 357–363, 1979.

[15] W. M. Boerner, M. B. El-Arini, C. Y. Chan, and P. M. Mastoris, "Polarization dependence in electromagnetic inverse problems," *IEEE Transactions on Antennas and Propagation*, AP-29, pp. 262-271, 1981.

[16] A.P. Agrawal, and W. M. Boerner, "Redevelopment of Kennaugh's target characteristic polarization state theory using the polarization transformation ratio for the coherent case," *IEEE Transactions on Geoscience and Remote Sensing*, GE-27, pp. 2-14, 1988.

[17] S. R. Cloude and E. Pottier, "A review of target decomposition theorems in radar polarimetry," *IEEE Transaction on Geoscience and Remote Sensin.*, vol. 34, no. 2, pp. 498–518, 1996.

[18] S. R. Cloude and E. Pottier, "An entropy based classification scheme for land applications of polarimetric SAR," *IEEE Trans. Geosci. Remote Sens.*, vol. 35, no. 1, pp. 68–78, Jan. 1997.

[19] E. Pottier, "Radar target decomposition theorems and unsupervised classification of full polarimetric SAR data," *IEEE Proceedings*, pp. 1139-1141, 1994.

[20] J.S. Lee, M.R. Grunes, R. Kwok, "Classification of multi-look polarimetric *SAR* imagery based on the complex Wishart distribution," *International Journal* of *Remote Sensing*, vol. 15, ,no. 11, pp. 2299-2311,1994.

[21] J.S. Lee, M.R. Grunes, T.L. Ainsworth, L. Du, D.L. Schuler and S.R. Cloude "Unsupervised classification of polarimetric *SAR* images by applying target decomposition and complex Wishart distribution," *IEEE Trans. on Geoscience and Remote Sensing*, vol.37, no.5, pp. 2249-2258, 1999.

[22] J.S. Lee, M.R. Grunes, Eric Pottier, and L. Ferro-Famil "Unsupervised terrain classification preserving polarimetric scattering characteristics," vol. 42, no. 4, 2004.

[23] Ferro-Famil, E. Pottier, and J.S. Lee, "Unsupervised classification of multi-frequency and fully polarimetric SAR images based on the H/A/Alpha-Wishart classifier," *IEEE Transactions on Geoscience and Remote Sensing*, vol. 39, no. 11, pp. 2332–2342, 2001.

[24] E. Pottier and Ferro Famil, "Dual frequency polarimetric SAR data classification and analysis," *Progress In Electromagnetics Research*, PIER 31, pp.247–272, 2001.

[25] M Ouarzeddine, and B Souissi, "Unsupervised Classification Using Wishart Classifier," *USTHB, F.E.*BP no. 32, El Alia Bab Ezzouar, Alger.

[26] Cao Fang, Hong Wen, Wu Yirong, "An improved Cloude-Pottier decomposition using H/α/span and complex Wishart classifier for polarimetric SAR classification," *International Conference on Radar*, 2006.

[27] Sang-Eun Park, and W. M. Moon "Unsupervised classification of scattering mechanisms in polarimetric SAR data using fuzzy logic in entropy and alpha plane," *IEEE Trans. Geosci. Remote Sensing*, vol. 45, no. 8, pp. 2652-2664, 2007.

[28] J. Praks, E. C. Koeniguer, and M. T. Hallikainen, "Alternatives to Target Entropy and Alpha Angle in SAR Polarimetry," *IEEE Trans. Geosci. Remote Sensing* , vol. 47, no. 7, pp. 2262-2274, 2009.

[29] J.S. Lee, M.R. Grunes, and E. Pottier, "Quantitative Comparison of Classification Capability: Fully Polarimetric Versus Dual and Single-Polarization SAR," *IEEE Trans. Geosci. Remote Sensing*, vol. 39, no. 11, 2001

[30] A. Freeman and S. L. Durden, "A three-component scattering model for polarimetric SAR data," *IEEE Trans. Geosci. Remote Sens.*, vol. 36, no. 3, pp. 963–973, 1998.

[31] Yoshio Yamaguchi, Toshifumi Moriyama, Motoi Ishido, and Hiroyoshi Yamada, "Four-component scattering model for polarimetric SAR image decomposition", *IEEE Transactions on Geoscience And Remote Sensing*, vol. 43, no. 8, pp. 1699- 1706, 2005.

[32] Yoshio Yamaguchi, Yuki Yajima, and Hiroyoshi Yamada, "A four-component decomposition of POLSAR images based on the coherency matrix," *IEEE Transactions on Geoscience And Remote Sensing Letters,* vol. 3, no. 3, pp. 292-296, 2006.

[33] Yuki Yajima, Yoshio Yamaguchi, Ryoichi Sato, Hiroyoshi Yamada, and W. M. Boerner, "POLSAR image analysis of wetlands using a modified four-component scattering power decomposition," *IEEE Transactions on Geoscience and Remote Sensing,* vol. 46, no. 6, pp. 1667-1673, 2008.

[34] Lamei Zhang, Bin Zou, Hongjun Cai, and Ye Zhang "Multiple-component scattering model for polarimetric SAR image decomposition," *IEEE Trans. Geosci. Remote Sens. Letters*, vol. 5, no. 4, 2008.

[35] Lamei Zhang, Bin Zou ,Junping Zhang and Ye Zhang, "An extended multiple-component scattering model for PolSAR images," *International Journal of Remote Sensing*, vol. 30, no. 21, pp. 5515–5525, 2009.

[36] M. Mahmudur Rahman, Josaphat Tetuko Sri Sumantyo, "ALOS PALSAR data for tropical forest interpretation and mapping," *The International Archives of the Photogrammetry, Remote Sensing and Spatial Information Science,* vol. xxxvii, part b,2008.

[37] J. W. Goodman, "Some fundamental properties of speckle," *J. Opt. Soc. Amer. 66,* No. 11, pp. 1145-1150, 1976.

[38] J. S. Lee, "Speckle analysis and smoothing of synthetic aperture radar images," *Computer Graphics and Image Process*, vol. 17, pp. 24-32, 1981.

[39] J. S. Lee, M. R. Grunes, and G. de Grandi, "Polarimetric SAR speckle filtering and its implication on classification," *IEEE Trans. Geosci. Remote Sens.*, vol. 37, no. 5, pp. 2363–2373, 1999.

[40] V. S. Frost, et al. "A model for radar image and its application to adaptive digital filtering of multiplicative noise," *IEEE Transactions on Geoscience and Remote Sensing*, vol. 4, no.2, pp. 157-166, 1982.

[41] Yongwei Sheng and Zong-Guo Xia, "A comprehensive evaluation of filters for radar speckle suppression," *Proc. IGARSS- 96*, vol. 3, pp.1559-1561, 1996.

[42] E. Nezry, F. Yakam Simen, "On the preservation of polarimetric signatures and polarimetric texture signatures by fully polarimetric MAP filters," *Geoscience and Remote Sensing Symposium, IGARSS '99, Proceedings, IEEE International*, 1999.

[43] F. N. S. Medeiros, et al. "Evaluating an adaptive windowing scheme in speckle noise map filtering," SIBIGRAP2002, Fortaleza Brazil, pp. 281-285, 2002.

[44] W. M. Boerner, "Recent Advances in Polarimetry and Polarimetric Interferometry," *Geoscience and Remote Sensing Symposium, IGARSS '06, Proceedings, IEEE International*, pp. 49-51, 2006.

[45] W. M. Boerner et al., 'Polarimetry in Radar Remote Sensing: Basic and Applied Concepts,' Chapter 5 in F. M. Henderson, and A.J. Lewis, (ed.), *Principles and Applications of Imaging Radar*, vol. 2 of Manual of Remote Sensing, Third Edition, John Willey & Sons, New York, 1998.

[46] W. M. Boerner et al., "Determination of the characteristic polarisation states of the radar target scattering matrix [S(AB)] for the coherent, monostatic and reciprocal propagation space using the polarisation ratio," in *Direct and Inverse Methods in Radar Polarimetry, Kluwer Academic Publishers*, Netherlands, Kluwer Academic Publishers, pp. 297-349,1992 .

[47] W. M. Boerner, W-Ling Yan, An-Qing XI, and Y. Y, "On the basic principles polarimetry: the target of radar characteristic polarization state theory of Kennaugh, Huynen's polarization fork concept, and its extension to the partially polarized case," *IEEE Proceedings*, vol. 79, no. 10, pp. 1538-1550,1991.

[48] Guissard, "Mueller and Kennaugh matrices in radar polarimetry," *IEEE Transactions on Geoscience and Remote Sensing*, vol. 32, no. 3, pp. 590–597, 1994.

[49] W.M. Boerner and J. Morisaki, A. Danklmayer and Madhu Chandra, "On the statistical aspects of radar polarimetry, " *Geoscience and Remote Sensing Symposium, IGARSS '05, Proceedings, IEEE International*, vol. 3, pp. 1995 - 1998, 2005.

[50] C. M. H. Unal and L. P. Ligthart, "Decomposition theorems applied to random and stationary radar targets," *Progress In Electromagnetics Research*, PIER 18, pp. 45–66, 1998.

[51] Lamei Zhang, Junping Zhang, Bin Zou, and Ye Zhang, "Comparison of methods for target detection and applications using polarimetric SAR image," *PIERS online*, vol. 4, no. 1, pp. 140-145, 2008.

[52] S. R. Cloude, E. Pottier, W. M. Boerner, "Unsupervised Image Classification using the Entropy/Alpha/Anisotropy Method in Radar Polarimetry," *NASA-JPL, AIRSAR-02 Earth Science and Application Workshop*, 2002.

[53] S. R. Cloude, 'Polarimetry in Wave Scattering Applications', Chapter 1.6.2 in R Pike, P Sabatier (eds.), *Scattering*, vol. 1, Academic Press, 2001.

[54] S. R. Cloude, "Uniqueness of Target Decomposition Theorems in Radar Polarimetry," in W.M. Boerner et al. *(eds.), Direct and Inverse Methods in Radar Polarimetry*, Part 1, NATO-ARW, Kluwer Academic Publishers , ISBN 0-7923-1498-0, pp 267-296, 1992.

[55] Varsha Turkar and Y.S. Rao, "Classification of Polarimetric Synthetic Aperture Radar Images from SIR-C and ALOS PALSAR," *Proceedings of International Conference on Microwave – 08*, 2008.

[56] Brandt Tso, Paul Mather, *Classification Methods for Remotely Sensed Data*, 2nd ed. CRC Press, Taylor & Francis Group, LLC, 2009.

[57] Lillesand, M.T., and Kiefer, R.W., *Remote Sensing and Image Interpretation*, Fourth Edition. John Wiley & Sons, New York, 2000.

[58] J.A. Richards, *Remote Sensing Digital Image Analysis*, Springer-Verlag, Berlin, 1999.

[59] Moth'd Belal, and Al-Daoud, "A New Algorithm for Cluster Initialization," *J. World Academy of Science, Engineering and Technology*, 2005.

[60] J.M.Pena, J.A. Lozano, P. Larranaga, "An empirical comparison of four initialization methods for the K-Means algorithm," *Pattern Recognition Letters*, vol. 20, pp.1027-1040, 1999.

[61] N. Venkateswarlu, and P. Raju, "Fast isodata clustering algorithms," *Pattern recognition*, vol. 25 (3), pp. 335-342, 1992.

[62] Mahesh Pal, Paul M. Mather, "Decision tree based classification of remotely sensed data," *22nd Asian Conference on Remote Sensing*, 2001.

[63] Mahesh Pal, Paul M. Mather, "An assessment of the effectiveness of decision tree methods for land cover classification," *Remote Sensing of Environment*, vol. 86, no. 4, pp.554–565, 2003.

[64] Swain, P. H., and H. Hauska, 'The decision tree classifier: Design and potential," *IEEE Transactions on Geoscience and Remote Sensing*, vol.15, pp. 142–147, 1977.

[65] S. Rasoul Safavian and David Landgrebe, "A Survey of Decision Tree Classifier Methodology," IEEE Transactions on Systems, Man, and Cybernetics, *IEEE Transactions on Systems, Man, and Cybernetics*, vol. 21, no. 3, pp 660-674, 1991.

[66] Congalton, R.G., "A review of assessing the accuracy of classification of remotely sensed data," *Remote Sensing of Environment*, vol. 37, pp. 35–46, 1991.

[67] Gebhard Banko, "A review of assessing the accuracy of classifications of remotely sensed data and of methods including remote sensing data in forest inventory," *INTERIM REPORT IR-98-081 International Institute for Applied Systems Analysis*, 1998.

[68] Yoshio Yamaguchi, W. M. Boerner, Jian Yang, Ryoichi Sato, and Hiroyoshi Yamada, "ALOS-PALSAR quad. pol. images and their applications," *Proceedings IEEE*, 2009.

[69] C.P. Régis, Marques et al. "Filtering Effects on SAR Images Segmentation," *Springer-Verlag*, Berlin Heidelberg, LNCS 3124, pp. 1041–1046, 2004.

[70] SARSCAPE help document.

[71] P.Ferrazzoli et al., "The potential of multi-frequency polarimetric SAR in assessing agricultural and arboreous biomass," *IEEE Trans. Geosci. Remote Sensing*, vol.35, no.1, pp.5-17, 1997.

[72] H. Skriver, J. Dall, T. Le Toan, et al., "Agriculture classification using POLSARdata," in Proceedings of the 2nd International Workshop on Applications of SAR Polarimetry and Polarimetric Interferometry (POLinSAR '05), 2005.

[73] Ferrazzoli, P., L. Guerriero and G. Schiavon, "Experimental and model investigation on radar classification capability," *IEEE Trans. Geosci. Rem. Sens.*, vol. 37, no.2, pp. 960-968, 1999.

[74] Pascale C. Dubois, Jakob van Zyl, and Ted Engman, "Measuring Soil Moisture with Imaging Radars," *IEEE Trans. Geosci. Remote Sensing,* vol.33, pp.915-926, 1995.

[75] S. Baronti, F. Del Frate, P. Ferrazzoli, S. Paloscia, P. Pampaloni, and G. Schiavon, "SAR polarimetric features of agricultural areas," *Int. J. Remote Sensing*, vol. 16, pp. 2639–2656, 1995.

[76] Pierce, L.E., F.T. Ulaby, K. Sarabandi, and M.C. Dobson, "Knowledge-based classification of polarimetric SAR images," *IEEE Trans. Geosci. Remote Sensing*, vol.32, no.5, pp. 1081-1086, 1994.

[77] C. da Costa Freitas et al., "Land Use and Land Cover Mapping in the Brazilian Amazon Using Polarimetric Airborne P-Band SAR Data," *IEEE Trans. Geosci. Remote Sensing*, vol. 46, no. 10, 2008.

[78] G. Mittal, and D. Singh "Critical analysis of polarimetric PALSAR data for land cover classification," *Proceedings of International Conference on Microwave – 08*, pp. 434-437,2008.

[79] V. V. Chamundeeswari, D. Singh, and K. Singh, "An adaptive method with integration of multi-wavelet based features for unsupervised classification of SAR images," *J. Geophys. Eng.*, vol. 4, no. 4, pp. 384–393, Dec. 2007.

[80] V. Alberga ,"A study of land cover classification using polarimetric SAR parameters," *International Journal of Remote Sensing*, vol. 28, no. 17, pp. 3851–3870, 2007.

[81] Michael E. Hodgson, "What Size Window for Image Classification? A Cognitive Perspective," *Photogrammetric Engineering & Remote Sensing*, vol. 64, no. 8, pp. 797-807, August 1998.

APPENDIX

A. Classification results

A.1. Decision tree classification

Overall accuracy=88.0208

Kappa coefficient=0.8313

Table – A-1

Confusion matrix for decision tree classifier

Classes	P.A.(%)	U.A.(%)	Commission	Ommission
Water	99.67	88.96	11.04	0.33
Urban	80.31	99.05	0.95	19.69
Tall vegetation	95.71	97.10	2.09	4.29
Short vegetation	78.75	55.26	44.75	21.25
Bare soil	66.67	100.00	0	33.33

A.2. Classification based on Pauli decomposition

A.2.1. Parallelepiped classification

Overall accuracy =30.5952%

Kappa coefficient =0.2075

Table – A-2

Confusion matrix for parallelepiped classification based on Pauli decomposition

Classes	P.A.(%)	U.A.(%)	Commission (%)	Ommission (%)
Water	0	0	0	100
Tall vegetation	98.57	21	78.90	1.43
Short vegetation	93.43	30.62	69.38	6.57
Urban	3.77	100.00	0.0	96.23
Bare soil	75.76	67.57	32.43	24.24

A.2.2. Minimum distance classification

Overall accuracy = 66.4286%

Kappa coefficient = 0.5469

Table – A-3

Confusion matrix for minimum distance classification based on Pauli decomposition

Classes	P.A.(%)	U.A.(%)	Commission (%)	Ommission (%)
Water	78.81	79.33	20.67	21.19
Tall vegetation	48.57	58.62	41.38	51.43
Short vegetation	54.01	49.33	50.67	45.99
Urban	68.30	78.02	21.98	31.70
Bare soil	46.97	33.70	66.30	53.03

A.2.3. Maximum likelihood classification

Overall accuracy = 71.5476%

Kappa coefficient = 0.6203

Table – A-4

Confusion matrix for maximum likelihood classification based on Pauli decomposition

Classes	P.A.(%)	U.A.(%)	Commission (%)	Ommission (%)
Water	59.60	87.80	12.20	40.40
Tall vegetation	34.29	58.54	41.46	65.71
Short vegetation	73.72	49.03	50.97	26.28
Urban	91.32	82.03	17.97	8.68
Bare soil	81.82	62.07	37.93	18.18

A.3. Classification based on eigen value decomposition

A.3.1. Using H/A/Alpha as input to classifier

A.3.1.1. Parallelepiped classification

Overall accuracy = 38.2143%

Kappa coefficient = 0.2186

Table – A-5

Confusion matrix for parallelepiped classification based on H/A/Alpha

Classes	P.A.(%)	U.A.(%)	Commission (%)	Ommission (%)
Water	0.33	50.00	50.00	99.67
Tall vegetation	20.00	21.21	78.79	80.00
Short vegetation	69.34	34.30	65.70	30.66
Urban	56.98	56.98	58.17	43.02
Bare soil	90.91	44.78	55.22	9.09

A.3.1.2. Minimum distance classification

Overall accuracy= 40.1190%

Kappa coefficient= 0.2431

Table – A-6

Confusion matrix for Minimum distance classification based on H/A/Alpha

Classes	P.A.(%)	U.A.(%)	Commission (%)	Ommission (%)
Water	17.88	35.53	64.47	82.12
Tall vegetation	80.00	29.02	70.98	20.00
Short vegetation	37.96	34.67	65.33	62.04
Urban	43.02	50.67	49.33	56.98
Bare soil	92.42	51.69	48.31	7.58

A.3.1.3. Maximum likelihood classification

Overall accuracy= 40%

Kappa coefficient= 0.2772

Table – A-7

Confusion matrix for Maximum likelihood classification based on H/A/Alpha

Classes	P.A.(%)	U.A.(%)	Commission (%)	Ommission (%)
Water	11.92	43.37	56.63	53.28
Tall vegetation	45.71	22.22	77.78	54.29
Short vegetation	46.72	37.43	62.57	53.28
Urban	55.09	41.48	58.52	44.91
Bare soil	87.88	64.44	35.56	12.12

A.3.2. Using H/Alpha as input to classifier

A.3.1.1. Parallelepiped classification

Overall accuracy = 39.0476%

Kappa coefficient = 0.2325

Table – A-8

Confusion matrix for parallelepiped classification based on H/A/Alpha

Classes	P.A.(%)	U.A.(%)	Commission (%)	Ommission (%)
Water	0	0	0	100
Tall vegetation	30	22.83	77.17	70
Short vegetation	78.10	33.13	66.86	21.90
Urban	52.96	42.81	57.19	46.04
Bare soil	86.36	62.64	37.36	13.64

A.3.1.2. Minimum distance classification

Overall accuracy= 40.2381%

Kappa coefficient= 0.2444

Table – A-9

Confusion matrix for Minimum distance classification based on H/A/Alpha

Classes	P.A.(%)	U.A.(%)	Commission (%)	Ommission (%)
Water	17.88	35.53	64.47	82.12
Tall vegetation	80.00	29.02	70.98	20
Short vegetation	37.96	34.67	65.33	62.04
Urban	43.02	50.67	49.33	56.98
Bare soil	93.94	51.67	48.33	6.06

A.3.1.3. Maximum likelihood classification

Overall accuracy= 42.6190%

Kappa coefficient= 0.2642

Table – A-10

Confusion matrix for Maximum likelihood classification based on H/A/Alpha

Classes	P.A.(%)	U.A.(%)	Commission (%)	Ommission (%)
Water	11.26	43.04	56.96	88.74
Tall vegetation	55.71	26.53	73.47	44.29
Short vegetation	52.55	38.92	61.08	47.45
Urban	56.98	44.54	55.46	43.29
Bare soil	93.94	68.89	31.11	6.06

A.4. Classification based on three D decomposition

A.4.1. Without filter

A.4.1.1. Parallelepiped classification

Table – A10

Classification based on three D decomposition by parallelepiped classification

Window size	O.A.	Kappa	Water		Urban		Vegetation	
			P.A.	U.A.	P.A.	U.A.	P.A.	U.A.
3x3	88.8430	0.8286	79.41	100.00	99.34	92.64	84.67	72.99
5x5	89.1185	0.8338	78.31	100.00	99.34	94.08	88.00	75.00
11x11	90.0826	0.8473	81.62	100.00	99.34	93.50	86.67	74.71
15x15	91.0468	0.8615	84.19	100.00	99.34	93.50	86.67	75.58

A.4.1.2. Minimum distance classification

Table – A11

Classification based on three D decomposition by minimum distance classification

Window size	O.A.	Kappa	Water		Urban		Vegetation	
			P.A.	U.A.	P.A.	U.A.	P.A.	U.A.
3x3	88.9807	0.8353	75.74	100.00	96.71	99.66	97.33	76.04
5x5	89.6694	0.8449	77.21	100.00	97.04	99.66	97.33	76.04
11x11	89.6917	0.8464	77.21	100.00	97.04	99.66	96.67	78.80
15x15	90.4959	0.8571	80.15	100.00	97.04	99.66	96.00	79.12

A.4.1.3. Maximum likelihood classification

Table – A12

Classification based on three D decomposition by maximum likelihood classification

Window size	O.A.	Kappa	Water		Urban		Vegetation	
			P.A.	U.A.	P.A.	U.A.	P.A.	U.A.
3x3	38.3459	0.0000	100.00	38.35	0.00	0.00	0.00	0.00
5x5	98.4962	0.9773	98.04	100.00	97.73	100.00	100.00	95.00
11x11	99.2481	0.9886	100.00	100.00	97.73	100.00	100.00	97.44
15x15	99.2481	0.9886	100.00	100.00	97.73	100.00	100.00	97.44

B. MATLAB CODES

B.1. Three D decomposition

(a) Without filtering

```
%3 D freeman decomposition
%%
clc
clear all;
close all;
%% Memmory Initialization
   S_hh(400,400)=0;
   S_hv(400,400)=0;
   S_vh(400,400)=0;
   S_vv(400,400)=0;
   alpha(400,400)=0;
   beta(400,400)=0;
   Fs(400,400)=0;
   Fd(400,400)=0;
   Fv(400,400)=0;

%% importing ASCII files
path_1= importdata('E:\50003\wo filtering\resized\ascii\hh_cal.txt');
path_2= importdata('E:\50003\wo filtering\resized\ascii\hv_cal.txt');
path_3= importdata('E:\50003\wo filtering\resized\ascii\vh_cal.txt');
path_4= importdata('E:\50003\wo filtering\resized\ascii\vv_cal.txt');
 for m= 1:1:400
   for n=1:1:400
      S_hh(m,n)=path_1( m, 2*n-1 )+sqrt(-1)* path_1( m , 2*n);
    S_hv(m,n)=path_2(m , 2*n-1)+sqrt(-1) * path_2( m , 2*n);
     S_vh(m,n)=path_3(m , 2* n-1)+sqrt(-1)* path_3( m , 2*n);
     S_vv(m,n)=path_4( m, 2* n-1)+sqrt(-1)* path_4( m , 2*n);
   end
end
```

```
'file reading done'

%% Formulation of covariance terms
hh = S_hh .* conj(S_hh);
vv= S_vv .* conj(S_vv);
hv = S_hv .* conj(S_hv);
vvC= conj(S_vv);
hhvv= S_hh .* vvC;
%% Ensemble averaging
HH = imfilter (hh, 15);
VV = imfilter (vv, 15);
HV = imfilter (hv, 15);
HHVV = imfilter (hhvv, 15);

re= real(HHVV);
im= imag(HHVV);

% CALCULATION OF TERMS Fs,Fd,Fv
for i=1:400
  for j =1:400
    [i j];
if re(i,j) >0
  alpha(i,j)=-1;
Fs(i,j) = (alpha(i,j).^2).*(VV(i,j).^2 - 2.* alpha(i,j).*HHVV(i,j).*VV(i,j) +
        HHVV(i,j).^2)./(VV(i,j).*alpha(i,j).^2 - 2.*HHVV(i,j).*alpha(i,j) + HH(i,j));
Fd(i,j) =  -(HHVV(i,j).^2 - HH(i,j).*VV(i,j))./(VV(i,j).*alpha(i,j).^2 - 2.*HHVV(i,j).*alpha(i,j)
        + HH(i,j));
beta(i,j) = (HH(i,j) - alpha(i,j).*HHVV(i,j))./(HHVV(i,j) - alpha(i,j).*VV(i,j));
else
      beta(i,j)=1;
Fs(i,j) =-(HHVV(i,j).^2 - HH(i,j).*VV(i,j))./(VV(i,j).*beta(i,j).^2 - 2.*HHVV(i,j).*beta(i,j) +
       HH(i,j));
Fd(i,j) =(beta(i,j).^2.*VV(i,j).^2 - 2.*beta(i,j).*HHVV(i,j).*VV(i,j) +
        HHVV(i,j).^2)./(VV(i,j).*beta(i,j).^2 - 2.*HHVV(i,j).*beta(i,j) + HH(i,j));
```

```
  alpha(i,j) =(HH(i,j) - beta(i,j).*HHVV(i,j))./(HHVV(i,j) - beta(i,j).*VV(i,j)) ;

      end
   end
end

 ps= Fs .*(1 + abs (beta .* beta));
 pd=Fd .*(1+ abs (alpha.*alpha));
 pv=8.* HV;

 Ps= abs(ps);
 Pd= abs(pd);
 Pv= abs(pv);
%
dlmwrite('3D_Ps.dat',Ps,'delimiter','\t','precision', '%.4f');
dlmwrite('3D_Pd.dat',Pd,'delimiter','\t','precision', '%.4f');
dlmwrite('3D_Pv.dat',Pv,'delimiter','\t','precision', '%.4f');
```

(b) With polarimetric filtering

```
% 3 d decomposition with polarimetric filter
clc
clear all;
close all;
%%  ASCII files import
path_1= importdata('E:\50003\with pol filter\resize\ascii\polv_1.txt');
path_2= importdata('E:\50003\with pol filter\resize\ascii\polv_2.txt');
path_3= importdata('E:\50003\with pol filter\resize\ascii\polv_3.txt');
path_4= importdata('E:\50003\with pol filter\resize\ascii\polv_4.txt');
path_5= importdata('E:\50003\with pol filter\resize\ascii\polv_5.txt');
path_6= importdata('E:\50003\with pol filter\resize\ascii\polv_6.txt');
path_7= importdata('E:\50003\with pol filter\resize\ascii\polv_7.txt');
path_8= importdata('E:\50003\with pol filter\resize\ascii\polv_8.txt');
path_9= importdata('E:\50003\with pol filter\resize\ascii\polv_9.txt');

for m= 1:1:400
   for n=1:400
      hh_vv(m ,n)=path_4( m, n )+sqrt(-1)* path_5( m ,n);
      hh_hv(m, n)=path_6(m , n)+sqrt(-1) * path_7( m , n);
      vv_hv(m, n)=path_8(m , n)+sqrt(-1)* path_9( m ,n);
    end
end
 'file reading done'

% SPATIAL AVERAGING
HH  = path_1;
VV  = path_2;
HV  = path_3;
HHVV = hh_vv;

re= real(HHVV);
im= imag(HHVV);
```

```
% CALCULATION OF TERMS Fs,Fd,Fv
for i=1:400
  for j =1:400
    [i j];
      if re(i,j) >0
            alpha (i, j)=-1;
Fs( i, j) = (alpha(i,j).^2).*(VV(i,j).^2 - 2.* alpha(i,j).*HHVV(i, j).*VV(i,j) +
        HHVV(i,j).^2)./(VV(i, j).*alpha(i,j).^2 - 2.*HHVV(i ,j).*alpha(i,j) + HH(i,j));
Fd(i,j) =  -(HHVV(i,j).^2 - HH(i, j).*VV(i, j))./(VV(i, j).*alpha(i ,j).^2 -
        2.*HHVV(i,j).*alpha(i,j)  + HH(i,j));
beta(i,j) = (HH(i,j) - alpha(i,j).*HHVV(i,j))./(HHVV(i,j) - alpha(i,j).*VV(i,j));
      else
            beta(i,j)=1;
Fs(i,j) =-(HHVV(i,j).^2 - HH(i,j).*VV(i,j))./(VV(i,j).*beta(i,j).^2 - 2.*HHVV(i,j).*beta(i,j) +
      HH(i,j));
Fd(i,j) =(beta(i,j).^2.*VV(i,j).^2 - 2.*beta(i,j).*HHVV(i,j).*VV(i,j) +
      HHVV(i,j).^2)./(VV(i,j).*beta(i,j).^2 - 2.*HHVV(i,j).*beta(i,j) + HH(i,j));
alpha(i,j) =(HH(i,j) - beta(i,j).*HHVV(i,j))./(HHVV(i,j) - beta(i,j).*VV(i,j)) ;
    end
  end
end
ps = Fs .*(1 + abs (beta .* beta));
pd= Fd .*(1+ abs (alpha.*alpha));
pv=8.* HV;
Ps= abs(ps);
Pd= abs(pd);
Pv= abs(pv);
Ps(isnan(Ps))=0;
Pd(isnan(Pd))=0;
Pv(isnan(Pv))=0;

dlmwrite('3D_Ps.dat',Ps,'delimiter','\t','precision', '%.4f');
dlmwrite('3D_Pd.dat',Pd,'delimiter','\t','precision', '%.4f');
dlmwrite('3D_Pv.dat',Pv,'delimiter','\t','precision', '%.4f');
```